Technische Universität Berlin

Master's thesis

Acoustical Behaviour of Buckling Dielectric Elastomer Actuators

by

Michael Gareis

Supervisors:

Prof. Dr. Stefan Weinzierl FG Audiokommunikation
Prof. Dr. Jürgen Maas FG Elektromechanische Konstruktion

February 25, 2019

Fakultät |
Geisteswissenschaften

Prüfungsausschüsse

Studiendekan und Vorsitzender

Prof. Dr. Friedrich Steinle

Eidesstattliche Erklärung

Ist jeder an der TU Berlin verfassten schriftlichen Arbeit eigenhändig unterzeichnet beizufügen!

Hiermit erkläre ich an Eides statt gegenüber der Fakultät I der Technischen Universität Berlin, dass die vorliegende, dieser Erklärung angefügte Arbeit selbstständig und nur unter Zuhilfenahme der im Literaturverzeichnis genannten Quellen und Hilfsmittel angefertigt wurde. Alle Stellen der Arbeit, die anderen Werken dem Wortlaut oder dem Sinn nach entnommen wurden, sind kenntlich gemacht. Ich reiche die Arbeit erstmals als Prüfungsleistung ein. Ich versichere, dass diese Arbeit oder wesentliche Teile dieser Arbeit nicht bereits dem Leistungserwerb in einer anderen Lehrveranstaltung zugrunde lagen.

Titel der schriftlichen Arbeit

VerfasserIn/VerfasserInnen*

Name Vorname Matr.-Nr.

Betreuende/r DozentIn

Name Vorname

Mit meiner Unterschrift bestätige ich, dass ich über fachübliche Zitierregeln unterrichtet worden bin und verstanden habe. Die im betroffenen Fachgebiet üblichen Zitiervorschriften sind eingehalten worden.

Eine Überprüfung der Arbeit auf Plagiate mithilfe elektronischer Hilfsmittel darf vorgenommen werden.

Ort, Datum Unterschrift**

*Bei Gruppenarbeiten sind die Unterschriften aller VerfasserInnen erforderlich.
**Durch die Unterschrift bürgen Sie für den vollumfänglichen Inhalt der Endversion dieser schriftlichen Arbeit.

Abstract

Dielectric elastomers (DE) are regarded as a potentially alternative to conventional actuator technologies. They feature low weight, high strains and low material costs. A soft dielectric (here: silicone) is sandwiched between two compliant electrodes. Upon voltage, the material compresses in thickness and expands in area due to incompressibility. Their scope of application ranges from sensors, energy generators, smart textiles to biomimetic robots and much more. A few concepts of loudspeakers using DE have been demonstrated by the research community. One of the disadvantages of previously concepts was the need for mechanical bias (e.g. by air pressure). This work proposes a new concept of loudspeaker, which does not need prestretch or other means of mechanical bias. Buckling dielectric elastomer actuators use the area expansion of actuated DE to buckle up. This mechanism is used to construct a milli-meter-scale loudspeaker with good frequency response in the range above 5 kHz. The concept is implemented using automatically fabricated multi-layer membranes of 3 to 8 layers. The multilayer structure allows to generate more force and higher flexural rigidity than a single-layer setup. 6 samples with different amount of layers and a diameter of 8 mm are fabricated.
A full analytical model is derived. Measurements of the static deflection, the frequency response and the total harmonic distortion validate the model. Ways of optimizing and tuning the loudspeaker are discussed in the latter part of this thesis. Sound pressure level increases with ∼18 dB/octave until the peak SPL of almost 80 dB (in 1 m distance in half-space) is achieved at a frequency of 5 kHz. The small scale of the speaker allows it to be installed in large arrays and thus might offer a hardware platform for high-resolution beam forming or wave field synthesis.

Zusammenfassung

Dielektrische Elastomere (DE) werden als mögliche Alternative zu konventionellen Aktortechnologien angesehen. Sie bieten große Verformung, geringes Gewicht und potentiell niedrige Material- sowie Produktionskosten. Ein weiches Dielektrikum mit flexiblen Elektroden auf beiden Seiten erfährt unter angelegter Spannung eine Kompression. Das Material gilt als inkompressibel und dehnt sich im Zuge der Kompression in der Fläche aus. Frühe Anwendungen bezogen sich fast ausschließlich auf künstliche Muskeln in der Robotik, doch immer mehr Anwendungsbereiche werden durch diese Technologie erschlossen. Das Prinzip kann nicht nur als Aktor, sondern auch als Sensor und Generator verwendet werden.
Diese Arbeit stellt einen neuartigen Lautsprecher vor, der die Flächenexpansion der Folie ausnutzt. Eingespannt in einem festen Rahmen kann das Material nicht zur Seite hin ausweichen, und bei angelegter Spannung zwischen den Elektroden wölbt sich das Elastomer auf. Ein mehrschichtiger Aufbau erlaubt es, einen höheren Druck zu generieren und die entstehende Wölbung stabiler zu machen. Das System wird in dieser Arbeit analytisch beschrieben. 6 Exemplare eines Lautsprechers mit einem Durchmesser von 8 mm und unterschiedlicher Anzahl Schichten (3 bis 8 Schichten) werden hergestellt und vermessen. Anschließend wird die Verformung unter statischer Spannung sowie der Frequenzgang und die *total harmonic distortion* (THD) vermessen. Die Messergebnisse validieren das analytische Modell weitestgehend.
Der Lautsprecher kann eindeutig als Hochtöner identifiziert werden. Der Frequenzgang steigt mit etwa ∼18 dB/Octave an, bis bei 5 kHz der maximale Schalldruckpegel von fast 80 dB (in 1 m Abstand im Halbraum) erreicht wird. Der THD liegt mit ca. 30 dB etwas höher als bei konventionellen Lautsprechern.
Gegenüber früherer Konzepte von DE-Lautsprechern bietet der hier vorgestellte Prototyp den Vorteil, dass kein mechanischer Bias in Form von Luftdruck oder Vorspannung nötig ist.
Möglichkeiten, die akustische Performance zu verbessern werden diskutiert. Möglicher Anwendungsbereich für den vorgestellten Schallwandler erstrecken sich von Mikrolautsprechern in mobilen Geräten bis hin zu einer Hardwareplattform für hochauflösende Wellenfeldsynthese- und Beamforming-Systeme.

Acknowledgements

I want to thank all members of *FG Audiokommunikation (FG AK)* and of *FG Elektromechanische Konstruktion (FG EMK)* to support me with my work. Special thanks to Prof. Weinzierl and Prof. Maas to allow me pursue my ideas and encouraging me.
This work wouldn't have been possible without the help of labaratory manager Thomas Schütze of *FG EMK* for assisting me with the processing of the material and providing me with the multilayer samples used for this thesis. Also special thanks to Florian Straube, Fabian Brinkmann for assisting me with the audio equipment and test engineer Roman Tschakert, who allowed me to use the acoustic test facility, i.e. the excellent anechoic room of TU Berlin and.
I would also like to thank Abdelkarim Masoud and Ozan Cabuk for their help and assistance and who shared their expertise of dielectric elastomers with me. Thanks to Johann Ranzinger, wo left the department too early, for the fruitfull discussions about technologies and his help to establish the test setup for static measurements.

Contents

List of Tables

List of Figures

Chapter 1

Introduction

1.1 Motivation

Multi-channel audio systems are becoming increasingly popular as they become more affordable even for consumers. A wide range of 5.1 and 7.1 systems are meanwhile available and enjoy great popularity. Larger systems in cinemas, theatres or event halls provide good spatiality and the sound can be adjusted to the specific location using complex audio signal processing methods, to enhance audio quality. But multi-channel audio is becoming increasingly difficult to implement. While software algorithms can easily control large arrays of loudspeakers with modern wave field synthesis (WFS) programs or beam forming algorithms, hardware limits the amount of channels for most applications. *Dolby Atmos*, for example, is able to individually control up to 128 loudspeakers, which is seldomly actually implemented in theatres. Conventional acoustic transducers with reasonable performance are often expensive, heavy, large and require high input power. Large installations, as they exist in movie theatres or in auditoriums (e.g. *WellenFeld H 104*, see Fig. 1.1), are therefore only possible in large rooms.

In theory, an infinite amount of loudspeakers is required to fully satisfy the WFS equations [52].

Figure 1.1: Auditorium H 104 at TU Berlin. Multichannel system of 832 separate channels for wave field synthesis. More than 2700 loudspeaker arranged in 10 cm distance on ear-level around the audience.

Hence, to make WFS and beam forming appealing for consumers, new approaches to transducer design are needed. Lightweight, small and inexpensive loudspeakers with good overall performance are required. The variety of possible interiors calls for loudspeakers, that can be manufactured on demand and potentially very small.

The rise of dielectric elastomer actuators (DEA) over the past 20 years offer these opportunities. A thin polymeric film is used to generate sound. Films can be of any shape and size, are of cheap material (e.g. silicone) and thus, can be produced on demand in large scales with novel manufacturing techniques like 3D-printing.

Films are usually only about 10 µm to 500 µm thick and are supported by a rigid frame, which accounts for most of the actuators overall weight. The absence of permanent magnets, coils or other metallic structures in DEA leads to potentially lower weight than that of conventional electrodynamic or electrostatic systems.

The low weight of dielectric elastomer (DE) loudspeakers might also offers the opportunity, to install sound systems in weight restricted environments as automotive or aerospace. Small size and low weight are also advantageous for mobile applications like phones, headphones or portable speakers.

Recent prototypes of DE loudspeakers confirmed the capability of this technology. However, more accurate models and studies on the dynamic behaviour and acoustical optimizations are required to introduce these actuators to the consumer market.

1.2 Overview of Dielectric Elastomer (DE) Technology

Smart materials have become of great interest in recent decades, especially electroactive polymers (EAP) received a lot of attention by the research community [8]. Applications of EAPs cover a large variety of industries.
As a subclass of EAPs, dielectric elastomers (DE) have emerged as promising actuation technology for various kinds of applications.
In its basic configuration, a dielectric elastomer actuator (DEA) consists of a thin film of elastomer, usually only tens to hundreds of micrometers thick, sandwiched between two compliant electrodes. An applied voltage attracts the electrodes and compresses the elastomer. Because elastomers are rubber-like materials, they can be assumed to be incompressible and thus, their area will increase in the process of thickness compression. (see Fig.1.2)
In Chapter 2, it will be derived that the pressure on the material induced by an applied voltage is given by [41]

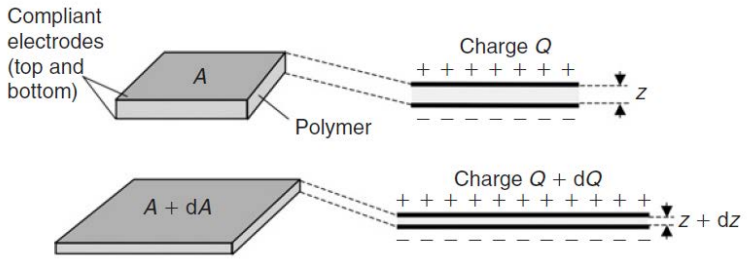

Figure 1.2: Dielectric elastomer actuator [8]

$$p = \epsilon_0 \epsilon \frac{V^2}{d^2} \tag{1.1}$$

where ϵ is the dielectric constant of the elastomer with thickness d, ϵ_0 the free-space permittivity and V the applied voltage.

With equations of *linear* elasticity, the strain in thickness direction (z-direction) is

$$s_z = -\frac{p}{E} = -\epsilon_0 \epsilon \frac{V^2}{E d^2} \tag{1.2}$$

with E the Young's modulus of the elastomer. [41]
The resulting increase in area (x-y-plain) is obtained by making use of the incompressibility of the material

$$(1 + s_x)(1 + s_y)(1 + s_z) = (1 + s_x)^2(1 + s_z) = 1 \tag{1.3}$$

Substituting typical values for an elastomer gives a good approximation of the achievable are strains. For a material with a dielectric constant of $\epsilon = 3$, a modulus of elasticity of $E = 1\,\mathrm{MPa}$ and the vacuum permittivity of $\epsilon_0 = 8.85 \times 10^{-12}\,\mathrm{F\,m^{-1}}$ this becomes

$$\begin{aligned} s_z &= -3 \frac{8.85 \times 10^{-12}\,\frac{\mathrm{F}}{\mathrm{m}}}{1\,\mathrm{MPa}} \frac{V^2}{E d^2} \\ &= -2.66 \times 10^{-17}\,\frac{\mathrm{F}}{\mathrm{m\,Pa}} \cdot E^2 \end{aligned} \tag{1.4}$$

With $d = d_0(1 + s_z)$ and an initial thickness $d_0 = 100\,\mu\mathrm{m}$, a third order polynomial of s_z is obtained

$$\begin{aligned} &s_z(1 + s_z)^2 = \\ &s_z + 2s_z^2 + s_z^3 = -2.66 \times 10^{-9}\,\frac{1}{\mathrm{V}^2} \cdot V^2. \end{aligned} \tag{1.5}$$

Fig- 1.3 shows the voltage induced strain in the elastomer. The maximum strain in this model of $-33\,\%$ is achieved at $\approx$7.5 kV. This corresponds to an increase in area of 50 %! [41]

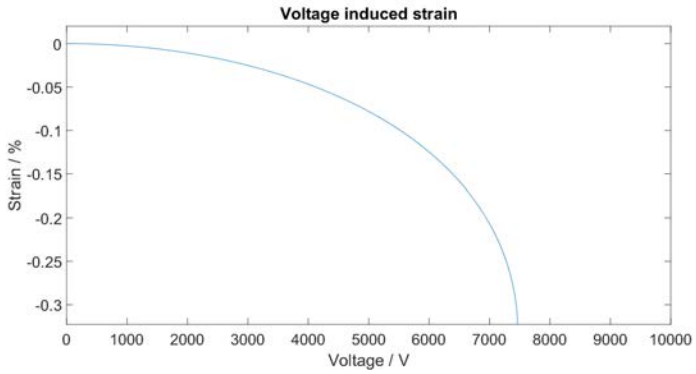

Figure 1.3: Strain-voltage in linear elasticity. A maximum thickness strain of 33 % is possible. (Graph is plotted for 0.1 mm membrane thickness, E=1.0 MPa and $\epsilon = 3.0$)

However, far greater strains have been observed, which highlights the limitations of the linear model. In reality the modulus of elasticity is strain dependent. But for low strains $< 20\,\%$ this model gives a good approximation. [40]

The idea of electricity induced deformation is not new. The volume of early capacitors in the 18th century (*Leyden jars*) was observed to change, when charged [33]. About 100 years later, Roentgen observed deformations of rubber, when supplied with an electric field [42]. This may be seen as the first ever dielectric elastomer actuator [4]. However, the observed strains were small and the potential of this form of actuation was not seen.
Another $\sim$ 100 years later, researchers began experimenting with EAPs as actuators, and with their extraordinary results introduced this technology to the research community [41, 58].

A lot of effort has been made on developing more precise models [11, 53] and on how to improve performance of DE i.e. reduce driving voltage and increase response. Different fabrication techniques [41], prestretching of the elastomer [23] and adding substrates into the material [28, 49, 57] show considerable success.

1.3 Materials

A wide range of polymers have been tested for suitability as dielectric elastomers [4], with Fluorelastomers, Polyurethanes, silicones and acrylics being more frequently used as DE [38].
Elastomers, or rubber-like materials consist of long, flexible polymer chains, which are at some points linked to each other, i.e. cross-linked or end-linked when the intermolecular linking is randomly distributed or only at the ends of the molecules, respectively [5].
This allows stretching of the material up to large strains of several hundred percent. Upon re-

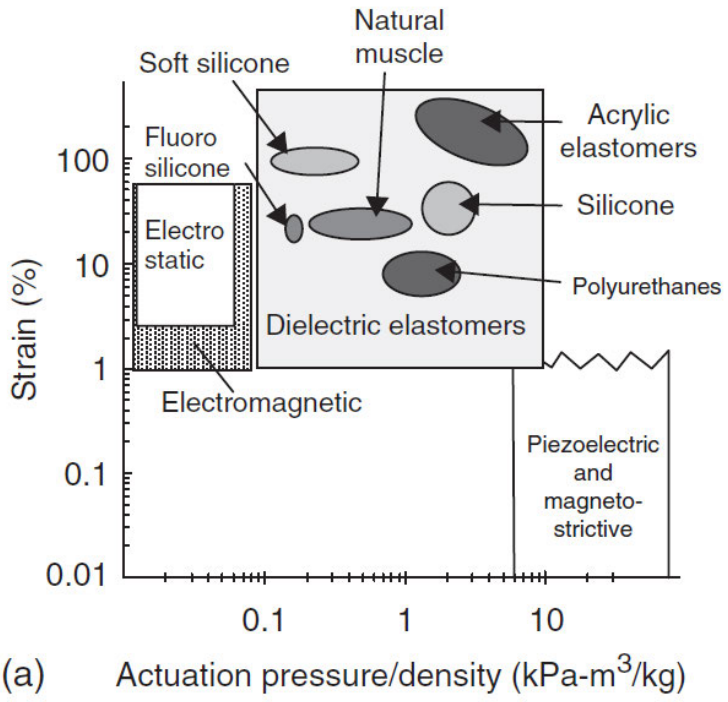

Figure 1.4: Comparison of high-speed actuator technologies [8]

lease, the molecular chains form back to their initial configuration.

Different applications for DEA require specific properties of the material. Fig. 1.4 shows performance of various DE materials in comparison to conventional actuators (electrostatic, electromagnetic, piezoelectric and magnetostrictive). The abscissa shows the actuation pressure per material density. This is an important measure for applications, where weight is a limiting factor, such as mobile devices, automotive or robots. The maximal strain observed with the materials is displayed on the ordinate.
Not displayed in this figure are important features such as reaction time and output force. This lack of information in the graphic leads to the assumption, that acrylic elastomers are the best choice, as they are positioned in the up right corner. A more sophisticated overview of material performance with respect to more properties including the impact of prestrain on performance is shown in Tab. 1.1.

While Polyurethane shows maximum strains of less than 20 % and low pressure-density, it has a large output force and good permittivity [41]. This may make it useful for applications, where low voltage and high force is required, but large strains are not. However, because of the limitations to low strains it is seldom used for DE, as conventional actuator technologies offer similar strains but much larger output forces.

Material	Prestrain (x,y) %	Energy density $\frac{MJ}{m^3}$	Actuation pressure MPa	Thickness strain %	Area strain %	Young's Modulus MPa	Electric Field (Breakdown) $\frac{MV}{m}$	Dielectric Constant
Silicone (Nusil CF19-2186)	0,0	0.22	1.36	32		1	235	2.8
Silicone (Nusil CF19-2186)	45,45	0.75	3	39	64	1	350	2.8
Silicone (Dow Corning HS3)	0,0	0.026	0.13	41		0.135	72	2.8
Silicone (Dow Corning HS3)	68,68	0.098	0.3	48	93	0.1	110	2.8
Polyurethane (Deerfied PT6100S)	0,0	0.087	1.6	11		17	160	7
Polyurethane (Estane TPU588)	0,0	0.0025	0.14	8			8	6
Fluorsilicone (Dow Coring 730)	0,0	0.0055	0.39	28		0.5	80	6.9
Fluorelastomer (Lauren L143HC)	0,0	0.0046	0.11	8		2.5	32	12.7
Acrylic (3M VHB 4910)	15,15	0.022	0.13	29	40		55	4.8
Acrylic (3M VHB 4910)	300,300	3.4	7.2	61	158	3.0	412	4.8

Table 1.1: Material Overview [4]

Fluorelastomers show high permittivity but lower performance in most other respects. Thus, these materials are also uncommon in actuators.

Acrylics and silicones seem to be most promising and are mainly used in actuators. In most applications the acrylic elastomer *VHB 4910* by *3M* is used because of its strains and its availability as commercial adhesive tape. Strains of 380 % have been recorded [24].
However for applications where fast response time is important, such as in loudspeakers, silicone seems to be more promising [31] (see Fig 1.5) and few loudspeaker prototypes have been already built [12, 14, 17, 48].
The elastomer used in this work is the silicone foil *Elastosil 2030* provided by *Wacker Chemie AG*.

1.4 Applications and Configurations

In most applications, the elastomer film is suspended in a frame, which supplies an antagonist force. The force stretches the elastomer in absence of applied voltage (pre-stretch). By turning on a voltage, the film elastically succumbs to the antagonist force and experiences a positive area stretch. Turning off the voltage (and thus the attractive force between the electrodes), the elastomer will return to its pre-stretched state.
As Kornbluh in [8] puts it: 'You can't push a rope', DEs are not able to exert a pushing force to an attached load. Instead DEs will only succumb to a mounted stretching/antagonist force. This, of course, only refers to 'ropes' considerably longer than thick.

For 'ropes', the same as for DEs, above a certain threshold-ratio of diameter to length, the material is able to exert a pushing force and will not uncontrollably buckle up.

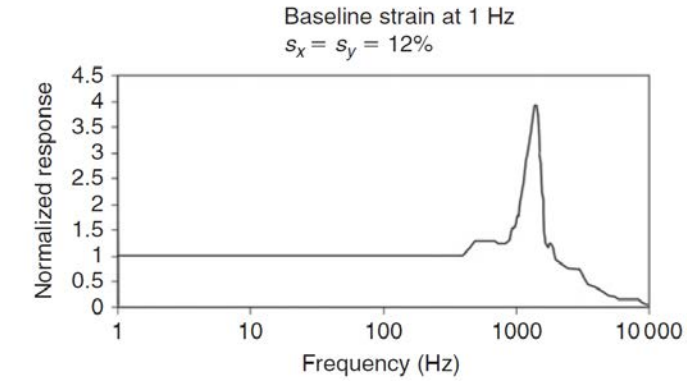

(a) Silicone

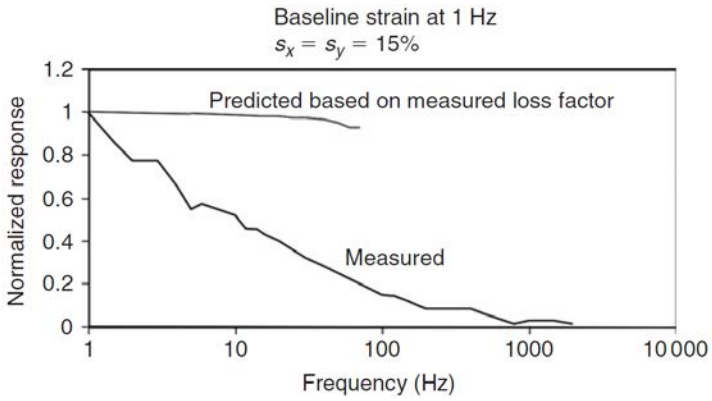

(b) Acryl

Figure 1.5: Frequency-dependent strain response of a circular DE actuator. Acrylic compared to silicone. Silicone shows no dependency on applied signal frequency up to a resonance at 1425 Hz [8]

Figure 1.6: Schematic view of one spring roll actuator. Left: Spring; Middle: electrode pattern; Right: Actuator. [37]

Figure 1.7: Hexapod robot *MERbot* using six spring roll actuators [37].

As artificial muscles, EAPs provide promising features for robotics [22]. In contrast to conventional actuators such as hydraulic-, pneumatic-, electric-motors or even combustion engines, EAPs are flexible, lightweight, potentially thin, can induce large strains, are inexpensive and easy to manufacture. Thus, they are of great interest as driving units in robotics. [22].
At *SRI International*, researchers have developed a range of biomimetic robots, including imitations of birds, fishes and insects, with various kinds of dielectric elastomer actuators [39].
Pei et al [37] proposed so-called spring roll actuators for the design of artificial muscles in robotic applications. With these, a hexapod robot called MERbot was successfully built.
The actuators consist of acrylic elastomers, which are prestrained 25-fold in area. The films were then coated in a specific pattern with carbon based electrodes, see Fig. 1.6.
Wrapped around a spring, the prestrained films cause a compressive force on it. By applying a voltage, stress on the activated side of the film is released and causes deformation of the spring. Six of these actuators are attached to a robot, see Fig. 1.7. With a weight of only 29 g per

Figure 1.8: Powered Clothing by *Seismic*. `https://www.myseismic.com/`. Artificial muscles in the suit enhance the wearer's physique.

leg these actuators do not contribute much to a potential robots total weight as conventional actuators usually do.
Similar mechanisms have been used to propel snake-like robots [39], which can be used for underwater manoeuvres.

Besides of developing imitations of organisms, EAPs may be integrated into existing organisms, e.g. as artificial blood pumps [7, 11], prosthetics [8] or as complex biomedical systems to control biological phenomena [13]. These applications are possible, because most polymers (e.g. silicone) are biocompatible and thus, can be integrated into organisms.

Smart textiles can be used to design clothing, that adapt to its environment, protect the wearer, monitor his/her medical condition or to generate power. [50]
A recent example of smart textile with EAP technology builds the *Powered Clothing* bei *Seismic*. An overall-like suit comprising various sensors and artificial muscles shall help elderly or injured people to move, by enhancing the wearers' own muscle force, see Fig. 1.8.

The ability to act as sensors and actuators at the same time, can be used to develop actuators that respond to their own feedback [21].
As generators, they are able to harvest power in small scale applications. [19, 56]

The capabilities of these materials are great, as they can be manufactured on demand and can be used as generators-, sensors-, and/or actuators simultaneously. The impact of EAPs on the commercial market is potentially immense, and research on this field is expected to extend

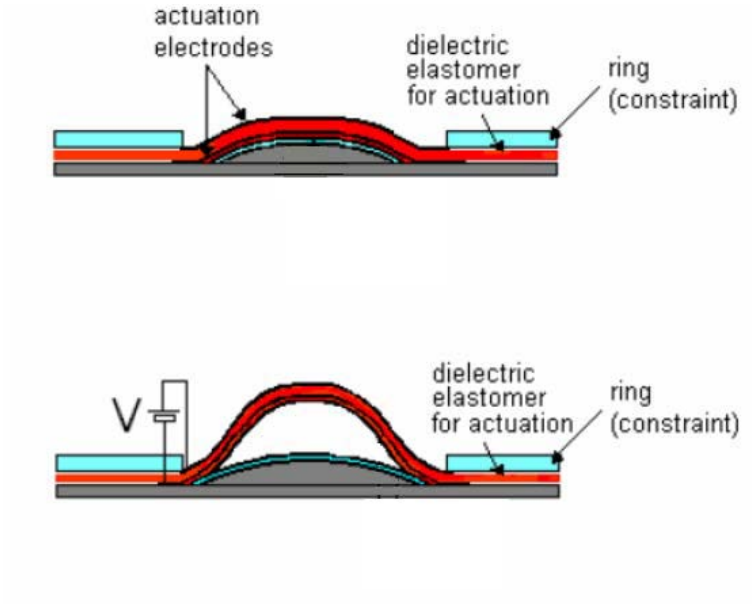

Figure 1.9: Schematic view of a buckling dielectric elastomer actuator. Top: inactive; Bottom: active [25]

the variety of applications. [43]

In the case of a buckling dielectric elastomer actuator (BDEA) the buckling is used to make use of the contracting force between the electrodes.
When said rope is sufficiently short, it will buckle up with only one antinode of buckling upon pushing it towards a fixed object. The same principle accounts for the BDEA, except for the fact, that the elastomer is not pushed, but its length will increase upon thickness contraction. Transformed to three-dimensions, the membrane will buckle up forming a cap, which may be assumed as spherical. The spherical buckling can then be used to move a mass or, for loudspeakers, air.
Fig. 1.9 shows the principle of a BDEA.
Prototypes of pumps [7] or robotic motors [6] using BDEAs have been successfully demonstrated. Lampani [25] studied the behaviour of a prototypic BDEA for its use in aerospace applications. This thesis will examine its suitability for loudspeakers.

1.5 DE Loudspeakers

Of special interest for this work is the suitability of DEs as loudspeakers. The earliest prototype using this technology as acoustic transducer was designed at *SRI International* and introduced DE as a potentially well performing type of transducer. [15]

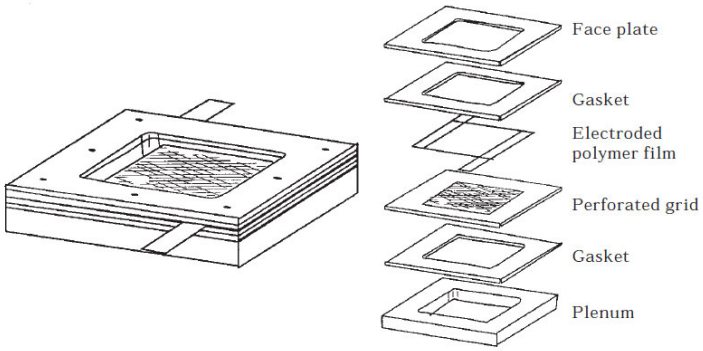

Figure 1.10: Exploded-view of the DE loudspeaker by [14].

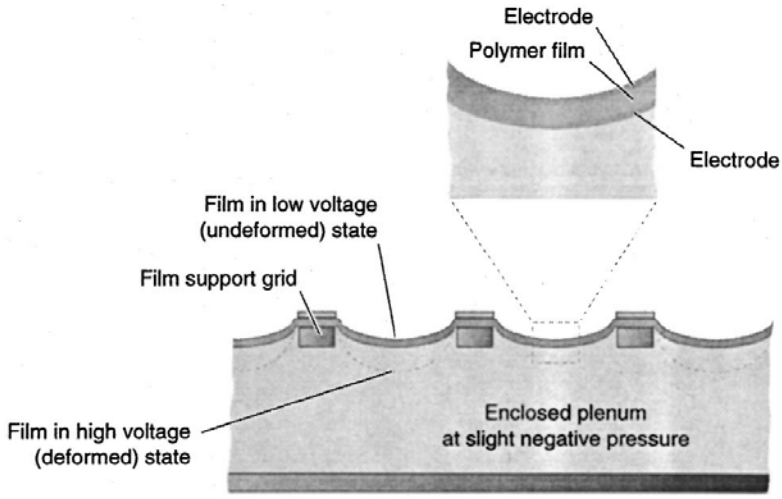

Figure 1.11: Cross sectional view of the DE loudspeaker by [14].

A silicone-rubber foil sandwiched between two compliant graphite electrodes is placed on top of a plate with a dense matrix of holes (1.10). A negative pressure on one side of the film pulls it through the holes, forming bubbles as seen in Fig. 1.11. Under applied bias- and signal voltage the bubbles shrink/grow and thus generate sound.
Despite having a good frequency response above resonance frequency (see Fig. 1.12), it features high harmonic distortion, as film displacement is dependent on the square of applied voltage (Eq. 1.1). Square rooting the audio signal provided significant improvement. Above resonance frequency, total harmonic distortion (THD) was reduced to $<1\,\%$.
With a bubble diameter of 5.5 mm, film thickness of 86 µm and a prestrain of only 10 % the resonance frequency was at $\approx$1.5 kHz.

Despite providing good performance, one might keep in mind, that the pressure beneath the film has to be kept at constant level (relative to atmosphere) in order to provide unvarying sound

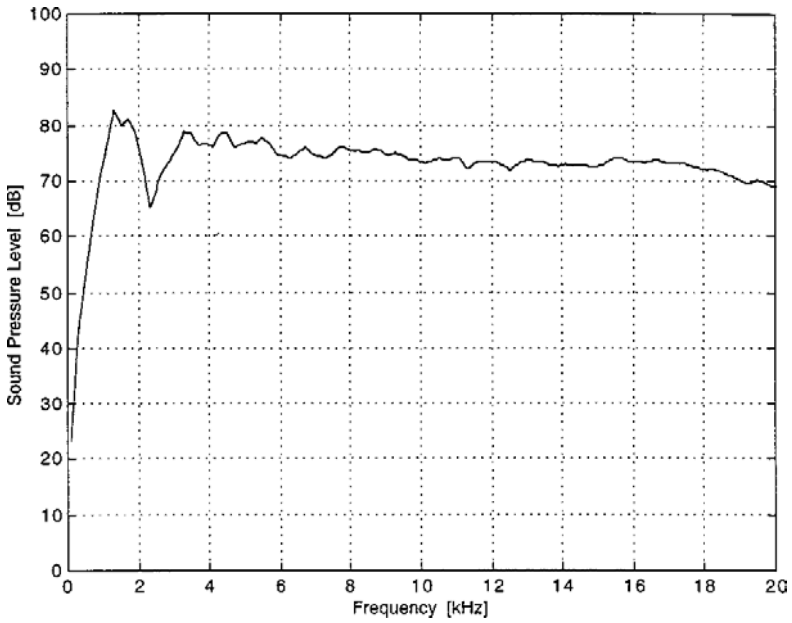

Figure 1.12: Frequency response of the loudspeaker by [15]. Resonance frequency at 1450 Hz. Measured in 1m distance.

generation. In ordinary applications, such as in consumer electronics, this is not feasible.
The frequency response of this loudspeaker is different from the strain-response of a silicon DE actuator as in Fig. 1.5a, indicating a frequency dependent sound radiation compensating the decline in strain for high frequencies.

Sugimoto et. al. [48] proposes a different approach to DE loudspeaker design. A transducer in push-pull operation is built in order to achieve much lower THD, without the need of square rooting the audio signal or mechanically biasing the film with static pressure, yet featuring a less flat frequency response.
Two circular framed DE films of polyurethane are symmetrically positioned on both sides of a small plate with mass $m = 60\,\mathrm{g}$. Stretching the films, by moving the frames away from each other makes the plate stay in place.
By feeding the signal with opposite phase to the upper and lower film, push-pull operation of the speaker is enabled. The mass allows tuning of the actuator without much effort. By adding/removing some weight to the plate, the resonance can be tuned to the desired frequency. Transducers with different resonance frequencies and low THD can be produced.
However, this approach withdraws the advantage of DE actuators being easily manufactured by hand, as the setup is more complex compared to push/pull-only configurations.

A desirable loudspeaker would show a flat frequency response comparable to Fig. 1.12, with

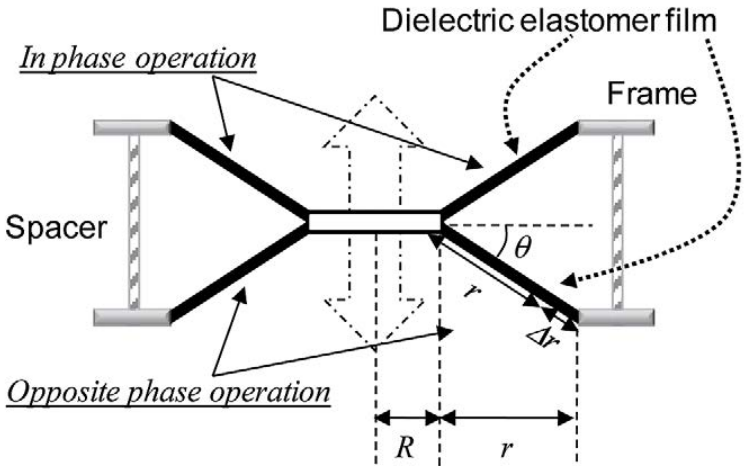

Figure 1.13: Two opposite phase operated membranes act as a Push-Pull transducer [48].With center mass of $m = 60\,\mathrm{g}$, the resonance frequency is at 115 Hz.

low resonance frequency and without the need of keeping constant air pressure as in [48]. Easily producible speakers might offer the chance of fabricating vast amounts with new manufacturing methods like 3D printing.

A possible approach to achieve these features, might be the use of the mentioned buckling actuator. The DE film, mounted on top of a rigid hemispheric cap and surrounded by a boundary ring, will lift up (see Fig. 1.9). Without the underlying support, the actuator would form uncontrolled buckles and would not force out any air to generate sound.
Several studies exist on the modelling of circular membranes as well as their dynamic behaviour [10, 11, 27, 51, 53, 55, 60] and good accordance with experimental data were achieved.
In his paper, Vertechy et. al. [51] uses a silicone foil with a thickness of $d_0 = 900\,\mu\mathrm{m}$ and a Youngs's modulus of 60 kPa. The initial height h_0 of the cap was 3 mm and its base radius 14 mm. Loudspeakers using this form of DEA remain to be developed. By applying a bias-voltage, the membrane can be 'lifted up' to a state of instability. An added signal voltage would then force the membrane to oscillate around this state, generating sound.
The simple approach of not having a mechanical bias air-pressure or any other kind of external force (e.g. foam) on the diaphragm makes this design configuration auspicious for loudspeaker design. Besides that, it is more easy to be crafted manually and further reduces the already low weight.
By using a thinner membrane, lower voltages may be required to achieve similar strains, since the electric field is $\propto \frac{1}{d_0}$. Using a multilayer actuator then should increases the actuation pressure, i.e. the sound pressure.

1.6 Scope

This thesis reviews the application of buckling dielectric elastomer actuators as loudspeakers. Different prototypes are tested in order to find a concept capable of sound generation.
A prototypic loudspeaker is developed and characterised. The work covers the analytical description of the system, i.e. the transfer function of voltage to sound pressure and the experimental validation of the model. Other characteristics, like total harmonic distortion and various resonance frequencies are discussed and measured.
The design and development of the actuator is thoroughly described. Goal of this thesis is to introduce an innovative way of sound generation using smart materials. A functioning prototype is presented. Possible ways of optimisation are considered in the latter part.

Chapter 2

Theory and Fundamentals

In this chapter, the principle of dielectric elastomers will be explained. Special attention will be given to buckling actuators, as those will be the driving unit for the loudspeaker.
The first part will describe the dielectric elastomer itself, where a general relation of applied voltage and resulting stress in the elastomer is derived.
Principles of sound generation are discussed in the second part.
A linearised model of the the dynamic behaviour of the buckling actuator follows.
Last, all results will be combined, to estimate the generated sound pressure of the BDEA.

2.1 Electromechanical Transduction in DE

In this section, an energy approach will be used, to deduce a relation of voltage and stress. [8]

The basic structure of a dielectric elastomer sandwiched between two compliant electrodes can be seen as a capacitor of area A and thickness z with capacitance

$$C = \frac{\epsilon_0 \epsilon A}{z} \tag{2.1}$$

where ϵ_0 is the permittivity of free space and ϵ the permittivity of the dielectric.
The electrical energy U_e stored in a capacitor with charge Q is [8]

$$U_\mathrm{e} = \frac{Q^2}{2C} = \frac{zQ^2}{2\epsilon_0 \epsilon A} \tag{2.2}$$

Unlike conventional capacitors, the dielectric elastomer is able to change its shape and size upon charging. An incremental change of energy $\mathrm{d}U_e$ therefore will have to consider changes of size.

$$\begin{aligned}\mathrm{d}U_e &= \frac{\partial U_\mathrm{e}}{\partial Q}\mathrm{d}Q + \frac{\partial U_\mathrm{e}}{\partial z}\mathrm{d}z + \frac{\partial U_\mathrm{e}}{\partial A}\mathrm{d}A \\ &= \frac{Q}{C}\mathrm{d}Q + U_\mathrm{e}\left[\frac{1}{z}\mathrm{d}z - \frac{1}{A}\mathrm{d}A\right] \\ &= V\mathrm{d}Q + U_\mathrm{e}\left[\frac{1}{z}\mathrm{d}z - \frac{1}{A}\mathrm{d}A\right]\end{aligned} \tag{2.3}$$

Here, the first terms represents the electrical energy provided by an external source, charging the capacitor. The second term describes the conversion of electrical to mechanical work. [8]
It only depends on changes of the geometry $\mathrm{d}z$ and $\mathrm{d}A$. So, the work on the polymer from an external power (i.e. the electrical field force) is [8]

$$\mathrm{d}W = -U_\mathrm{e}\left[\frac{1}{z}\mathrm{d}z - \frac{1}{A}\mathrm{d}A\right] \tag{2.4}$$

For the frequently used assumption of constant volume $Vol = A \cdot z$ (incompressibility of the elastomer) the electrical energy U_e reads as

$$\mathrm{d}U_\mathrm{e} = V\mathrm{d}Q + 2U_\mathrm{e}\frac{1}{z}\mathrm{d}z \tag{2.5}$$

The mechanical work done by a pressure p is obtained by

$$\mathrm{d}W = Ap\mathrm{d}z \tag{2.6}$$

or

$$p = \frac{1}{A}\frac{\mathrm{d}U_\mathrm{e}}{\mathrm{d}z} \quad \text{(when charge Q is kept constant)} \tag{2.7}$$

Here, the actuation pressure is generated by the opposed charged electrodes. [8]
Derivation, considering constant volume yields

$$p = \epsilon_0\epsilon\frac{V^2}{z^2} = \epsilon_0\epsilon E^2 \tag{2.8}$$

which is often called the Maxwell stress in dielectric elastomers.
This result will be later used in order to receive a relation for applied voltage and resulting strain and is thus the underlying equation for modelling of the loudspeaker.

The supplied voltage from the external amplifier (V_AMP) does not equal the voltage applied at the dielectric (V_C). Fig.2.1 shows the circuit diagram of the typical DEA setup. V_C is then

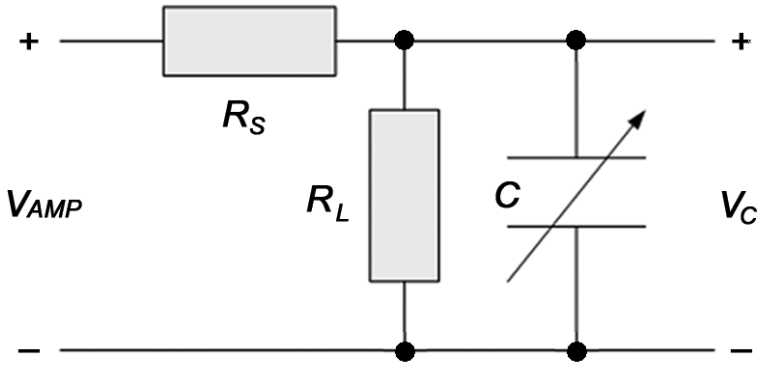

Figure 2.1: Circuit diagram of a dielectric elastomer actuator. R_S: combined resistance of electrode and feed line; R_L: resistance of the dielectric (leakage current); C: capacitance of the DE. [46]

given by

$$V_\mathrm{C} = V_\mathrm{AMP} \cdot \frac{R_\mathrm{L}}{R_\mathrm{L} + R_\mathrm{S}} \tag{2.9}$$

For many applications the electrode resistance is orders of magnitude lower than the resistance of the isolating layer and no leakage current can be assumed. For alternating current applications, the complex impedance of the circuit is given by

$$\begin{aligned} Z &= R_\mathrm{S} + R_\mathrm{L} \frac{1}{1 + i\omega C R_\mathrm{L}} \\ &= R_\mathrm{S} + \frac{R_\mathrm{L}}{1 + \omega^2 C^2 R_\mathrm{L}^2} \cdot (1 - i\omega C R_\mathrm{L}) \\ &= \Re(Z) + \Im(Z) \end{aligned} \tag{2.10}$$

To calculate the power consumption of the DE, only the real part of the impedance is of interest. The imaginary impedance only contributes to the energy in the electric field of the capacitor and is recovered after each cycle.
The electroded area of the DE is 8 mm × 8 mm large, the thickness d_0 is 50 µm and its permittivity is 2.8. Substituting gives a capacitance at zero strain of

$$C_0 = 3.2 \times 10^{-11}\,\mathrm{F} \tag{2.11}$$

Wacker specifies the volume resistivity of the utilised silicone as $1 \times 10^{14}\,\Omega\,\mathrm{m}$, so

$$R_\mathrm{L} = \frac{d}{A} \cdot 1 \times 10^{14}\,\Omega\,\mathrm{m} = \frac{d_0}{A_0}\lambda^2 = \lambda^2 \cdot 7.8 \times 10^{13}\,\Omega = R_{\mathrm{L},0} \cdot \lambda^2 \tag{2.12}$$

The real part of the impedance is then

$$\Re(Z) = R_\mathrm{S} + \frac{R_{\mathrm{L},0}\lambda^2}{1 + \omega^2 C_0^2 R_{\mathrm{L},0}^2} \tag{2.13}$$

The resistance of the electrode is in the range of 100 kΩ. Electrode quality and thus the resistance varies widely and is different for each sample. Uniform electrode design is a present topic of DE research and progress is being made.
The approximate impedance at zero strain is

$$\begin{aligned} \Re(Z) &= 100\,\mathrm{k\Omega} + \frac{7.8 \times 10^{13}\,\Omega}{1 + \omega^2 (3.2 \times 10^{-11}\,\mathrm{F})^2 (7.8 \times 10^{13}\,\Omega)^2} \\ &= 100\,\mathrm{k\Omega} + \frac{7.8 \times 10^{13}\,\Omega}{1 + \omega^2 \cdot 6.2 \times 10^{6}\,\mathrm{s}^2} \end{aligned} \tag{2.14}$$

For an applied signal of $\omega = 2\pi \cdot 1\,\mathrm{kHz}$ the right part of the equation is negligible compared to the electrode resistance. Hence, only electrode resistance will be considered when calculating the power consumption. Following Ohm's Law, that is

$$P_\mathrm{el} = \frac{V_\mathrm{AMP}^2}{R_\mathrm{S}} \tag{2.15}$$

When supplied by a voltage $V_\mathrm{AMP} = V_\mathrm{bias} + V_\mathrm{signal}$, the bias voltage will not contribute to the overall power consumption as the leakage current is low enough to be neglected.

For multilayer actuators, N layers of DE are connected in parallel and the total impedance is approximated by

$$Z \approx \frac{R_\mathrm{S}}{N} \tag{2.16}$$

The electrical power supplied to he system follows

$$P_\mathrm{el} = N \frac{V_\mathrm{AMP}^2}{R_\mathrm{S}} \tag{2.17}$$

and will later be used to calculate the efficiency.
It is neglected, that with increasing electrode resistance, the electric field takes more time to spread over the surface of the membrane. For lager membranes than the utilised 8 mm × 8 mm of this work, this may have considerable effect on performance.

2.2 Continuum Mechanics

The loudspeaker presented in this work consists of a circular DE-membrane clamped into a rigid frame.
Modelling of dielectric elastomers usually requires hyperelastic theory because of the large in-

duced strains.
For the DEs used in this work, strains $< 10\,\%$ are achieved and linear material behaviour can be assumed [41].

This section will cover the static behaviour of the membrane. A short introduction on viscoelasticity is found at the end of the section.

The governing equation for the static deformation of a circular plate in z-direction is [1].

$$D\Delta^2 w = p_z. \tag{2.18}$$

In the following, all elements of the expression will be derived and explained. A static model of the membrane will then estimate the expected shape of the membrane under uniform normal stress (i.e. the maxwell stress derived in the previous Chapter 2.1).
For high-speed actuated DEAs (as for loudspeakers) viscoelastic properties have to be considered.

Let a particle P be initially at position $\mathbf{X}$. After a displacement $\mathbf{u}$, the particles are at location $\mathbf{x}$

$$\mathbf{x} = \mathbf{X} + \mathbf{u} \tag{2.19}$$

A deformation gradient $\mathbf{F}$ can be defined as

$$\mathrm{d}\mathbf{x} = \frac{\partial \mathbf{x}}{\partial \mathbf{X}}\,\mathrm{d}\mathbf{X} = \mathbf{F}\,\mathrm{d}\mathbf{X} \tag{2.20}$$

Its determinant J gives information about the change of volume of a body before and after deformation V and v, respectively [16].

$$\mathrm{d}v = \det(\mathbf{F})\,\mathrm{d}V = J\,\mathrm{d}V \quad \text{with} \quad J > 0 \tag{2.21}$$

The deformation is therefore reversible (because $\det(F) < 0$) and the reverse deformation is

$$\mathrm{d}\mathbf{X} = \mathbf{F}^{-1}\,\mathrm{d}\mathbf{x} \tag{2.22}$$

The Green-Lagrangian strain tensor $\mathbf{E}$ is defined as

$$\mathbf{E} = \frac{1}{2}(\mathbf{F}^T\mathbf{F} - \mathbf{I}) \tag{2.23}$$

It provides information about the strains inside the structure. [2] The displacement $\mathbf{u}$ can then be written in terms of $\mathbf{F}$ and the identity matrix $\mathbf{I}$ as

$$\mathrm{d}\mathbf{u} = \mathrm{d}\mathbf{x} - \mathrm{d}\mathbf{X} = (\mathbf{F} - \mathbf{I})\,\mathrm{d}\mathbf{X} = \mathbf{H}\,\mathrm{d}\mathbf{X} \tag{2.24}$$

with the displacement gradient **H**

$$H_{ij} = \frac{\partial u_i}{\partial X_j} = \frac{\partial u_i}{\partial x_k}\frac{\partial x_k}{\partial X_j} = \frac{\partial u_i}{\partial x_k}\left(\delta_{kj} + \frac{\partial u_k}{\partial X_j}\right) \tag{2.25}$$

And the strain tensor **E** becomes

$$E_{ij} = \frac{1}{2}\left(\frac{\partial u_i}{\partial X_j} + \frac{\partial u_j}{\partial X_i} + \frac{\partial u_k}{\partial X_i}\frac{\partial u_k}{\partial X_j}\right) \tag{2.26}$$

In linear elasticity, the displacements of a particle are considered small with respect to the dimensions of the structure $\frac{\partial u_i}{\partial X_j} << 1$ and H_{ij} reads as

$$H_{ij} = \frac{\partial u_i}{\partial X_j} = \frac{\partial u_i}{\partial x_j} \tag{2.27}$$

Now, under this assumption of infinitesimal small strains, **E** equals the strain tensor ϵ [2]

$$\epsilon_{ij} = \frac{1}{2}\left(\frac{\partial u_i}{\partial x_j} + \frac{\partial u_j}{\partial x_i}\right) = \frac{1}{2}(u_{ij} + u_{ji}) \tag{2.28}$$

2.2.1 Stress-Strain

The theory of elasticity was defined in the last section. Now, the equations of strains shall be linked with the physical world using the stress tensor σ.
In linear elasticity, Hooke's Law states that, the strains are linear to an external stress

$$\sigma = \mathbf{c} : \epsilon \quad \text{or} \quad \sigma_{ij} = c_{ijkl}\epsilon_{kl} \tag{2.29}$$

with the elasticity tensor **c**. The 4^{th} order tensor **c** holds several symmetries, especially for isotropic materials.
Isotropy states, that the material's behaviour stays the same under rotation. 4^{th} order tensors with this property can be generally written as [2]

$$c_{ijkl} = \lambda\delta_{ij}\delta_{kl} + \mu(\delta_{ik}\delta_{jl} + \delta_{il}\delta_{jk}) + \kappa(\delta_{ik}\delta_{jl} - \delta_{il}\delta_{jk}) \tag{2.30}$$

with arbitrary constants λ, μ and κ.
In linear elasticity, the last term drops, because of $\sigma_{ij} = \sigma_{ij}$, which follows indirectly from Newton's Laws.
Substituting into Eq. 2.29 yields [2]

$$\sigma_{ij} = \lambda\epsilon_{kk}\delta_{ij} + 2\mu\epsilon_{ij} \tag{2.31}$$

The remaining constants λ and μ are called *Lamé parameters*. They can be written in terms of the more common material parameters E (Young's modulus) and ν (Poisson ratio). [2]

$$\lambda = \frac{\nu E}{(1-\nu)(1-2\nu)}, \qquad \nu = \frac{E}{2(1+\nu)}. \tag{2.32}$$

Then, Hooke's Law solved by the strains and substituting the symmetries and constants reads as (using summation convention)

$$E\epsilon_{ij} = (1+\nu)\sigma_{ij} - \nu\sigma_{kk}\delta_{ij} \tag{2.33}$$

Now, the relationship of stress and strain is specified and can be applied to the membrane using plate theory.

2.2.2 Kirchhoff-Love Plate Theory

The deformation of the silicone membrane shall be handled by the Kirchhoff-Love Plate Theory [2].
Plate theory tries to describe the elastic behaviour of structures thin compared to its in-plane dimensions (x, y). [2]
All material points are assumed to be in the midplane of the plate. The deflection in z-direction of a material point is a function of the in-plane dimensions [2]

$$w = w(x, y). \tag{2.34}$$

and is only due to a transverse distributed load p_z.
The second assumption of plate theory demands, that normal-stresses are negligible. This, of course, is not true for DE-membranes, as the normal stress is the driving force of actuation.
Redefining of the geometry can handle that problem. Instead of the membrane being compressed in z-direction by a stress σ_z and expanding in area direction, the plate is regarded as being subject to a radial compressive force q acting along the clamped edge leading to a fictive transverse load p_z. [1]
Both mechanics result in the buckling of the membrane and plate theory is applied to this problem.

Consider a plate with thickness h in the $x-y$-plane deflected in z-direction as depicted in Fig. 2.3 The displacements u and v for small angles $w_{x,y}$ are given by

$$\begin{aligned} u(x, y, z) &= -z\frac{\partial w(x, y)}{\partial x} \\ v(x, y, z) &= -z\frac{\partial w(x, y)}{\partial y} \end{aligned} \tag{2.35}$$

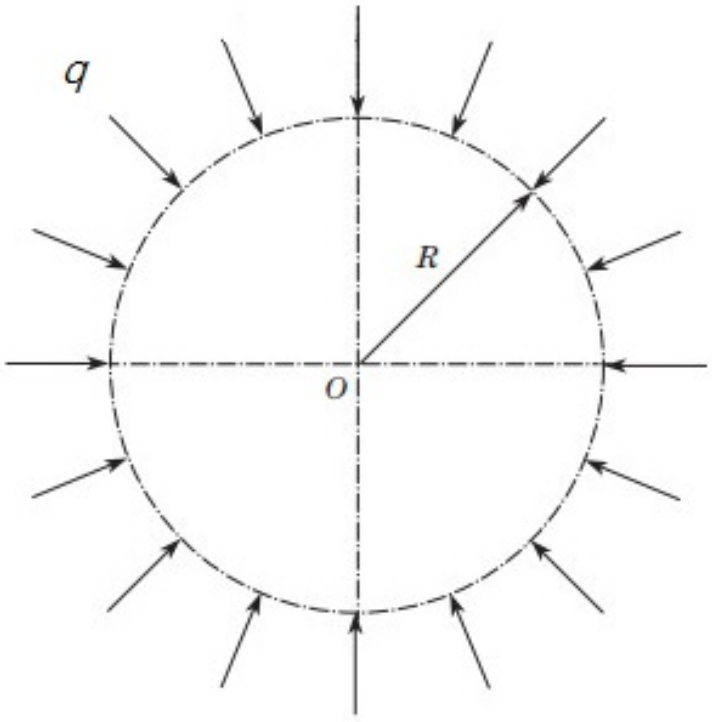

Figure 2.2: Schematic drawing of the circular plate of Radius R subject to a radial compressive force q [30], as analogy to a plate subject to radial extension.

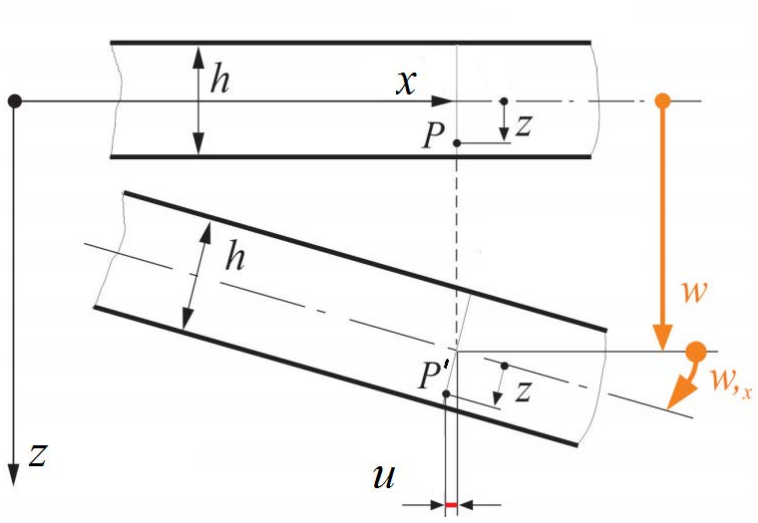

Figure 2.3: Plate bending in the $x-z$-plane. In-plane displacement in x-,y- direction are u and v, respectively. Displacement if the midplane in z-direction is w. Plate bending in $y-z$-plane is alike.

The strains are with Eq. 2.28

$$\begin{aligned} \epsilon_x &= \frac{\partial u}{\partial x} = -z\frac{\partial^2 w}{\partial x^2} \\ \epsilon_y &= \frac{\partial v}{\partial y} = -z\frac{\partial^2 w}{\partial y^2} \\ \epsilon_{xy} = \gamma_{x,y} &= \frac{\partial u}{\partial x} + \frac{\partial v}{\partial y} = -z\frac{\partial^2 w}{\partial x \partial y} \end{aligned} \tag{2.36}$$

All other strains in Kirchhoff Plate Theory are considered as negligible [1]. For the DEA with no prestretch, a strain in z-direction of less than 5 % is expected, and the assumption seems acceptable.
Solving Eq. 2.33 by σ and substituting the strains yields [2]

$$\begin{aligned} \sigma_x &= -\frac{Ez}{1-\nu^2}\left(\frac{\partial^2 w}{\partial x^2} + \nu\frac{\partial^2 w}{\partial y^2}\right) \\ \sigma_x &= -\frac{Ez}{1-\nu^2}\left(\frac{\partial^2 w}{\partial y^2} + \nu\frac{\partial^2 w}{\partial x^2}\right) \\ \sigma_{xy} = \tau_{xy} &= -\frac{Ez}{1+\nu}\frac{\partial^2 w}{\partial x \partial y} \end{aligned} \tag{2.37}$$

It is convenient to define internal forces Q and internal moments M as

$$\begin{aligned} Q_i &= \int_{-h/2}^{h/2} \tau_{iz}\ \mathrm{d}z \\ M_{ij} &= \int_{-h/2}^{h/2} \sigma_{ij} z\ \mathrm{d}z. \end{aligned} \tag{2.38}$$

Internal moments are obtained by substituting Eq. 2.37 and integrating

$$\begin{aligned} M_x &= -\frac{Eh^3}{12(1-\nu^2)}\left(\frac{\partial^2 w}{\partial x^2} + \nu\frac{\partial^2 w}{\partial y^2}\right) \\ M_y &= -\frac{Eh^3}{12(1-\nu^2)}\left(\frac{\partial^2 w}{\partial y^2} + \nu\frac{\partial^2 w}{\partial x^2}\right) \\ M_{xy} &= -(1-\nu)\frac{Eh^3}{12(1-\nu^2)}\frac{\partial^2 w}{\partial x \partial y} \end{aligned} \tag{2.39}$$

while the constant parameter is defined as the *flexural rigidity* D

$$D = \frac{Eh^3}{12(1-\nu^2)}. \tag{2.40}$$

The internal forces Q can not be obtained by integration, as it was stated that $\tau_{xz} = \tau_{yz} = 0$. But they can be calculated with the equilibrium conditions for an infinitesimal small plate element

under transverse load p_z. It holds

$$\frac{\partial Q_x}{\partial x} + \frac{\partial Q_y}{\partial y} = p_z \tag{2.41}$$

and

$$Q_x = \frac{\partial M_x}{\partial x} + \frac{\partial M_{xy}}{\partial y} \quad \text{and} \quad Q_x = \frac{\partial M_y}{\partial y} + \frac{\partial M_{xy}}{\partial x}. \tag{2.42}$$

Applying all equations for moments and forces one finally yields [1]

$$D\Delta^2 w = p_z. \tag{2.43}$$

To apply the formula to the given problem of a radially compressed disc as stated earlier, the fictive load p_z has to be determined. Fictive, because there is no actual load in z-direction when radially compressed. But plate theory requires a z-load.
For polar coordinates, a fictive load can be represented in terms of internal forces T_r and T_θ in radial and angular directions, respectively [1] as

$$p_z = T_r \frac{\partial^2 w}{\partial r^2} + T_\phi \left(\frac{1}{r} \frac{\partial w}{\partial \phi} + \frac{1}{r^2} \frac{\partial^2 w}{\partial \phi^2} \right) \tag{2.44}$$

where shear forces are neglected.
Substituting into Eq. 2.43 and using the Laplace operator in polar coordinates yields

$$D \left(\frac{\partial^2}{\partial r^2} + \frac{1}{r} \frac{\partial}{\partial r} + \frac{1}{r^2} \frac{\partial^2}{\partial \phi^2} \right)^2 w = T_r \frac{\partial^2 w}{\partial r^2} + T_\phi \left(\frac{1}{r} \frac{\partial w}{\partial \phi} + \frac{1}{r^2} \frac{\partial^2 w}{\partial \phi^2} \right) \tag{2.45}$$

Substituting $-q$ from Fig. 2.2 in T_r and T_θ

$$T_r = T_\theta = -q \tag{2.46}$$

and supposing axisymmetric deformation, Laplacians can be reduced and the solution is given by the Bessel functions of the first and second kind J_n Y_n, respectively. [1]

$$w = C_1 J_0(kr) + C_2 Y_0(kr) + C_3 \ln(kr) + C_4 \tag{2.47}$$

where $k^2 = q/D$. Deflections in the centre $r = 0$ of the membrane must not be infinite, so the constants C_2 and C_3 become zero.
In the specific problem of the membrane being clamped all around the edge

$$w(r = R_b) = \frac{\partial w(r = R_b)}{\partial} = 0 \tag{2.48}$$

it follows [1],

$$J_1(kR_b) = 0 \quad \text{so} \quad kR_b = 3.832 \tag{2.49}$$

and

$$C_4 = -C_1 J_0(kR_b) \tag{2.50}$$

and therefore

$$w(r) = C_1[J_0(kr) - J_0(kR_b)] \tag{2.51}$$

Now, to apply this to the problem of a DE membrane the constant C_1 has to be determined. The compressive maxwell stress Eq. 1.1 leads to an elastic deformation of the material according to linear elasticity (with $\lambda = \epsilon_z + 1$). Considering a multilayer actuator, with N electrodes and N dielectric layers, the equation becomes

$$NE \cdot (\lambda - 1) = (N-1)\epsilon\epsilon_0 \frac{V^2}{d_0^2 \lambda^2}. \tag{2.52}$$

The restriction of constant volume Vol in incompressible materials as silicone states that

$$Vol = A_0 \cdot d_0 = A \cdot d = A \cdot d_0 \lambda = \text{const.} \tag{2.53}$$

and the strain λ is the ratio of area before and after deformation, where it is assumed that the strain is homogeneous over the whole membrane surface.

$$A = \frac{A_0}{\lambda} = \frac{\pi R_b^2}{\lambda} \quad \text{or} \quad \lambda = \frac{\pi R_b^2}{A} \tag{2.54}$$

By calculating the surface of the deformed membrane given by Eq. 2.51 and substituting, C_1 can be calculated.

The shape is given by

$$f = \begin{pmatrix} r\cos(\phi) \\ r\sin(\phi) \\ w(r) \end{pmatrix} \quad \text{for} \quad r < R_b \tag{2.55}$$

and its surface area is calculated by

$$\begin{aligned} A &= \int_{\partial f} \mathrm{d}A \\ &= \int_0^{2\pi} \int_0^{R_b} \left| \frac{\partial f}{\partial r} \times \frac{\partial f}{\partial \phi} \right| \mathrm{d}r\mathrm{d}\phi \\ &= \int_0^{2\pi} \int_0^{R_b} \sqrt{1 + w'^2(r)} r \ \mathrm{d}r\mathrm{d}\phi \\ &= 2\pi \int_0^{R_b} \sqrt{1 + C_1^2 k^2 J_1^2(kr)} \ r \ \mathrm{d}r \end{aligned} \tag{2.56}$$

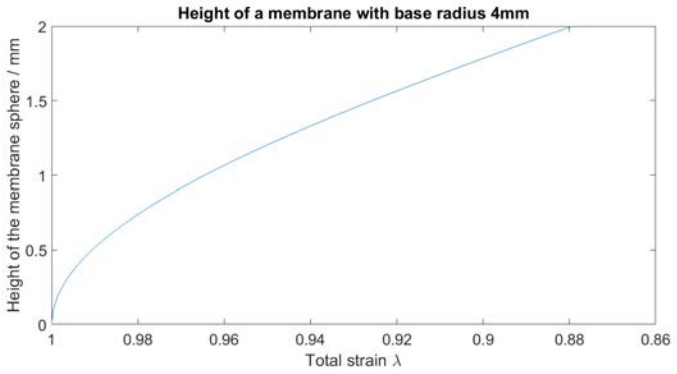

Figure 2.4: Cap height of a membrane by area-strain. The shape determined by plate-theory and homogeneously distributed stress and strain are assumed.

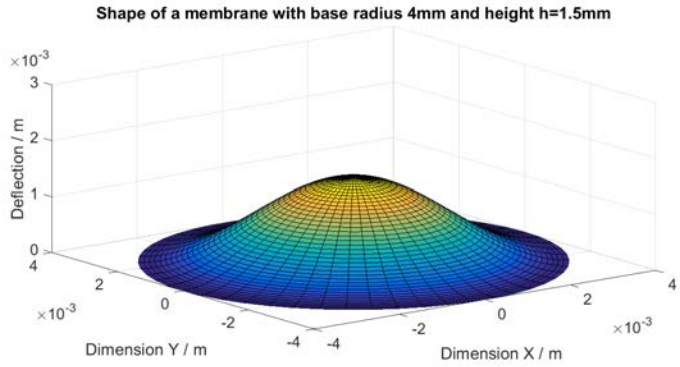

Figure 2.5: Shape of a membrane determined by plate-theory.

which has to be solved numerically using the *integral*-function in *Matlab*
with the cap height of the membrane of

$$h = w(0) = C_1 \cdot 1.402 \tag{2.57}$$

The cap height can be plotted over the strain, see Fig. 2.4. The shape of the membrane is illustrated in Fig. 2.5. As can be seen, strain near the base is expected to be much lower than near the apex of the cap. Therefore, homogeneous strain leads to an overestimation of height/strain. By what extend this model represents the actual shape of the membrane has to be tested. Possible deviations are because of the membrane being too thick, to neglect thickness.

2.2.3 Analytical Model

For an analytical model of the membrane deflection, it is more convenient to approximate the shape of the membrane by a sphere. Its geometry is specified as in Fig. 2.6

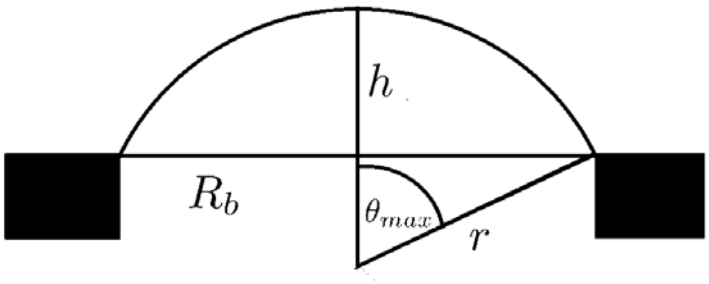

Figure 2.6: Geometry of the spherical membrane

As the membrane is initially supported by a spherical cap, its shape is spheric. Furthermore, it is assumed, that the membrane is still in the shape of a spherical cap when under electrostatic load, which is a sufficient approximation [51], despite Zhu et al [60] pointing out that, at high voltages, the shape of the membrane will slightly differ from a sphere.
The initial, or reference configuration is the unstretched membrane, i.e. planar. All material points are on a flat surface defined by

$$\mathbf{X} = \begin{pmatrix} R \cdot \cos(\phi) \\ R \cdot \sin(\phi) \\ 0 \end{pmatrix} \tag{2.58}$$

where $R \leq R_b$, with R_b the base radius of the cap and r_0 and h_0 the radius of the sphere and the cap height, respectively. The thickness is neglected and will be calculated from the area stretch. When supplied on the rigid cap, the particles form into spherical shape, defined by

$$\mathbf{x}_{pre} = \begin{pmatrix} r_0 \cdot \cos(\phi) \cdot \sin(\theta) \\ r_0 \cdot \sin(\phi) \cdot \sin(\theta) \\ r_0 \cos(\theta) - r_0 + h_0 \end{pmatrix}. \tag{2.59}$$

The restriction

$$\theta \leq \arcsin\left(\frac{R_b}{r_0}\right) = \arccos\left(\frac{r_0 - h_0}{r_0}\right) = \theta_{\max}. \tag{2.60}$$

follows from the rigid boundary ring and counts for all sphere radii.
Strains are calculated again by the area ratio of the undeformed and deformed membrane as before.

$$\lambda_{pre} = \frac{\pi R_b^2}{\pi(R_b^2 + h_0^2)} \tag{2.61}$$

When subject to an applied voltage, the radius/height of the the cap height will shrink/increase, respectively. All particles will move to the new position $\mathbf{x}_{act}$

$$\mathbf{x}_{act} = \begin{pmatrix} r \cdot \cos(\phi) \cdot \sin(\xi) \\ r \cdot \sin(\phi) \cdot \sin(\xi) \\ r \cdot \cos(\xi) - r + h \end{pmatrix}, \tag{2.62}$$

with

$$\xi \leq \arcsin\left(\frac{R_b}{r}\right) = \arccos\left(\frac{r-h}{r}\right) = \xi_{max}. \tag{2.63}$$

The total strains follow in analogy to the pre-strains. New cap height being substituted:

$$\lambda = \frac{\pi R_b^2}{\pi(R_b^2 + h^2)} \tag{2.64}$$

The total area strains are the product of pre- and actuation-strains $\lambda = \lambda_{act} \cdot \lambda_{pre}$, hence the activation strain in normal direction reads as

$$\lambda_{act} = \frac{\lambda}{\lambda_{pre}} = \frac{R_b^2 + h_0^2}{R_b^2 + h^2} \tag{2.65}$$

The total strain plotted versus the cap height of this analytical, spherical model differs from the previous model by a factor of $f \approx 1.3$ as seen in Fig. 2.7. So, as previously stated, the calculated height using the model for the shape of the membrane is an overestimation.
The assumption of homogeneously distributed strain is expected to slightly overestimate the deflection of the membrane. Strains near the apex of the cap will be greater, than those near the boundary ring. A more sophisticated model may be done in future research.

Early experiments showed, that the unloaded membrane is not stretched over the rigid support. It rather takes on a relaxed hemispherical shape, when clamped into the ring, see Fig. 2.8. This is probably due to the material being squeezed by clamping and thus displaced into the centre ring cavity.
Pre-strain is therefore neglected: $\lambda = \lambda_{act}$ (similar assumption is made in [51]) and the equation for static deflection then becomes

$$NE \cdot (\lambda_{act} - 1) = (N-1)\epsilon\epsilon_0 \frac{V^2}{d_0^2 \lambda_{act}^2}. \tag{2.66}$$

Solved by the voltage this allows to estimate the capheight of the membrane. The result is plotted in Fig. 2.9. At a voltage of about 4.3 kV the electrostatic attraction is stronger than the

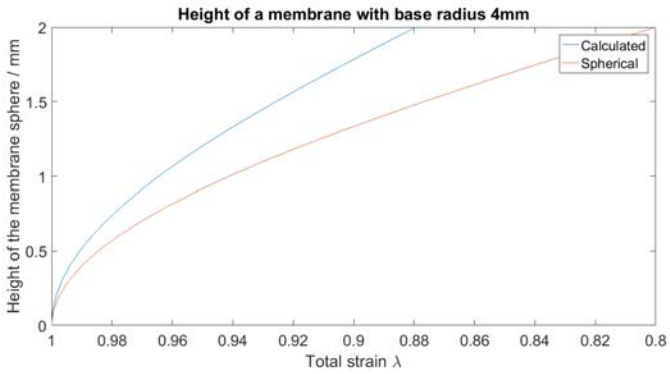

Figure 2.7: Comparison of strain-to-height for the calculated model of Ch. 2.2.2 and the more convenient approach of assuming spherical shape.

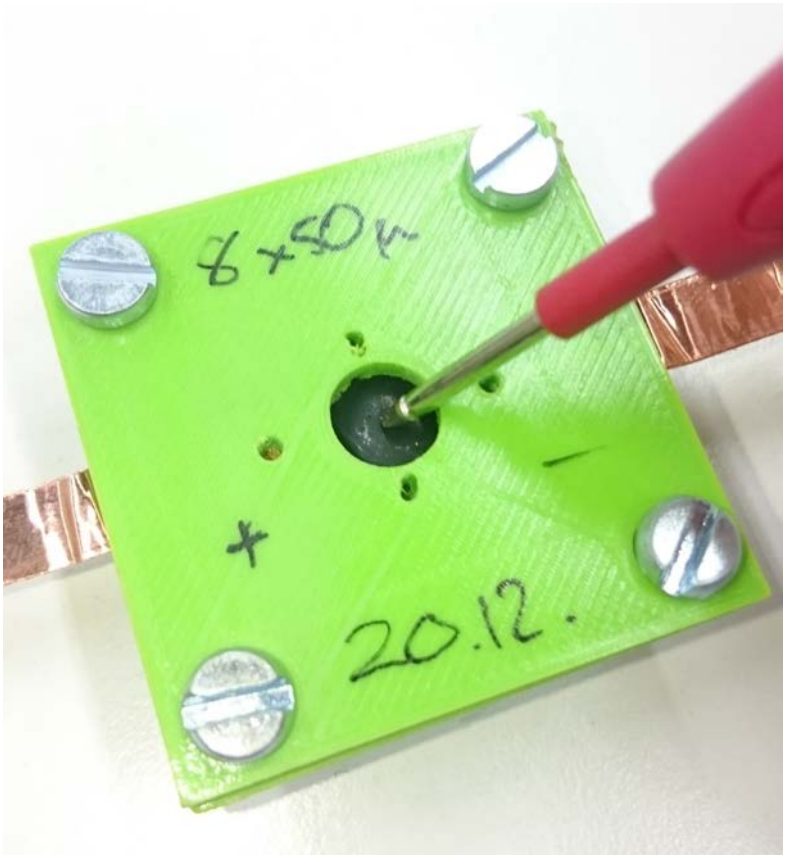

Figure 2.8: Assembled actuator. At $V = 0$ membrane does not stretch over the rigid cap. It takes on a (presumed) spherical shape of height h_0, which is made visible by carefully denting it.

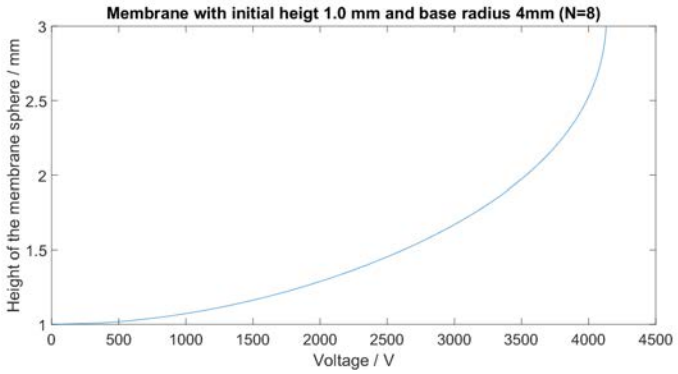

Figure 2.9: Estimation of cap height for a 8-layered BDEA with $R_b = 4.0\,\text{mm}$ and $h_0 = 1.0\,\text{mm}$, Youngs' modulus $E = 1.0\,\text{MPa}$, thickness $d_0 = 50\,\mu\text{m}$ and permittivity $\epsilon = 2.8$.

elastic repulsion and the breakdown voltage is reached. However, such high voltages may not be applied to the polymer, as the dielectric strength does not allow such high electric field strengths. Inhomogeneities in the membrane and the electrode usually further decrease the possible voltage significantly, and material failure is reached at far lower voltages.

2.2.4 Viscoelasticity

Until now, only pure elasticity was discussed. Most polymers also exhibit an viscous response to stress and strain as well. [36]
This behaviour is usually called the viscoelastic behaviour. The strain here is not only dependent on the applied stress, but also changes over time. The material shows creep strains and 'lags' behind the applied stress. For the modelling in this work a basic Kelvin-Voigt model is applied. Several viscoelastic models exist in literature. The Kelvin-Voigt model is chosen, as it is the simplest model for polymers at the beginning of loading. As this work is dedicated to the design of a loudspeaker, a high-frequency-driven unit, it can be considered as constantly being at the beginning of loading.

The material response is modelled by a parallel spring of elastic modulus E and a dashpot η (see Fig. 2.10). The stress is stated as

$$\sigma = E\xi(t) + \eta\dot{\xi}(t), \tag{2.67}$$

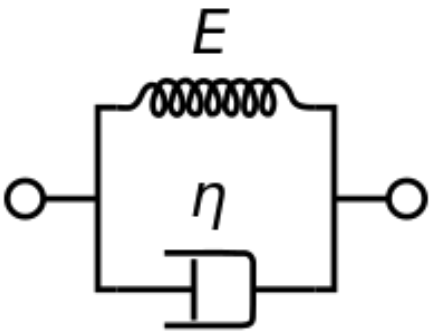

Figure 2.10: Schematic representation of the Kelvin-Voigt viscoelastic model. Two elements are coupled via a spring with spring constant E and a dashpot with friction η

with the displacement ξ. [36]
Considering the stress σ as constant σ_0, the strain is easily obtained by

$$\xi(t) = \frac{\sigma_0}{E}\left(-e^{-\frac{t}{\tau}}\right) \tag{2.68}$$

with $\tau = \frac{\eta}{E}$
For harmonic oscillating displacements of the system, Eq. 2.67 becomes

$$\hat{\sigma}e^{i(\omega t+\delta)} = E\hat{\xi}e^{i\omega t} + i\omega\eta\hat{\xi}e^{i\omega t} \tag{2.69}$$

which simplifies to

$$\hat{\sigma}e^{i\delta} = E\hat{\xi} + i\omega\eta\hat{\xi}. \tag{2.70}$$

Now, a complex modulus

$$\hat{E} = E' + iE'' = |E|e^{i\delta} \tag{2.71}$$

with $E' = E$ and $E'' = \eta\omega$ can be defined, so

$$\hat{\sigma} = \hat{E}\hat{\xi} \tag{2.72}$$

The angle δ provides information of how far the material lags behind the actuation under harmonic excitation. The loss factor is defined as

$$\tan\delta = \frac{\eta\omega}{E} \tag{2.73}$$

and is for dielectric elastomers in the range of a few percent [4].

The loss factor is an important measure for efficiency of the system. The efficiency of a DE can be calculated by the ratio of electrical energy supplied to the DE and mechanical energy received from it.

The electrical energy applied to the actuator per cycle can be calculated considering the DE as capacitor as in Ch.2.1. The capacitance is

$$C = \frac{\epsilon_0 \epsilon A}{d} = \frac{\epsilon_0 \epsilon A_0}{d_0 \lambda^2} \tag{2.74}$$

And the energy is thus

$$U_e = \frac{1}{2} C V^2 = \frac{\epsilon_0 \epsilon A_0 V^2}{2 d_0 \lambda^2} \tag{2.75}$$

For an harmonically driven DEA with viscoelastic effects according to Eq. 2.72 and Eq. 1.1, the electrical energy in the system becomes

$$\hat{U}_e(\omega) = \frac{1}{2} A_0 d_0 \hat{E} \hat{\xi} \tag{2.76}$$

The elastically stored energy is given by

$$\hat{U}_m(\omega) = A_0 d_0 E \hat{\xi}^2 \tag{2.77}$$

And thus, the efficiency becomes

$$\nu = \frac{\int_0^T \frac{\mathrm{d}U_m}{\mathrm{d}t} \mathrm{d}t}{\int_0^T \frac{\mathrm{d}U_e}{\mathrm{d}t} \mathrm{d}t} = \frac{E}{E + i\omega\eta} = \frac{1}{1 + \tan(\delta)} \tag{2.78}$$

So, with an increase of viscosity, the efficiency drops as one would expect.

To model the viscoelastic behaviour of a DE with arbitrary voltage the equation (with $\lambda = 1 - \xi$)

$$\frac{\epsilon \epsilon_0}{E d_0^2} \frac{V(t)^2}{\lambda^2(t)} = \xi(t) + \tau \dot{\xi}(t) \tag{2.79}$$

has to be solved.
A simple method to measure the viscosity of the material is to apply a static stress, switch it off and measure the time of material relaxation. Substituting zero stress yields

$$0 = \xi(t) + \tau \dot{\xi}(t) \tag{2.80}$$

leads to

$$\xi(t) = \xi_0 \cdot e^{-t/\tau} \tag{2.81}$$

with ξ_0 the initial strain under constant voltage.

Determination of viscoelastic properties of the membrane under use is not subject to this thesis. The loss factor is expected to have values of 0.1 %, which is large enough to dampen resonances, but low enough to allow movements at high velocities.

2.3 Sound Radiation

In acoustics engineering, various ways of generating sound exist. Engineers have always been looking for new methods of generating sound in an innovative way. Plasma loudspeakers, thermoacoustic transducers, magnetostatic transducers and many more. The most common types however, transfer the force of an electrostatic, piezoelectric or electromagnetic transducer via a membrane to the surrounding air. In these, the membrane (the coupling element of the transducer to the air) is one of the most crucial part of the system. While being lightweight to decrease the necessary driving force of the transducer it should be rigid enough to accelerate the surrounding mass of air even at high velocities, i.e. at high frequencies. Many manufacturers focus on improving stiffness of the membrane and accepting high membrane masses, as high driving force is easily achieved with large electromagnetic transducers and the price per power of amplifiers has dropped in recent decades [3]. The acoustical efficiency of these systems often reduces below 1 %.
Powerful speaker systems, though being able to generate high pressure amplitudes hence are often far less efficient. Not only the mass of the membrane but also the electronics of such systems decrease the overall efficiency.

For large arrays and portable devices (including headphones) the quest for energy efficient acoustic conversion is still relevant. [3]
Hence, for mobile applications, headphones, car- and aerospace aswell as for applications where a large number of loudspeakers is desired, more efficient technologies are requested.
The presented DE loudspeaker does not focus on membrane stiffness. Instead low membrane weight and low electronic losses are of interest to increase efficiency. Efficiency of DEs are reported to be significantly higher than that of conventional actuators. [18]

In a linear and time-invariant system, the mathematics can be handled in the frequency domain. For convenience the system can be split into two parts. One part for each domain transition.
The deflected membrane, coupled to the air, will emit sound pressure $\hat{p}$ in dependency to its membrane velocity $\hat{v}$. The first transfer function is

$$H_1(\omega) = \frac{\hat{p}}{\hat{v}} \tag{2.82}$$

The driving voltage $\hat{V}$ results in a deflection of the membrane according to a transfer function, which can be expressed in terms of speed in dependency of its driving voltage

$$H_2(\omega) = \frac{\hat{v}}{\hat{V}} \tag{2.83}$$

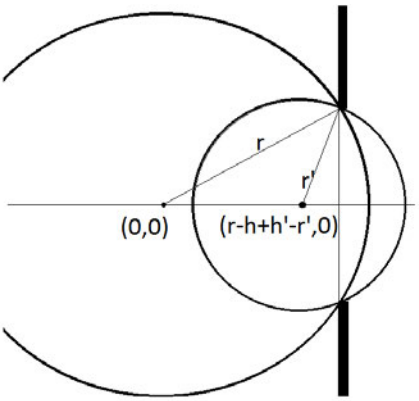

Figure 2.11: Geometry of the membrane, modelled as a ball

The overall frequency response is the product of both

$$H(\omega) = \frac{\hat{p}}{\hat{V}} = H_1(\omega) \cdot H_2(\omega) \tag{2.84}$$

In the following sections, both transfer functions are determined. Last, the results are combined with an estimation of the resonance behaviour to estimate the total frequency response of the system.

2.3.1 Frequency response

For the acoustical model an analytical approach will be used to estimate the frequency response. By calculating the membrane velocity and taking it as the boundary condition for the axial-symmetric wave equation, both the sound field and the frequency response may be calculated.
First, the geometry has to be defined. Assuming the membrane to be perfectly spherical at any times it shall be depicted by a ball vibrating along the x-axis while changing its radius in order to fit though a cavity, see Fig. 2.11. Its shape under bias voltage is then described by

$$\mathbf{x} = \begin{pmatrix} r \cdot \cos(\theta) \\ r \cdot \sin(\theta) \end{pmatrix} \tag{2.85}$$

with $\theta \leq \theta_{max} = \arcsin\left(\frac{R_b}{r}\right)$ and R_b its base radius. (see Fig. 2.6)
By changing the applied voltage, i.e. applying a signal, the centre and the radius of the sphere will change:

$$\mathbf{x} \rightarrow \mathbf{x}' = \begin{pmatrix} r' \cdot \cos(\theta') \\ r' \cdot \sin(\theta') \end{pmatrix} + \begin{pmatrix} (r-h) - (r'-h') \\ 0 \end{pmatrix} \tag{2.86}$$

with h the height of the membrane. Following assumptions are made.

- The stretch is equal everywhere on the sphere, so $\frac{\theta}{\theta_{max}} = \frac{\theta'}{\theta'_{max}} = \text{const.}$

- The radius vibrates harmonically around the bias radius: $r' = r + \hat{r}e^{i\omega t}$

- $\hat{r}$ is small compared to r: $\hat{r} \leqq r$

The velocity can be written as

$$\mathbf{v} = \dot{r}\left[\left(1 - \cos(\theta)\frac{r}{\sqrt{r^2 - R_b^2}}\right)\mathbf{e_r} - \left(\frac{\theta R_b}{\theta_{max}\sqrt{r^2 - R_b^2}} - \sin(\theta)\frac{r}{\sqrt{r^2 - R_B^2}}\right)\mathbf{e}_\theta\right] \tag{2.87}$$

The full derivation is found in the appendix 6.1 This shall be the boundary condition for solving the wave equation in terms of the acoustic potential Φ (with c the sound velocity in air)

$$\frac{1}{c^2}\frac{\partial^2\Phi}{\partial t^2} - \nabla^2\Phi = 0 \tag{2.88}$$

which translates under harmonic vibrations to

$$\begin{aligned} -\frac{\omega^2}{c^2}\Phi - \nabla^2\Phi = 0 \quad \text{or} \\ (k^2 + \nabla^2)\Phi = 0 \end{aligned} \tag{2.89}$$

In an axisymmetric system the solutions are the sum of Hankel functions $H_n^{(1)}(kR)$(representing ingoing waves) und $H_n^{(2)}(kR)$(representing outgoing waves). P_n are the Legendre Polynomials. [3]

$$\Phi = \sum_{n=0}^{\infty}\tilde{\Phi}_n\Big(A_{n+}H_n^{(1)}(kR) + A_{n-}H_n^{(2)}(kR)\Big)P_n(\cos(\theta)) \tag{2.90}$$

Ingoing waves are set zero to simulate the free field, so

$$\Phi = \sum_{n=0}^{\infty}A_nH_n^{(2)}(kR)P_n(\cos(\theta)) \tag{2.91}$$

To find the unknown coefficients A_n the boundary condition has to be met.

$$\mathbf{v} = \boldsymbol{\nabla}\Phi|_{R=r} \tag{2.92}$$

$$\mathbf{v_r} + \mathbf{v}_\theta = \frac{\partial\Phi}{\partial R}\mathbf{e_r} + \frac{1}{R}\frac{\partial\Phi}{\partial\theta}\mathbf{e}_\theta \Big|_{R=r_0} \tag{2.93}$$

Only the radial velocity component is relevant for the sound radiation, hence the governing relation is

$$\dot{r}\left[\left(1 - \cos(\theta)\frac{r}{\sqrt{r^2 - R_b^2}}\right)\right] = \frac{\partial}{\partial R}\sum_{n=0}^{\infty}A_nH_n^{(2)}(kR)P_n(\cos(\theta)) \Big|_{R=r} \tag{2.94}$$

To solve the equation, the orthogonality of the Legendre Polynomials is exploited. Both sides are multiplied by the m$^{\text{th}}$ Legendre Polynomial $P_m(\cos(\theta))$. Integration over the sphere eliminates the sum.
A full calculation and the expression for the A_n are in the appendix 6.2.

For the sake of simplicity the loudspeaker is considered as an acoustic monopole. As the diameter of the transducer is small compared to the acoustic wavelength in the air for the full audible spectrum it is a viable approach. The potential is then given by

$$\Phi = \frac{A}{R} e^{i(\omega t - kR)} \tag{2.95}$$

To calculate the sound pressure, the volume flux is calculated. The volume of the spherical cap is given by

$$Vol = \frac{\pi}{6}(3R_b^2 h + h^3) \tag{2.96}$$

and its time derivative is

$$\frac{\mathrm{d}Vol}{\mathrm{d}t} = Q = \frac{\pi}{6}\left(3R_b^2 \frac{\partial h}{\partial r}\dot{r} + 3h^2 \frac{\partial h}{\partial r}\dot{r}\right) \tag{2.97}$$

with $h = r - \sqrt{r^2 - R_b^2}$ it yields to

$$Q = \frac{\pi}{2}\left(1 - \frac{r}{\sqrt{r^2 - R_b^2}}\right)(R_b^2 + h^2)\dot{r}. \tag{2.98}$$

The displaced volume per time Q has to be equal to the volume flux given by a closed surface integral (sphere) of the sound particle velocity

$$Q = \int_{\mathbb{S}} \vec{v} \cdot \mathrm{d}\vec{S} = \int_{\mathbb{S}} \boldsymbol{\nabla}\Phi \cdot \mathrm{d}\vec{S} = 4\pi A e^{i\omega t} \tag{2.99}$$

The missing coefficient A is easily obtained

$$A = \frac{1}{8}\left(1 - \frac{r}{\sqrt{r^2 - R_b^2}}\right)(R_b^2 + h^2)\dot{r} \cdot e^{-i\omega t} \tag{2.100}$$

And finally the simplified acoustic potential is

$$\Phi = \frac{1}{8R}\left(1 - \frac{r}{\sqrt{r^2 - R_b^2}}\right)(R_b^2 + h^2)\dot{r} \cdot e^{-ikR} \tag{2.101}$$

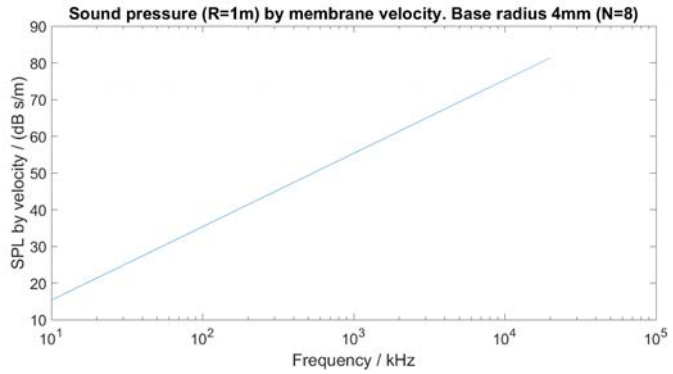

Figure 2.12: Sound pressure level in 1 m distance of the loudspeaker by membrane velocity. (Frequency response of a constant-speed ($1\,\mathrm{m\,s^{-1}}$) driven membrane).

which shall be the basis for further analysis.
The sound pressure is given by the time derivative of the acoustic potential Φ [9]

$$p = -\rho_0 \frac{\partial \Phi}{\partial t} = -i\omega\rho_0\Phi. \tag{2.102}$$

Then the radial impedance at the membrane surface is given by the ratio of pressure and radial velocity at $R = r$

$$Z_0 = \frac{\hat{p}(r,\omega)}{\hat{v}(r,\omega)} = -i\omega\rho_0 \frac{1}{8r}\left(R_b^2 + h^2\right)e^{-ikr} \tag{2.103}$$

Here Eq. 2.87 is used for small angles θ.
This radial impedance can be considered as additional damping for the membrane movement, similar to the viscoelastic damping. [47]
And the transfer function, which calculates the sound pressure in distance $R = 1\,\mathrm{m}$ relative to the membrane velocity, is

$$\begin{aligned} H_1(\omega) &= \frac{p(1\,\mathrm{m},\omega)}{\hat{v}(r,\omega)} = \\ &= -i\omega\rho_0 \frac{1}{8\,\mathrm{m}}\left(R_b^2 + h^2\right)\cdot e^{-ikR} \end{aligned} \tag{2.104}$$

Fig. 2.12 shows the calculated frequency response of the simplified model. The membrane moving with a constant velocity of $1\,\frac{\mathrm{m}}{\mathrm{s}}$ will emit sound as depicted. The curve shows an increase of the SPL with increasing frequency 6 dB/octave.

This model is expected to overestimate the actual sound emission as the membrane will not be in perfect spherical shape. It will rather flatten near the apex of the cap during movement, as the soft material will struggle to displace the surrounding air. But, it serves as useful approx-

imation by means of identifying the speaker clearly as a tweeter.
A numerical model and shape examination using laser vibrometry are ought to be done in future research.

2.3.2 Sound power

To estimate the efficiency of the loudspeaker, which is supposed to be one of the main benefits of DE technology, the sound power is calculated as

$$\begin{aligned} P_{ak} &= \int v \cdot p \, \mathrm{d}A \\ &= 2\pi \int p(1\,\mathrm{m}, \omega) \cdot v(1\,\mathrm{m}, \omega) \, \sin(\theta) \, \mathrm{d}\theta \end{aligned} \tag{2.105}$$

when the area of integration is chosen as a sphere with radius 1 m. The pressure p was calculated in the previous section relative to the membrane velocity as $H_1(\omega)$.
The velocity in 1 m distance can be calculated using the free-field impedance

$$\frac{p}{v} = \rho_0 \cdot c. \tag{2.106}$$

As the loudspeaker only performs well at high frequencies, 1 m can be considered as far-field and the free-field impedance a valid expression [34].
Substituting yields

$$\begin{aligned} P_{ak} &= 2\pi \int \frac{p^2(1\,\mathrm{m}, \omega)}{\rho c} \, \sin(\theta) \, \mathrm{d}\theta \\ &= \frac{4\pi}{\rho_0 c} H_1(\omega)^2 \cdot \hat{v}^2 \end{aligned} \tag{2.107}$$

considering the loudspeaker as an omnidirectional sound source, which was the assumption for the simplified acoustical model.

2.4 Dynamic Response of the Membrane

An accurate dynamic modelling of the non-linear behaviour of a DEA membrane is only possible with numerical approaches as the equations lead to a non-linear inhomogeneous differential equation. This thesis' aim is it to approximate the sound generation of a buckling DEA by means of an analytical model. The governing equations will be linearised and compared with existing studies [10, 20, 44] and with the results of acoustic measurements.

2.4.1 Membrane Frequency Response

Here, a dynamic model of the membrane is derived. For the dynamic modelling of the membrane, Newton's equation of motion is solved in order to obtain the frequency response.

$$A \cdot \sigma_{maxwell} - A \cdot \sigma_{elastic} = F \tag{2.108}$$

The elastic stress is assumed to be linear. As the motion of the membrane will be small compared to the bias-deflection it is a valid approach. F is the sum of the inertia, the air resistance in terms of the acoustic impedance Z_0 and viscous damping in terms of viscosity η. The acoustic impedance was derived in the previous section. The viscoelastic losses are approximated as 0.1 % using the results of [8] for other PDMS materials, as the loss-factor of the utilised *Elastosil 2030* is yet unknown.

$$F = m \cdot \frac{\mathrm{d}^2\mathbf{x}}{\mathrm{d}t^2} + A \cdot (Z_0 + \eta) \cdot \frac{\mathrm{d}\mathbf{x}}{\mathrm{d}t} \tag{2.109}$$

As was seen in 2.3, position and shape of the membrane $\mathbf{x}$ are represented by the surface of a sphere, which can be reduced to only two dimensions.

$$\mathbf{x} \approx r \begin{pmatrix} \cos\theta \\ \sin\theta \end{pmatrix} \quad \text{with} \quad \theta < \theta_{max} \tag{2.110}$$

As all forces are assumed to act along the radial direction, vectorial elements are reduced and the equation becomes one-dimensional. As can be seen from Eq. 2.87, the radial velocity of the membrane has to be adjusted by a factor dependent on the angle θ. For small angles, that is for membrane radii much larger than R_b, θ can be considered as zero and the correction factor becomes constant. With r the radius of the sphere under bias-voltage, radial velocity and acceleration become

$$\dot{\mathbf{x}} = \dot{r} \cdot \left(1 - \frac{r}{\sqrt{r^2 - R_b^2}}\right) \tag{2.111}$$

$$\ddot{\mathbf{x}} = \ddot{r} \cdot \left(1 - \frac{r}{\sqrt{r^2 - R_b^2}}\right) \tag{2.112}$$

For clearer synopsis, the factor is left out and will be added again later on.
Substituting into 2.109, together with 1.2, 1.1 and the geometrical relation

$$\lambda_{act} = \frac{\lambda}{\lambda_{pre}} = \frac{R_b^2 + h_0^2}{R_b^2 + h^2} \tag{2.113}$$

yields to to an inhomogeneous 2$^{\text{nd}}$ order non-linear differential equation for an actuator consisting of N layers. With a passive layer at the bottom, the first term representing the electrostatic

attraction reduces by 1.

$$\begin{aligned}(N-1)\cdot A\cdot\epsilon_0\epsilon\frac{V^2}{\lambda_{act}^2 d_0^2}+N\cdot A\cdot E(\lambda_{act}-1)-N\cdot m\ddot{r}-A(Z_0+N\cdot\eta)\cdot\dot{r}=0\\ \frac{N-1}{N}\cdot\epsilon_0\epsilon\frac{V^2}{d_0^2}+E(\lambda_{act}^3-\lambda_{act}^2)-\lambda_{act}^3 d_0\rho\cdot\ddot{r}-\lambda_{act}^2(\frac{Z_0}{N}+\eta)\cdot\dot{r}=0\\ \frac{N-1}{N}\cdot\epsilon_0\epsilon\frac{V^2}{d_0^2}+\lambda_{act}^3(E-d_0\rho\cdot\ddot{r})-\lambda_{act}^2\left((E+\frac{Z_0}{N}+\eta)\cdot\dot{r}\right)=0,\end{aligned}\tag{2.114}$$

To linearise the equation, a series expansion of λ_3^n at $r=r_0$ is conducted.

$$\lambda_{act}^n\approx\alpha_n+\beta_n\int\hat{r}e^{i\omega t}\mathrm{d}\omega\tag{2.115}$$

substituting yields

$$\begin{aligned}\frac{N-1}{N}\epsilon_0\epsilon\frac{V^2}{d_0^2}+&\left(\alpha_3+\beta_3\int\hat{r}e^{i\omega t}\mathrm{d}\omega\right)\left(E+d_0\rho\cdot\omega^2\int\hat{r}e^{i\omega t}\mathrm{d}\omega\right)\\ &-\left(\alpha_2+\beta_2\int\hat{r}e^{i\omega t}\mathrm{d}\omega\right)\left(E+i\omega(\frac{Z_0}{N}+\eta)\int\hat{r}e^{i\omega t}\mathrm{d}\omega\right)\\ &=0\end{aligned}\tag{2.116}$$

Let the voltage be given by $V=V_{bias}+\int\hat{V}(\omega)e^{i\omega t}\,\mathrm{d}\omega$, whereas $\frac{N-1}{N}\frac{\epsilon_0\epsilon}{d_0^2}V_{bias}^2=(\alpha_2-\alpha_3)E$, then

$$\begin{aligned}\frac{N-1}{N}\frac{\epsilon_0\epsilon}{d_0^2}&\left(2V_{bias}\int\hat{V}(\omega)e^{i\omega t}\mathrm{d}\omega+\left(\int\hat{V}(\omega)e^{i\omega t}\mathrm{d}\omega\right)^2\right)=\\ &=\left[(\beta_2-\beta_3)E-\alpha_3 d_0\rho\omega^2+\alpha_2(\frac{Z_0}{N}+\eta)i\omega\right]\int\hat{r}(\omega)e^{i\omega t}\mathrm{d}\omega\\ &+\left[\beta_2(\frac{Z_0}{N}+\nu)i\omega-\beta_3 d_0\rho\omega^2\right]\left(\int\hat{r}(\omega)e^{i\omega t}\mathrm{d}\omega\right)^2.\end{aligned}\tag{2.117}$$

Making use of the convolution theorem, integrals can be reduced.

$$\begin{aligned}\frac{N-1}{N}\frac{\epsilon_0\epsilon}{d_0^2}&\left(2V_{bias}+\left(\int\hat{V}(\xi)e^{i\xi t}\mathrm{d}\xi\right)\right)\hat{V}(\omega)=\\ &=\left[(\beta_2-\beta_3)E-\alpha_3 d_0\rho\omega^2+\alpha_2(\frac{Z_0}{N}+\eta)i\omega\right]\hat{r}(\omega)\\ &+\left[\beta_2(\frac{Z_0}{N}+\nu)i\omega-\beta_3 d_0\rho\omega^2\right]\left(\int\hat{r}(\xi)e^{i\xi t}\mathrm{d}\xi\right)\hat{r}(\omega)\end{aligned}\tag{2.118}$$

The relation has to be fulfilled for all times t. Assuming there is a moment in time for all frequencies where both, $\int\hat{V}(\xi)e^{i\xi t}\mathrm{d}\xi$ and $\int\hat{r}(\xi)e^{i\xi t}\mathrm{d}\xi$ are zero (e.g. in infinity after the signal has been turned off), the second terms in both sides of the equations vanish and the transfer function is calculated under consideration of the velocity correction factor which was dropped

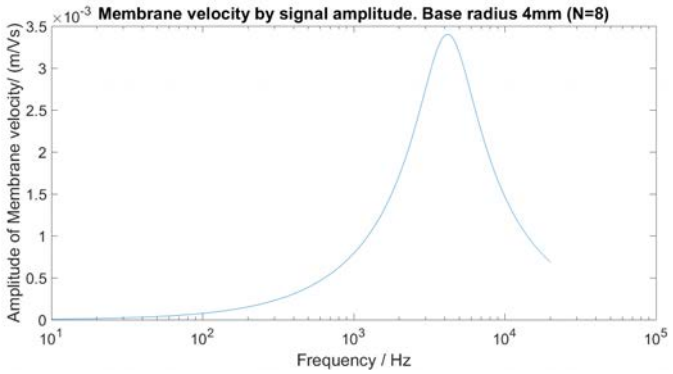

Figure 2.13: Membrane response with 2 kV applied bias voltage and 1 V signal voltage, mechanical loss of 0.1 %, density of the material $\rho = 1050\,\frac{\mathrm{kg}}{\mathrm{m}^3}$ and elastic modulus of $E = 1.2\,\mathrm{MPa}$.

earlier, by

$$\begin{aligned} H_2(\omega) = \frac{\hat{v}(\omega)}{\hat{V}(\omega)} = \frac{i\omega\hat{r}(\omega)}{\hat{V}(\omega)} \cdot \left(1 - \frac{r}{\sqrt{r^2 - R_b^2}}\right) = \\ = 2\epsilon_0\epsilon \frac{N-1}{N} \frac{V_{bias}}{d_0^2} \frac{i\omega}{(\beta_2 - \beta_3)E - \alpha_3 d_0 \rho\omega^2 + \alpha_2(\frac{Z_0}{N} + \eta)i\omega} \cdot \left(1 - \frac{r}{\sqrt{r^2 - R_b^2}}\right). \end{aligned} \tag{2.119}$$

Fig. 2.13 shows membrane velocity per applied voltage amplitude over the frequency. For a signal voltage of 1 V the velocity of the membrane is about $3.5\,\mathrm{mm\,s^{-1}}$ for frequencies close to its resonance.
The umber of layers barely affects the membrane velocity. The term $\frac{Z_0}{N} + \eta$ does not change much by varying amount of layers, as viscoelastic losses are orders of magnitude higher than the acoustic impedance. For other materials this might be different.
A clear resonance peak is found at 4.1 kHz. Higher values for viscoelastic losses dampen the resonance.

Compared to existing studies of dynamic DE membranes the equation seems valid. In his paper, Rosset et. al. [44] studies the behaviour of a buckling dielectric elastomer actuator made of silicone. The actuator has a diameter of only 2 mm. Though a different setup with ion-implanted electrodes was used, it may serve as comparison. Fig. 2.14 shows the measured response from literature and the modelled curve for the BDEA of this work. Up to a specific frequency, both curves are flat op to a specific resonance frequency, have a peak and then drop rapidly. Height of the peak decreases with increasing loss-factor.
Measured data suspect a small peak at the 2$^{\mathrm{nd}}$ natural frequency and a peak at the first subharmonic [44]. Fig. 2.14a shows the dynamic behaviour of the membrane. A resonance frequency of 1350 Hz is observed, which is very similar to the observed peak in Fig. 1.12 as well as in Fig. 1.5a and suggests good validity. As Heydt et al [15] found out, the frequency response of a silicone

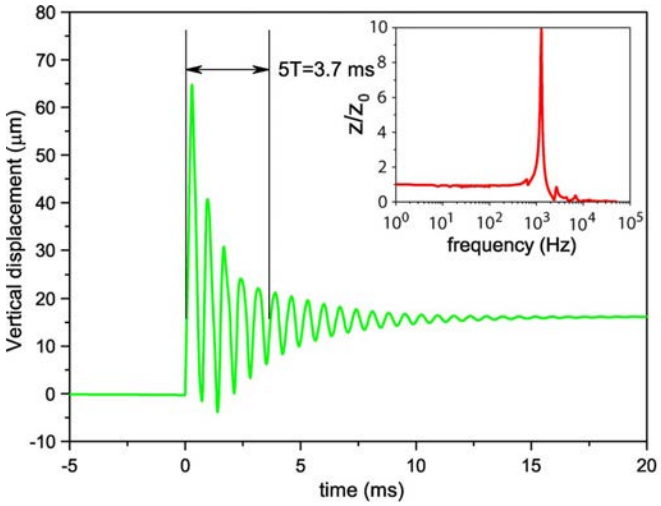

(a) Response of a circular buckling silicone actuator on a 700 V step signal. [44]

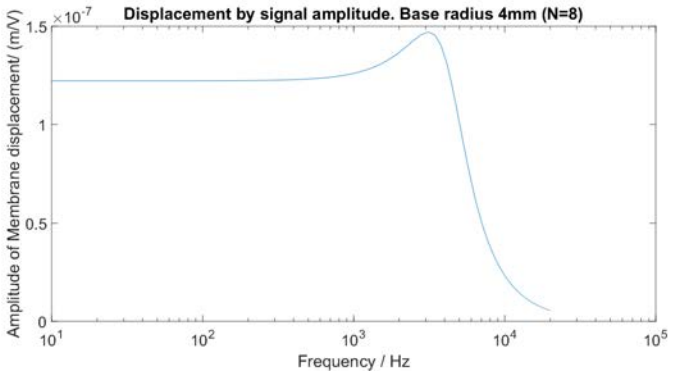

(b) Expected displacement-response of the BDEA of this thesis

Figure 2.14: Comparison of membrane response found in literature with the derived model.

DE loudspeaker is almost linear up from the mechanical resonance frequency.

The linearised equation is only a rough estimation of the membrane response. It is only valid for signal voltages small compared to the bis voltage.

2.4.2 Resonance Frequencies

The multilayer buckling actuators can be considered as an array of non-linearly-coupled parametric oscillators with each layer regarded as one oscillator subject to the non-linear driving force $\propto V^2$. [60]
As result of the quadratic excitation and the non-linear coupling, sub- and super-harmonic resonances occur [59].
That means, that for an excitation frequency Ω the oscillator will also show vibrations at frequencies $M \cdot \omega_0$ with M integers or inverses of integers and ω_0 the natural frequency.
Natural frequencies in comb-drive microcantilevers are given by

$$\omega_i = \sqrt{1 - 8Q \sin^2\left(\frac{i\pi}{2(N+1)}\right)}\omega_0 \tag{2.120}$$

with $Q = \frac{\epsilon\epsilon_0 A_0 V_{bias}^2}{2d_0^3 Y}$ and $\frac{\omega_0}{2\pi} \approx 4.1\,\text{kHz}$ the fundamental frequency (see Fig.2.13). [59]
If the frequency of excitation Ω, given by a signal $V = V_{bias} + \hat{V} \cdot \cos(\Omega t)$, is close to $2\frac{\omega_i}{j}$ $(i, j \in \mathbb{N})$, the system will resonate at frequencies ω_i.
Fig.2.15 shows the measured displacement of a circular DE membrane for a broad frequency range. High displacements are achieved at frequencies ω_i, but also at frequencies $\frac{\omega_0}{2}$ and $2\omega_0$, i.e. sub- and superharmonics. Vibrations in frequencies different from the excitation frequency contribute to the total harmonic distortion of loudspeaker. Hence, the total harmonic distortion (THD) is expected to have peaks at frequencies $\Omega = 2\omega_0$ and at $\Omega = \frac{\omega_0}{2}$.

Besides of the previously determined resonance frequency of $\sim$4.1 kHz, other natural frequencies in Eq.2.120 and its sub- and superharmonics, the geometry of the problem leads to infinitely many resonances. At high frequencies the movement of the membrane will decay in several modal patterns, leading to peaks and dips in the frequency response.
Oscillations of a circular membrane are a well studied problem. Similar to Eq. 2.43, the dynamic behaviour of a vibrating membrane is described by

$$D\Delta^2 w + \rho\frac{\partial^2 w}{\partial t^2} = 0. \tag{2.121}$$

Here, ρ is the mass per unit area [26]. Solutions for sinusoidal vibrations are given by

$$\hat{w}(k) = [A_n J_n(kr) + B_n I_n(kr)]\cos(n\phi), \tag{2.122}$$

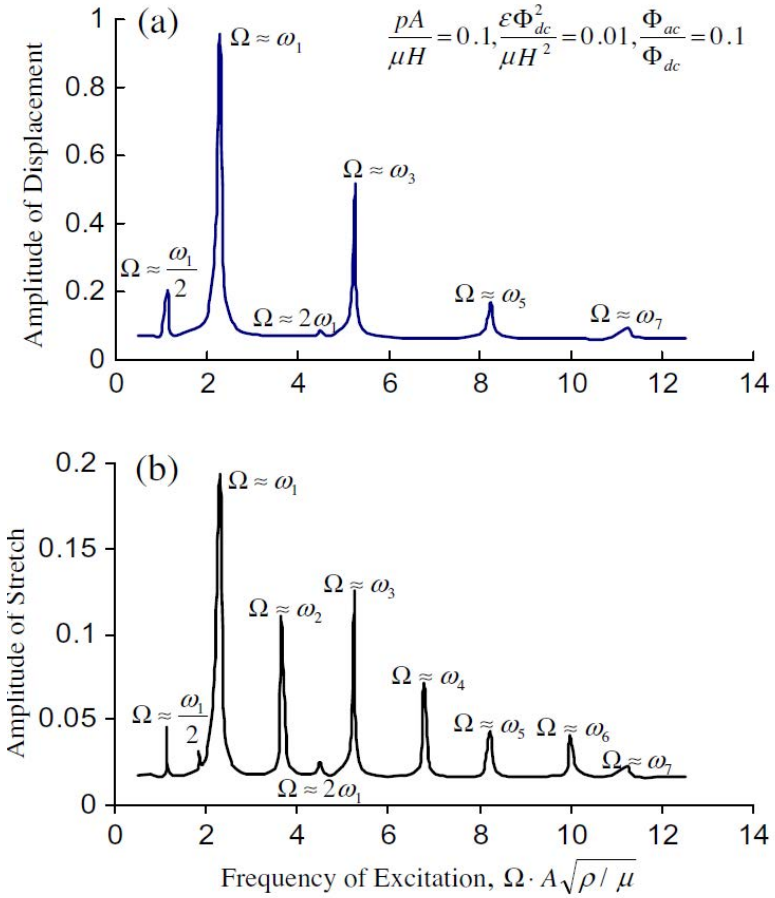

Figure 2.15: Displacements and stretches of a circular stretched DE membrane [60]. Resonances at natural frequencies ω_i as well as sub- and superharmonics. With A radius of the membrane, H its thickness, μ its shear modulus and ρ the density of the material.

s	n=0	n=1	n=2	n=3	n=4
1	3,196	4,611	5,906	7,144	8,347
2	6,306	7,800	9,197	10,54	11,84
3	9,439	10,96	12,40	13,80	15,15
4	12,58	14,11	15,58	17,01	18,40
5	15,72	17,26	18,74	20,19	
6	18,86	20,40			

Table 2.1: Values for κ from Eq. 2.125 to determinde resonance frequencies $\kappa^2 = \omega R_b^2 \sqrt{\rho/D}$

with J_n Bessel function of the first kind and I_n the modified Bessel function of the first kind [26]. Here, n represents the number of nodal lines as can be seen from the cos-term. Higher number of nodal lines will split the membrane into areas of upward and downward movement. Consequence will be drops in the frequency response as opposed movement will cancel air movement out. With the same boundary conditions as in the static case for a clamped membrane it yields to

$$\frac{A_n}{B_n} = -\frac{I_n(\kappa)}{J_n(\kappa)} \tag{2.123}$$

with $\kappa^2 = \omega R_b^2 \sqrt{\rho/D}$ [26]. So, the modal shapes are given by

$$\hat{w}(\kappa) = A_n \left[A_n J_n(kr) - \frac{J_n(\kappa)}{I_n(\kappa)} I_n(kr) \right] \cos(n\phi) \tag{2.124}$$

The values of κ are obtained by solving

$$J_n(\kappa) I_{n+1}(\kappa) + I_n(\kappa) J_{n+1}(\kappa) = 0 \tag{2.125}$$

and are listed in Tab.2.1 The lowest resonance frequency for the 8-layered actuator would be 458 Hz. As argued before, no sound generation is expected at such low frequencies, hence the first audible peaks in the spectrum are expected to be at 953 Hz and 1.56 kHz corresponding to the ($n = 1$, $s = 1$)- and($2 = 0$, $s = 1$)-modes, respectively.

2.5 Complete System

With the results of the previous sections, the overall performance is approximated. The frequency response is obtained by both transfer functions H_1 and H_2. Last, the efficiency of the actuator is calculated, as it is supposed to be one of the major advantages of DE-technology.

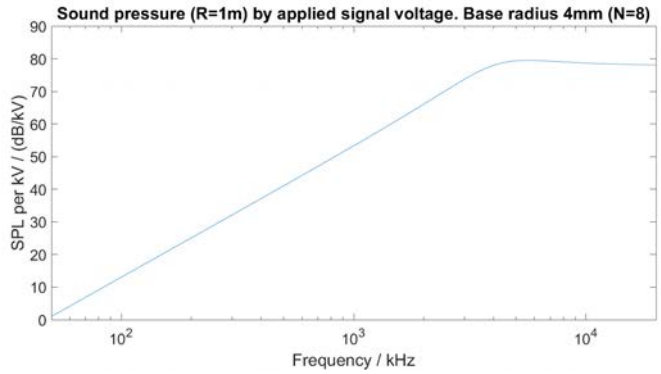

Figure 2.16: Frequency response of the experimental loudspeaker per kV of applied signal voltage.

2.5.1 Frequency response

Now, both transfer functions have been determined and it is possible to estimate the total sound output of the system by

$$H(\omega) = \frac{\hat{v}(\omega)}{\hat{V}(\omega)} \cdot \frac{\hat{p}(\omega)}{\hat{v}(\omega)} = \frac{\hat{p}(\omega)}{\hat{V}(\omega)} \tag{2.126}$$

Fig. 2.16 shows the estimated acoustic frequency response of the actuator. Viscoelastic losses are set to 0.1 % , density of air to $\rho_0 = 1.2\,\frac{\mathrm{kg}}{\mathrm{m}^3}$ and of silicone to $\rho = 1050\,\frac{\mathrm{kg}}{\mathrm{m}^3}$. The bias voltage is set to 2 kV.
The available audio amplifier to drive the unit supplies a signal voltage of up to 400 V. The level at 1 kHz will therefore be at about 45 dB [SPL] (−8 dB).
At ∼5 kHz the response reaches its maximum of almost $80\,\mathrm{dB\,kV^{-1}}$.
At high frequencies membrane movement decays into partial oscillations (see previous section) and the actual frequency response is expected to hold several peaks and dips.

For frequencies below 500 Hz no sound output is expected. With increasing frequency, SPL increases by ∼18 dB/octave. Low SPL for low frequencies is due to low membrane velocity (see Fig. 2.13) and low acoustic impedance (see Fig. 2.12).
For playback of music, the frequency range should be expanded into lower frequency domains. This may be achieved by increasing membrane mass (number of layers or other material), using thicker foil, increasing diameter or by using a material with lower elastic modulus E.

Non-linear behaviour has been widely ignored, as the transfer function is linearised

2.5.2 Efficiency

The overall acoustical efficiency ν is calculated by the ratio of supplied electrical power and the generated sound power.

Following from Eqs. 2.104,2.119 and 2.17 the efficiency is

$$\begin{aligned}\nu(\omega) &= \frac{P_{\mathrm{ak}}(\omega)}{P_{\mathrm{el}}(\omega)} \\ &= \frac{4\pi}{\rho_0 c} H_1^2(\omega) \cdot H_2^2(\omega) \cdot \frac{\hat{V}^2}{P_{\mathrm{el}}} \\ &= \frac{4\pi}{\rho_0 c} H_1^2(\omega) \cdot H_2^2(\omega) \cdot \frac{R_{\mathrm{S}}}{N}.\end{aligned} \tag{2.127}$$

And is below $\sim$1 % (assuming R_S again as in the range of 100 kΩ, $N = 8$), which is common for loudspeakers [3]. From this point of view the DE technology is not necessarily advantageous to conventional drivers. The benefits of being extraordinarily lightweight, easy to manufacture and scalable remain.

The equation, of course, is only valid under the assumptions made before. That is, electrode resistance far lower than isolating resistance of the dielectric $R_S << R_L$, high frequencies $f >> 100\,\mathrm{Hz}$ (see Section 2.1), and voltage amplitude lower than bias-voltage, so that H_2 is a valid linearisation.

Chapter 3

Experiments

After the proper concept of buckling dielectric elastomer actuators was found, static and acoustic measurements are conducted.
First, development and assembly of the loudspeaker is described, followed by a description of the experimental setup.

3.1 Preliminary Tests

The initial goal of the thesis was to develop a small scale buckling DEA for loudspeakers. Different actuator sizes with different membrane thicknesses were planned to be compared.
After frames for different actuator sizes were designed in *Solidworks* and 3D-printed using the *Ultimaker* 2^{Go} 3D-printer, experiments to figure out the optimal electrode mix were performed.

The electrode (ELASTOSIL LR 3162) was provided by *Wacker*. Following the manufacturing guide, two pasty-like components A and B are mixed with ratio 1:1. The mixture is then blended with an amount of volatile silicone (BELSIL DM 1 PLUS) to attain viscosity suitable for spraying onto the silicone foil. BELSIL is a silicone solvent which, upon spraying, dissolves the surface of the membrane. It allows the conducting carbon particles of A and B of the mixture to blend onto the membrane, creating an abrasion resistant, stretchable electrode with good conductivity even under stretch.

Results of earlier projects at the institute recommended a ratio of 1:1:40. Unfortunately this ratio did not perform well. The large amount of BELSIL broke the surface tension of the membrane and wrinkles formed during spraying. Gradually reducing the amount of BELSIL until a ratio of 2:2:40 showed inreasing performance. This ratio, while still suitable for spraying, did not corrode the membrane much and further allowed quick curing of the electrode.

Figure 3.1: Experimental buckling DEA with membrane thickness of 50 µm with 3 kV supplied voltage. One large electrode was expected to buckle-up through the 5 mm wide cavities. The deformation could not be assumed as spherical.

Next, different masking techniques were tested. First experiments were conducted using rigid 3D-printed PLA masks. Bad connection of mask and membrane lead to imprecise edges and big margins of the electrode. Better results were achieved using the carrier foil, on which the membranes were attached.

Carpi et al. [6] presented a buckling dielectric elastomer actuator with a diameter of 30 mm using a membrane with thickness 500 µm.
Many attempts of reproducing a downscaled version (5:2, 3:1, 5:1, 10:1) of a buckling dielectric elastomer actuator with the provided membrane thicknesses of 20 µm, 50 µm, 100 µm and 200 µm failed. Even with small diameters of the actuator, uncontrolled wrinkles formed (see Fig. 3.1), whereas the thicker membranes did not show any notable deformation at all. Therefore, the concept of a downscaled single layer actuator was dropped.

Eventually a multilayer actuator consisting of 3 to 8 membrane layers (50 µm thick) and a diameter of 8 mm showed the desired spherical deformation and provided audible sound generation down to frequencies of ∼500 Hz.

3.2 Fabrication

Fabrication of the loudspeaker elements consists of two steps. First the multi-layered membranes have to be produced.
The stacked membranes are then assembled into the 3D-printed frame.
Using 3D printer technology allowed quick prototyping and several concepts were tested before the final concept was devised.
In the following each step of fabrications is explained.

3.2.1 Multilayer Film Fabrication

A semi-automatic fabrication process allows to produce multilayer DE actors of high quality with very small variations. The produced membrane stacks have an active area of 8 mm × 8 mm. [29]

Within the development of multilayer actors, an automated dry deposition manufacturing sequential process was developed. Aim of the process is to automatically produce 192-layered stack actuators. The process uses prefabricated silicone films (Elastosil 2030 50 µm) by Wacker and is subdivided into six sub-processes.
The elastomer is delivered on rolls. The first step is to remove the film from the protective sheet and the carrier foil. A vacuum roller is used to avoid mechanical loading of the membrane in the process. The vacuum roller is a roll of porous material with negative pressure inside (see Fig. 3.2).
The film is then laminated on a vacuum folding table (see Fig. 3.3) by applying positive pressure in the roller and negative pressure in the table of the same porous material. A hot wire cutter is used to cut off the film. Once the film is placed on the vacuum folding table, the spraying mask is arranged above the film. Electrode (ELASTOSIL LR 3162) is sprayed in thin layers (4 µm to 5 µm) on the film. The cut-off membrane is large enough to contain 8 segments of 24 electrodes (active area: 8 mm × 8 mm) each.
Before the electrode is cured, the films are folded. The process is repeated until 8 layers of film and electrode are fabricated.
24 functioning actuators with 8 layers are ready to use after the electrode is cured.
A full overview of the fabrication facility is depicted in Fig. 3.4. For the multilayer buckling actuators the process ends here, as the maximum tested number of layers is 8. With this process, 24 samples of multilayer membranes for this work are automatically fabricated.

The purpose of the facility is to fabricate stack actuators of 192 layers.
To achieve this, the stacked segment is cut by an ultrasonic knife in 24 pieces and stacked by a vacuum gripper.

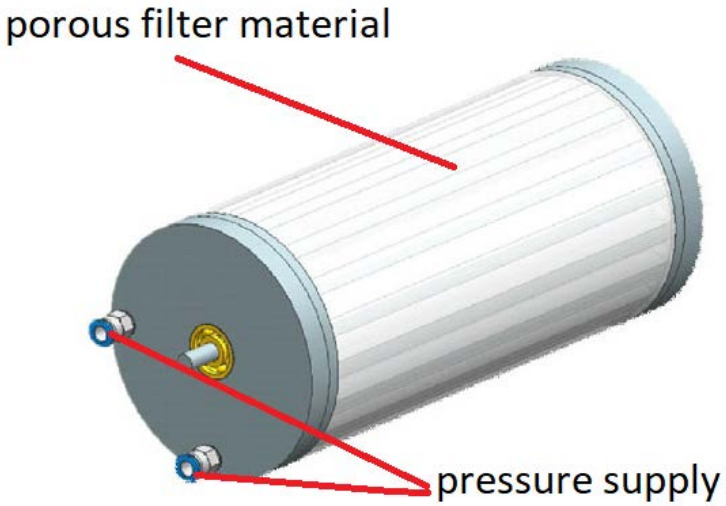

Figure 3.2: Vaccum roller to separate the film from the roll and to place it on the table [29]

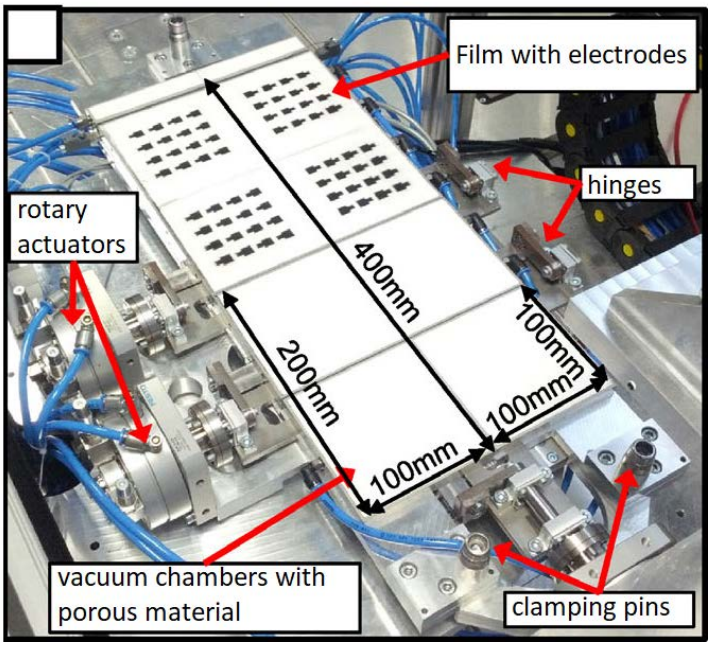

Figure 3.3: Vacuum folding table used to produce 8 layered actuators [29]

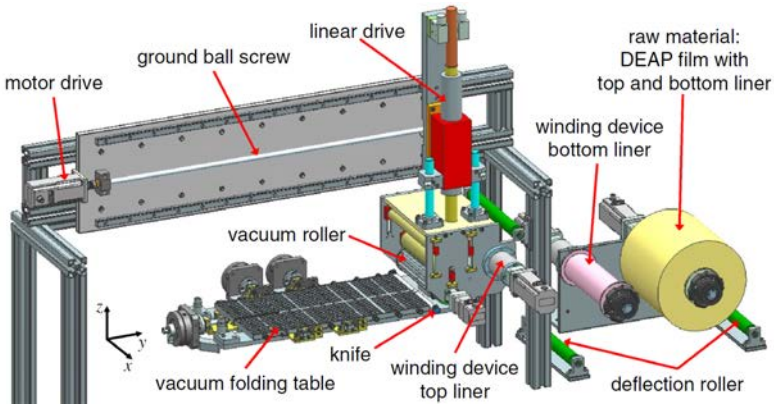

Figure 3.4: Sketch of the automatic multilayer production facility. [29]

Contacting is done using a contacting film. Last step is to encapsulate the stack actuator using the same elastomer. [29]

To build samples of BDEA with different amount of layers (3-8 layers are tested), layers are carefully removed subsequently. If electrode material was damaged in this process, additional spraying is needed to cover up.

3.2.2 Actuator Assembly

Fig. 3.6 shows a technical drawing of the frame. To assemble the multi-layered membrane into the frame, double sided adhesive tape is used. The membrane is not subject to any prestretch as it would decrease actuating capabilities [6]. Clamped between conducting copper tape and placed in the frame, the actuator is ready.
Fig. 3.7 shows the step-by-step assembly of the actuator. Post-treatment of the 3D-printed frame involves polishing the surface. Height of rigid cap support decreases slightly in the process.
A cavity (1 mm wide) at the centre of the rigid cap accounts for the pressure compensation, so the membrane may move freely without working against compressed air.

For better connection of the conducting copper tape, the actuator is frayed at the support region. Tightly clamped between copper tape, it is ensured that all layers are connected to the power supply.
Another tested method for connection was to pierce a wire through the membrane. Randomly occurring discharges from the wire to the membrane lead to highly non linear behaviour. Upon ramping up the voltage cracking sounds indicated sudden deformations. Measurements with a high precision laser confirmed the audible examination (see Fig. 3.5).
As the actuator assembly is very simple, an automatic fabrication process might be installed in the future. Together with an automatic fabrication process of multilayer membranes, which is

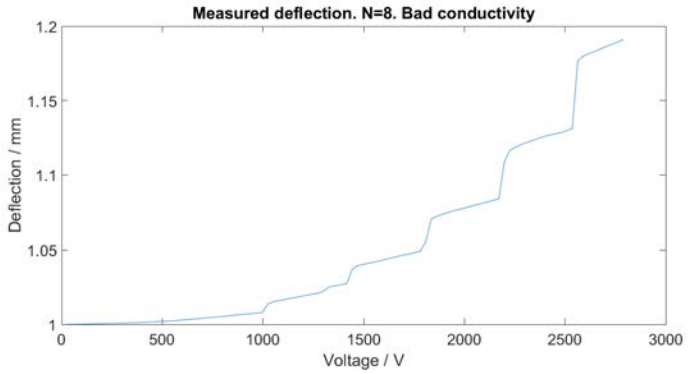

Figure 3.5: Sample with bad conductivity, where randomly occurring discharges led to erratic deflection changes during linear voltage ramping.

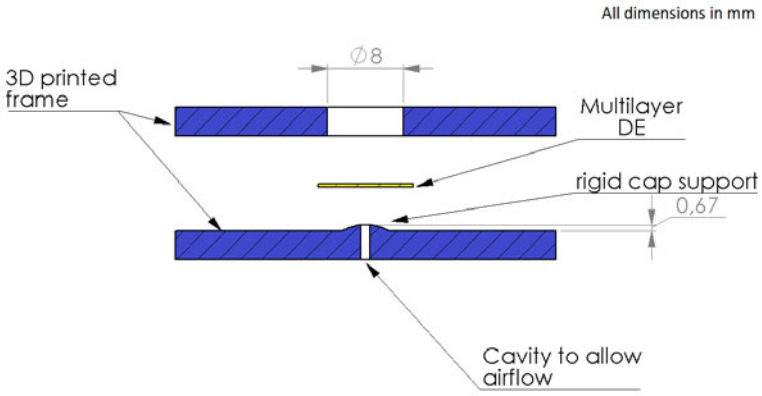

Figure 3.6: Technical drawing of the actuator. Total width is 40 mm. Frame is screwed together (M4 screws) for maximum stability.

subject to research at *FG Elektromechanische Konstruktion*, full-automatic production of loudspeakers seems to be possible in near future. In contrast to conventional electrodynamic loudspeakers the DE technology might offer extraordinarily low production costs.
The finished actuator is depicted in Fig. 3.8.

3.3 Static Deflection

Measurements of the static deflection are conducted in order to proof the static model of the membrane and to determine the Young's modulus E of dielectric elastomer.
For measurements of the deflection under static load, an automated process with *Simulink* and the *dSpace* micro-controller was implemented. Measurements are performed using a high-precision laser rangefinder (*Mirco-Epsilon optoNCDT*).
A laptop is used to run the micro-controller, which is connected to the high-voltage amplifier

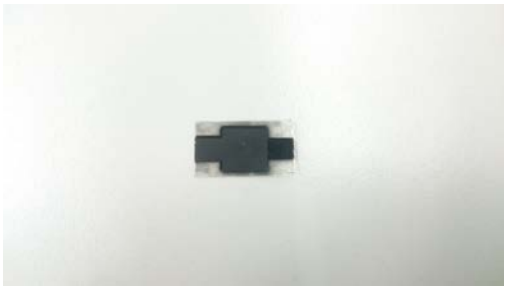

(a) Multilayer Membrane consisting of 8 layers with 8 electrodes. The bottom layer is a passive layer

(b) Double sided adhesive tape fixes the membrane in the boundary ring of 8 mm diameter.

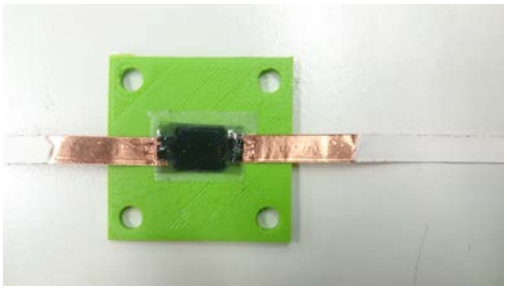

(c) Conductive copper tape is placed on the frame. Supply region of the actuator is frayed to ensure conductivity

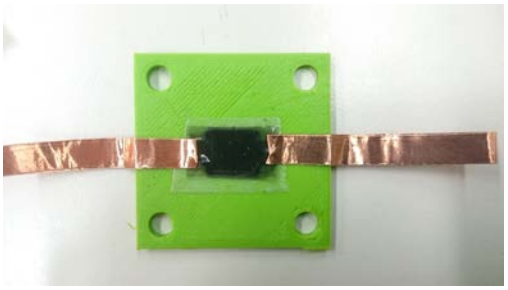

(d) Membrane is sandwiched between the adhesive copper tape and clamped into the frame.

Figure 3.7: Step-by-step assembly of the loudspeaker

Figure 3.8: The finished actuator

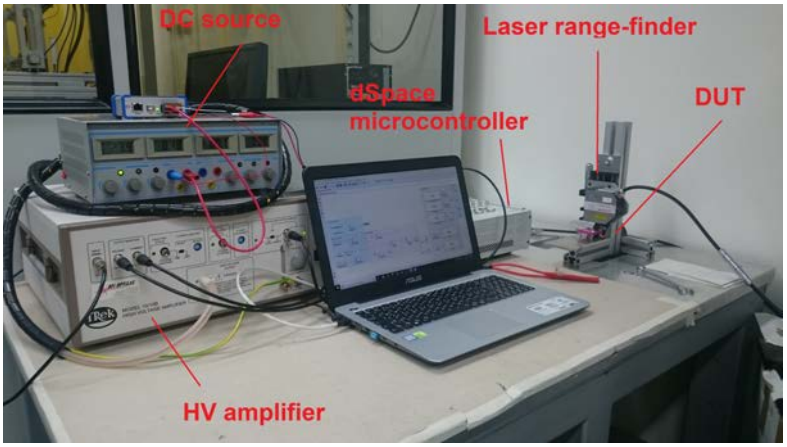

Figure 3.9: Setup for the static measurement

and the laser range-finder, measuring applied voltage, current and deflection of the membrane simultaneously, see Fig. 3.9.
The *dSpace*-microcontroller is able to provide an outgoing voltage of 0 V to 10 V, while the amplifier amplifies the input voltage by a fixed factor of 1000, so the necessary voltage of 0 V to 3000 V is easily achieved.

The BDE-sample is manually positioned below the laser leading to potential errors, as it is possibly not exactly centred.
The sample is connected to the amplifier, using clamps attached to the copper tape contacts.

First the initial height h_0 of each sample is measured to accurately calculate the strains from the membrane deflection.
During measurement, the voltage is ramped up from 0 V to 2800 V over a period of 20 s. A close-up view of the rangefinder and the BDE-sample is depicted in Fig. 3.10

3.4 Frequency Response

Acoustic measurements are conducted in the anechoic room of the *Institut für Strömungsmechanik und Technische Akustik*. It has a volume of 1070 m^3 and a lower cut-off frequency of 63 Hz. Below that cut-off frequency, measurements might be prone to noise.
The room is equipped with a net to walk on, so bottom reflections are eliminated.

The device under test is placed on a sound baffle so sound is emitted in the half-space above the speaker. The baffle rests on a foam mat. (see Fig. 3.11)
The microphone is located in 0.5 m distance above the DUT. Sound radiation in the half space

Figure 3.10: Close-up view of the sample under test.

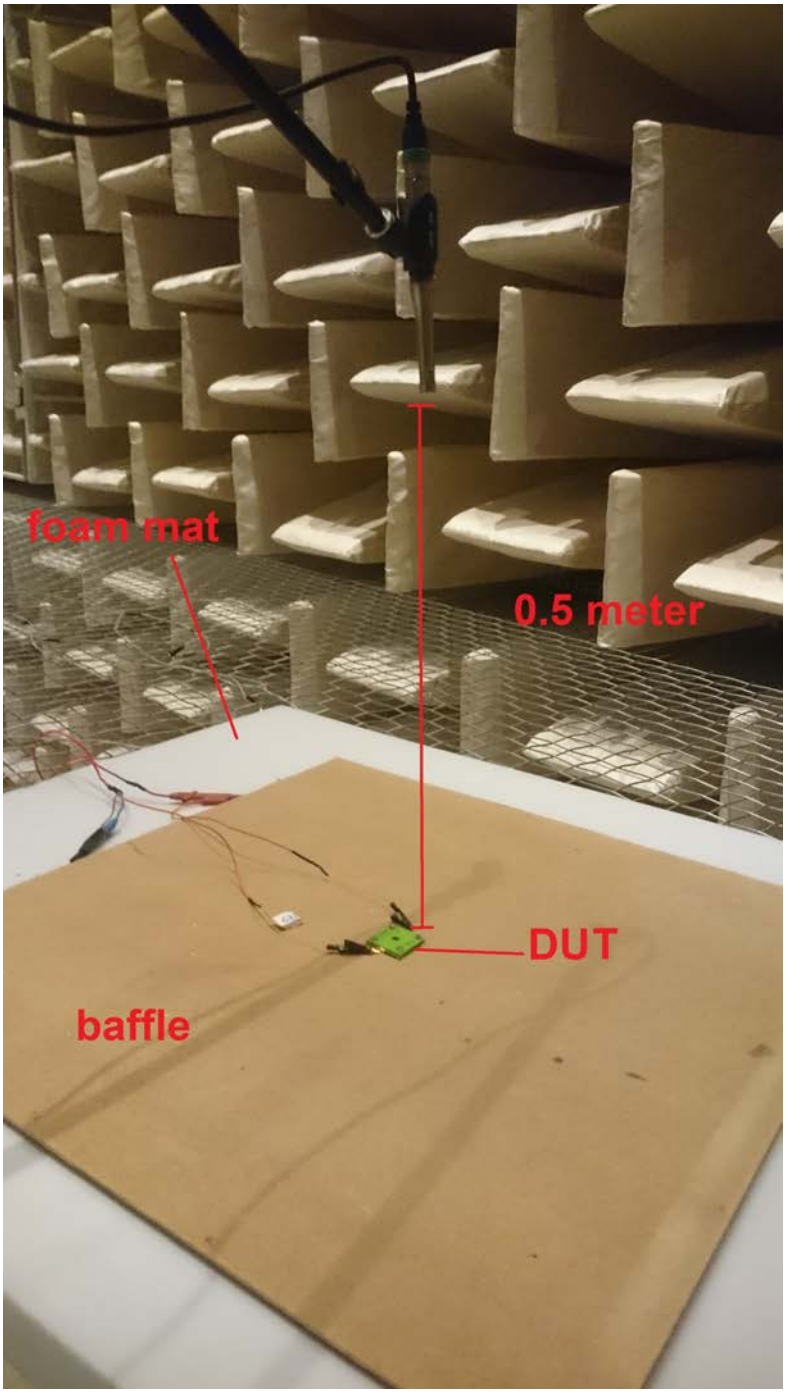

Figure 3.11: Acoustic measurement of the loudspeaker in the anechoic room of TU Berlin

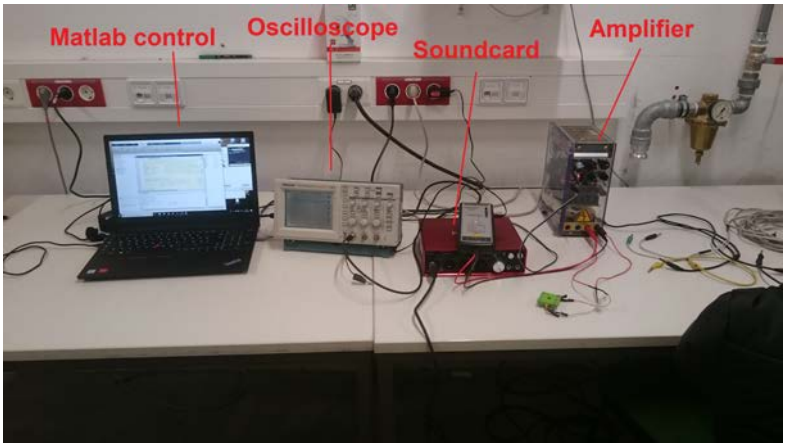

Figure 3.12: Hardware setup outside the anechoic room during the measurement of the frequency response

Device	Model
Sound card	Focusrite Scarlett 18i8
Microphone and Preamp	NTI M2230 and NTI MA220
Amplifier	Custom build
Software	AKtools-library for MatLab

Table 3.1: Equipment used for the measurement of the frequency response

(+6 dB) plus microphone distance of 0.5 m (+6 dB) result in a measured sound pressure level 12 dB higher than the modelled SPL, which is calculated for free space in 1 m distance.
The baffle is designed large enough to not affect the measurement with edge reflections for frequencies higher than 500 Hz, which is the expected operating range of the loudspeaker.

The test facility provides a cable management system, so all electronics (sound card, amplifier, PC, etc.) can be outside the anechoic room and noise can be reduced (see Fig. 3.12). The software library *AKtools* for audio measurements is provided by *Fachgebiet Audiokommunikation* and offers the possibility to measure various acoustic parameters using Matlab.
To observe the test signal during measurement, an oscilloscope is connected in parallel to the loudspeaker. A voltage divider (1/1000) is linked to the oscilloscope, to handle the high voltages. The flowchart depicting the setup is seen in Fig. 3.13
The amplifier provides a fixed bias-voltage of 2 kV and a maximum signal amplitude of 400 V. As test signal for measurement of the frequency response a logarithmic sweep with a sampling frequency of 44 100 Hz is used. The generated sweep has 2^{20} samples and thus, lasts 23.8 s. Signal amplitude is set to the maximum possible 400 V.

A frequency response measurement of the amplifier as reference is conducted in the same manner.

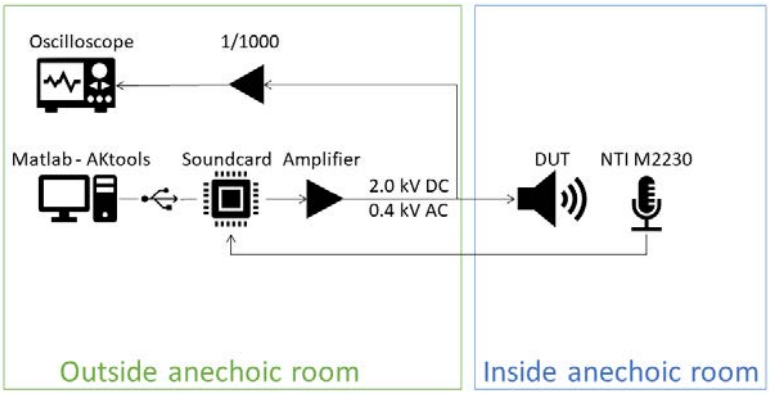

Figure 3.13: Flowchart of acoustic measurements

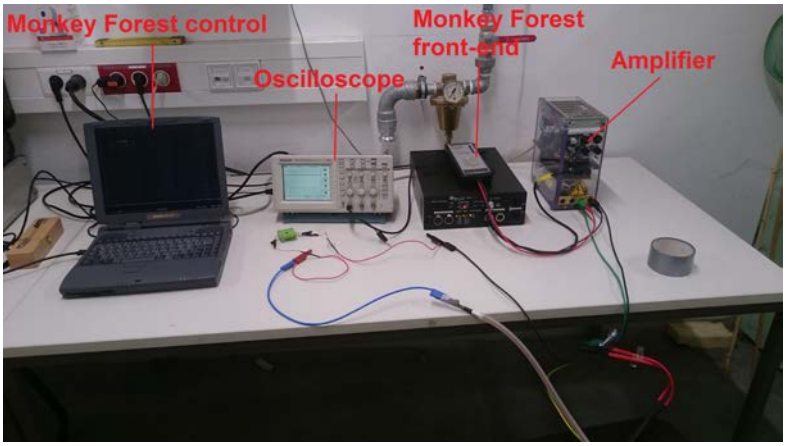

Figure 3.14: Hardware setup outside the anechoic room during the measurement of THD+N

Its inverse is used to adjust the frequency response of the loudspeaker.

3.5 Total Harmonic Distortion (THD+N)

Measurement of the total harmonic distortion (THD+N) is also conducted in the anechoic room. The same amplifier, microphone and preamplifier is used. Setup inside the test-facility is the same as in Fig. 3.11

The measurement system used is *Monkey Forest* by *Four Audio*. A DOS-based software with hardware front-end capable of measuring THD and various other acoustic parameters.
The setup is depicted in Fig. 3.14.

Total harmonic distortion is measured for each sample with signal voltages of 0.1 kV, 0.2 kV and 0.4 kV. Bias voltage is kept constant 2.0 kV.

Total harmonic distortion is calculated as the ratio of the fundamental p_1 to its harmonics p_i plus noise p_{noise}

$$\text{THD} + \text{N} = \sqrt{\frac{\sum_2^{\text{inf}} p_i^2 + p_{\text{noise}}^2}{p_1^2}} \tag{3.1}$$

and can be expressed in terms of percent or decibel [52]. The audio measurement system only measures (and calculates the THD) harmonics up to the 3$^{\text{rd}}$ order.
A sampling frequency of 44 100 Hz only allows measurement of the THD up to frequencies of ca.10 kHz as the frequency of the 2$^{\text{nd}}$ harmonic already reaches the Nyquist frequency.
Measurements of the fundamental, the 2$^{\text{nd}}$ and 3$^{\text{rd}}$ harmonics and the noise level are performed in the range of 0.1 kV to 10 kV. The 3$^{\text{rd}}$ harmonic is only possible to measure up to $f = \frac{44100/2}{3} = 7.35$ kHz. In contrast to the prior measurement of the frequency response, a stepped sine is used, with step size of a 1/20-octave (corresponding to a factor of 1.0353).

Chapter 4

Results

4.1 Static Deflection

As mentioned, the membrane formed a slight deflection upon assembling into the frame. Rigid cap support seems to be unnecessary for these small-scale buckling DEAs. Measured cap heights h_0 for each sample is shown in Fig. 4.1.
The initial cap height is presumably due to compression of the material between the plastic frames. Compressive force of clamping displaces the material into the cavity during actuator assembly, forming a cap.
The cap heights h_0 increase on average by 0.1 mm per added layer of dielectric material ($d_0 = 50\,\mu m$).
For further analysis a larger amount of samples have to be studied. A more precise numerical model might provide dependencies. Deflection tests are shown in Figs. 4.2-4.7.
A small hysteresis was measured (see Fig. 4.1). While ramping the voltage down, the measured deflection was slightly above the deflection of ramping up. Different speeds of voltage ramping were conducted with the same results. Hence, hysteresis is suspected to be not due viscoelastic effects in the DE. They rather emerge from the material creeping below and out of the plastic frame. Higher quality frames and clamping the material more tight might cover that problem. As the effect is different for each sample, analysing and considering the hysteresis in the dynamical model is challenging. Measured hysteresis is not further analysed but is expected to slightly decrease sound generation.
The measured data is fitted into

Number of layers N	3	4	5	6	7	8
Initial height h_0 [mm]	0.5	0.6	0.8	0.8	0.9	1.0

Table 4.1: Initial cap heights h_0 for each actuator.

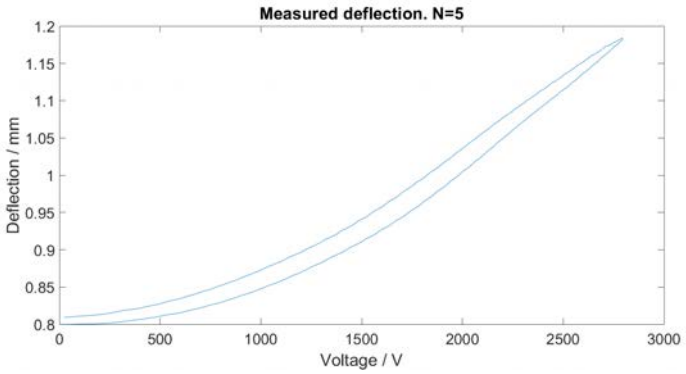

Figure 4.1: Deflection of the 5-layered actuator as measured while ramping voltage up to 2.8 kV in 20 s and down. A notable hysteresis occurs. It is expected to decrease the acoustic performance.

$$NE \cdot (\lambda - 1) = (N - 1)\epsilon\epsilon_0 \frac{V^2}{d_0^2 \lambda^2} \tag{4.1}$$

after the strain λ was calculated by

$$\lambda = \frac{R_b^2 + h_0^2}{R_b^2 + h^2} \tag{4.2}$$

Matlab's *fminsearch*-function is used to minimize the standard variance of measured to modelled data by the parameter E (elastic modulus).
A maximum deflection of almost $\sim$0.4 mm (50 % relative to h_0) was achieved using the 8-layered actuator. Similar relative displacements were achieved by the other actuators, widely confirming the model.

The measurement's aim was to validate the analytical model and to estimate the elastic Modulus E of the membrane.
Half of the produced samples (3-,5- and 8-layer) showed good accordance with the model and equal material parameters were fitted. The silicone is reported to have a Young's modulus of 1.1 MPa [29]. The low discrepancy to the measured value of $\sim$1.2 MPa is most probably due to electrode stiffness.

The large variation of elastic moduli determined by curve fitting confirms the apprehension of high tolerances in manufacturing. 3D printing, the automatic multilayer production as well as the assembly itself provide large sources of errors. In actuators with too high Young's Moduli, not all off the membranes seem to be conductively connected to the supply voltage. The applied electrostatic force is seemingly lower and less deflection is seen.
The reason may either be in the electrode itself (not conducting, too thin, damages, etc) or in the electrical contact itself.

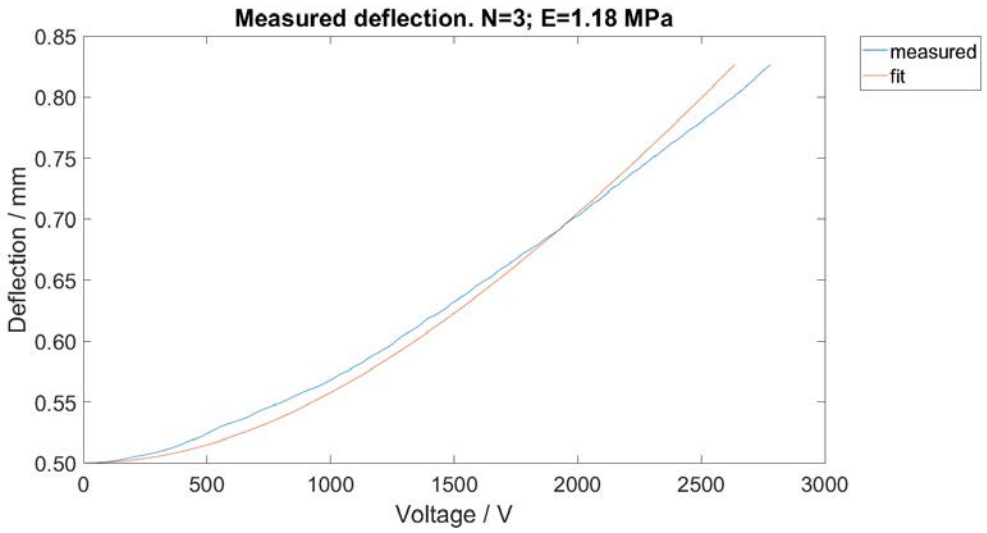

Figure 4.2: Deflection of the 3-layered actuator under static voltage. An elastic modulus of 1.2 MPa fits the curve.

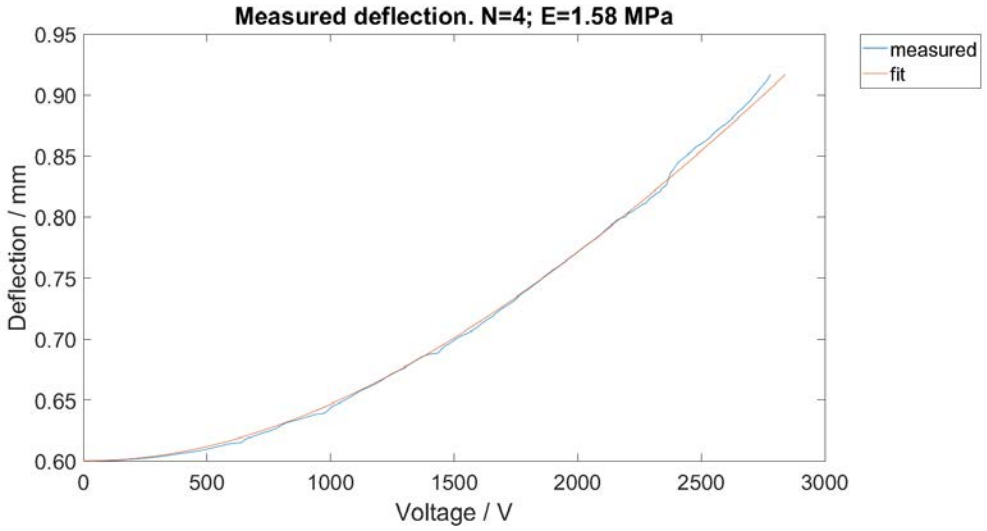

Figure 4.3: Deflection of the 4-layered actuator under static voltage. An elastic modulus of 1.6 MPa fits the curve.

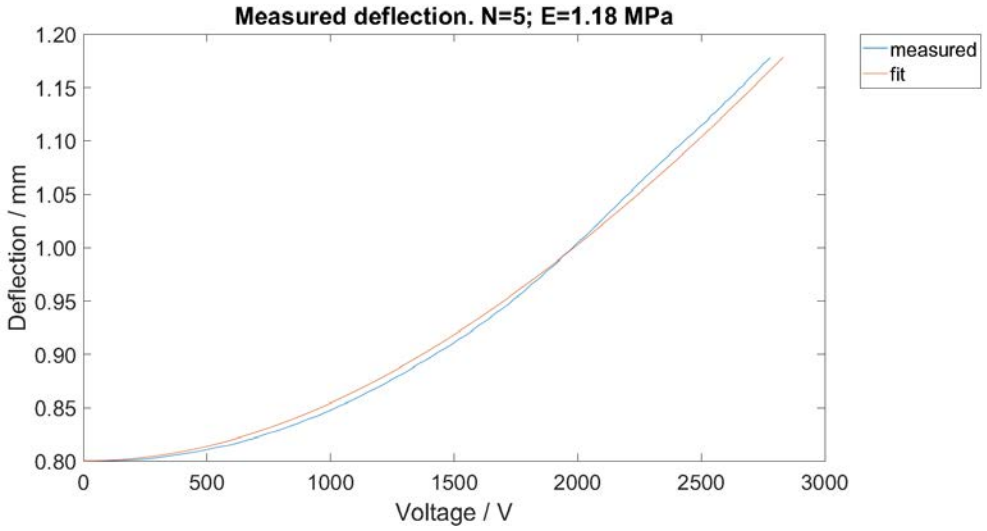

Figure 4.4: Deflection of the 5-layered actuator under static voltage. An elastic modulus of 1.2 MPa fits the curve.

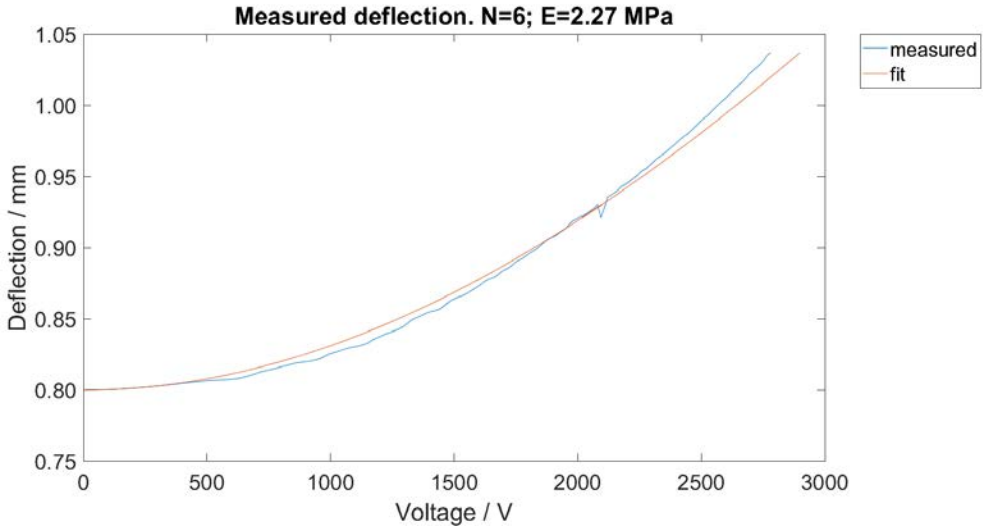

Figure 4.5: Deflection of the 6-layered actuator under static voltage. An elastic modulus of 2.3 MPa fits the curve.

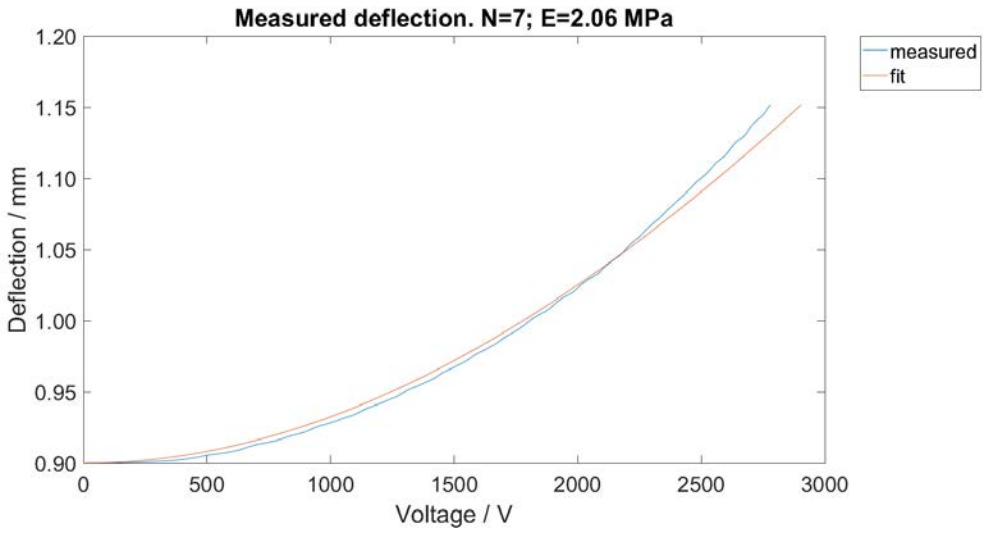

Figure 4.6: Deflection of the 7-layered actuator under static voltage. An elastic modulus of 2.1 MPa fits the curve.

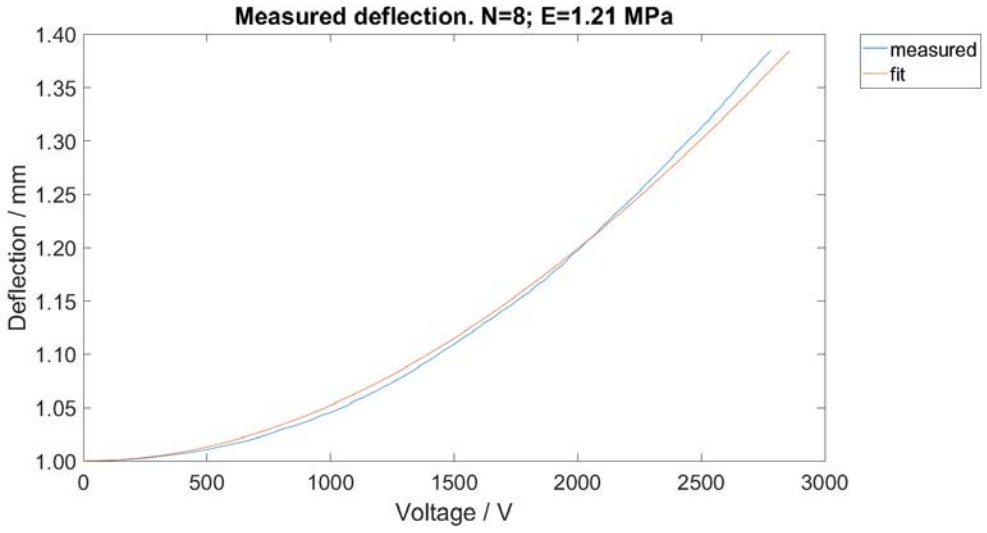

Figure 4.7: Deflection of the 8-layered actuator under static voltage. An elastic modulus of 1.2 MPa fits the curve.

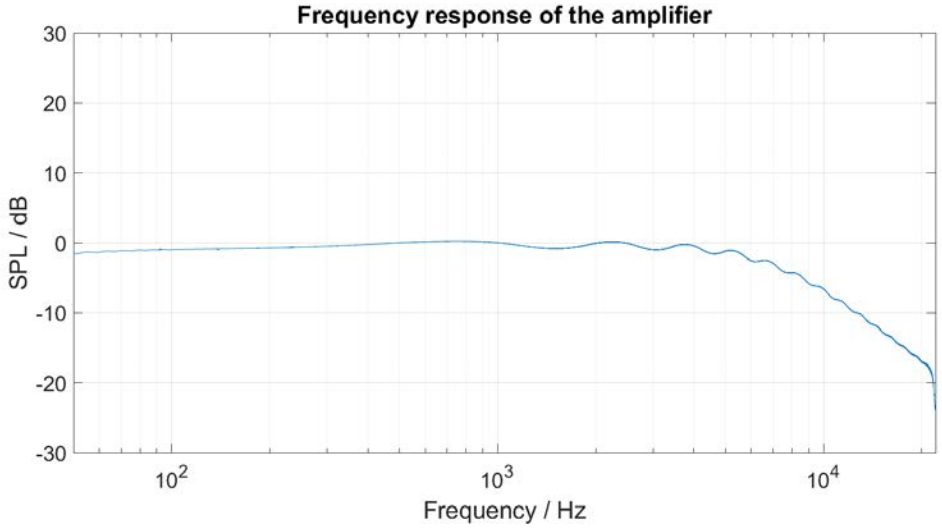

Figure 4.8: Frequency response of the custom built amplifier. Normalised to 1 kHz

The measurements confirm the analytical model, despite some samples performed badly due to manufacturing issues.

Compared to buckling actuators in literature, far lower relative displacements were achieved. Both, Vertechy et al [51] and Lampani [25], used materials with Young's Modulus of only 60 kPa and a permittivity of 5.3 (*Silicone TC-5005, BJB Enterprises Inc., USA*) and achieved relative displacement of >80 %.

4.2 Frequency Response

The frequency response of the amplifier, which is used to correct the acoustic measurements is depicted in Fig. 4.8. As can be seen, the response drops rapidly for frequencies $f > 6$ kHz by ca. 6 dB/octave. Adjusted values for the frequency response at high frequencies are thus more prone to noise.

Figs. 4.9-4.14 show the measured and adjusted frequency responses of each actuator compared to the modelled curves. In each figure, the modelled curve is adjusted for the fitted elastic modulus of the static tests. Of course, the elastic modulus is the same for every actuator, namely (1.2 MPa), as the same material is used. In this context however, it is rather regarded as a measure of the material's response to the electric stimulus and not as an intrinsic material parameter. The measurement distance of 0.5 m halves the measured curve, so values in 1.0 m are obtained. Radiation in half space and signal voltage amplitude are included in the calculated curve.

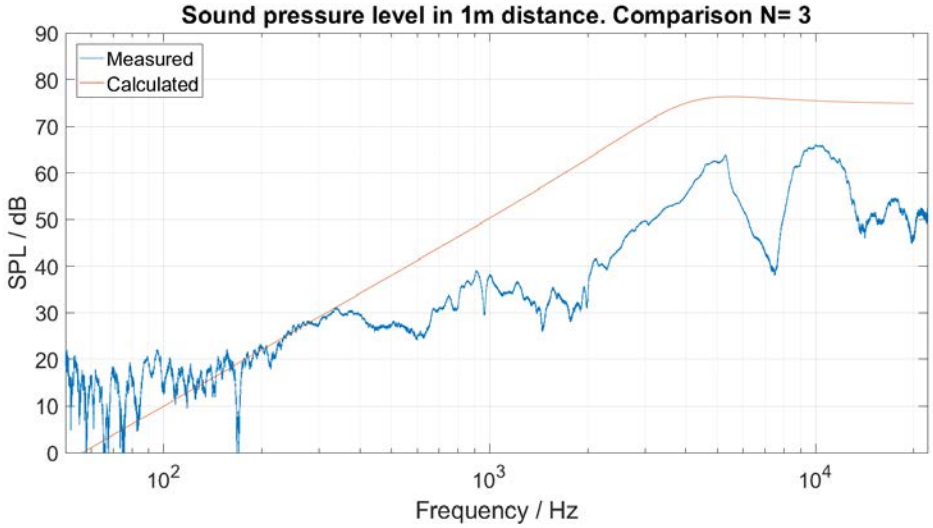

Figure 4.9: Measured frequency response of the 3-layered actuator. Measured with 2.0 kV bias voltage and 0.4 kV signal amplitude voltage. Compared to the model.

The 8-layered actuator shows great difference to the others. Far lower SPLs than expected are most probably due to fabrication issues. In the following it is regarded as faulty and is not subject to further analysis.

All other actuators show similar SPL with a prominent peak at the calculated $f_0 \approx 5\,\text{kHz}$ (see Fig. 4.15). Different amount of layers show different natural frequencies also in the model. Small variations ($< 5\,\%$) of the location of the peaks are due to inhomogeneities in the fabrication process.
The position of maximum SPL at about 5 kHz is observed for all samples.
This common property suggest high reproducibility of the membrane fabrication, as the position of this major resonance results from layer thickness and material properties rather than geometry. Largest source of errors therefore seems to be in the assembling of the actuator itself, that is clamping it stretch-free into the 3D-printed frame. Frame quality might also affect performance.
All samples share a small peak at around 1 kHz, which is most prominent in Fig. 4.12, where the measured and modelled curve coincide.

Audible sound radiation is from ∼500 Hz, though at very low levels. As expected, the presented loudspeaker clearly acts as a tweeter.
With increasing amount of layers, an increase in sound pressure is generated. A maximum SPL of 78.7 dB is achieved with the 7-layered actuator, while the 3-layered actuator only reaches an SPL of 66.0 dB at the 2^{nd} peak at 10 kHz.

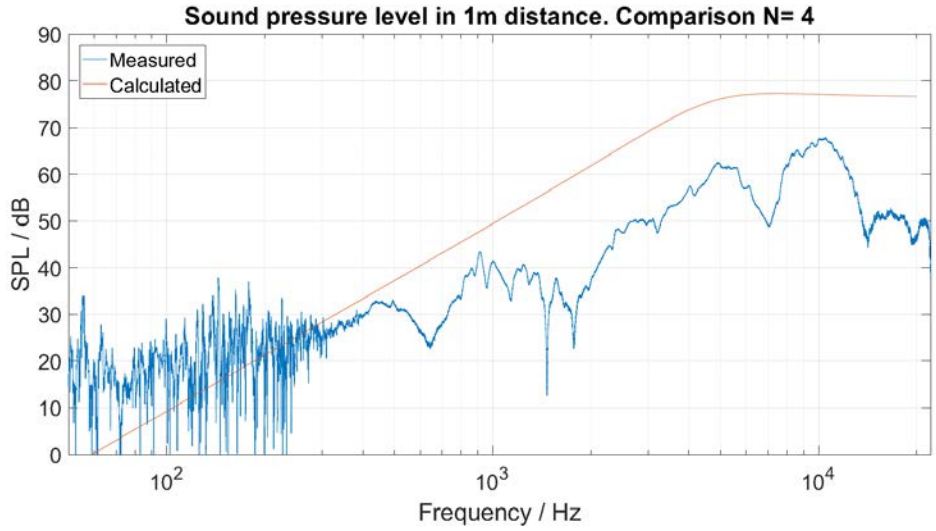

Figure 4.10: Measured frequency response of the 4-layered actuator. Measured with 2.0 kV bias voltage and 0.4 kV signal amplitude voltage. Compared to the model.

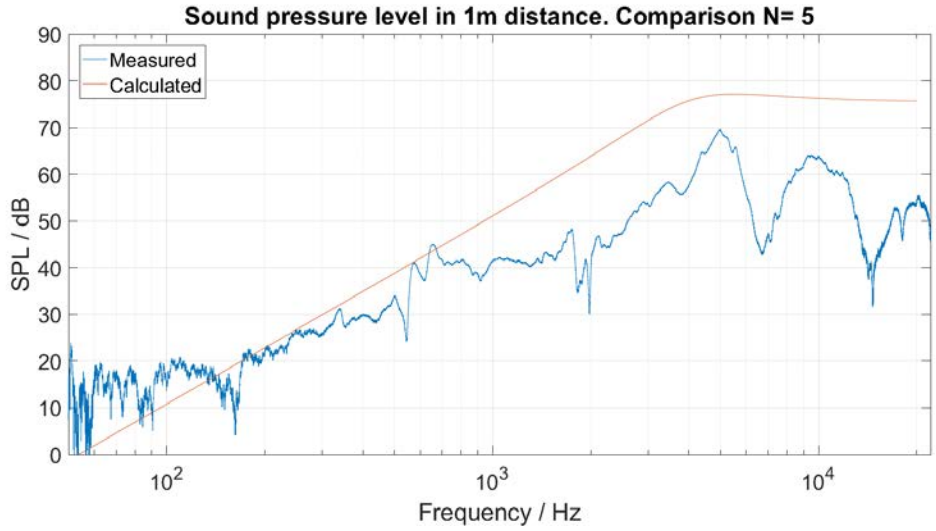

Figure 4.11: Measured frequency response of the 5-layered actuator. Measured with 2.0 kV bias voltage and 0.4 kV signal amplitude voltage.

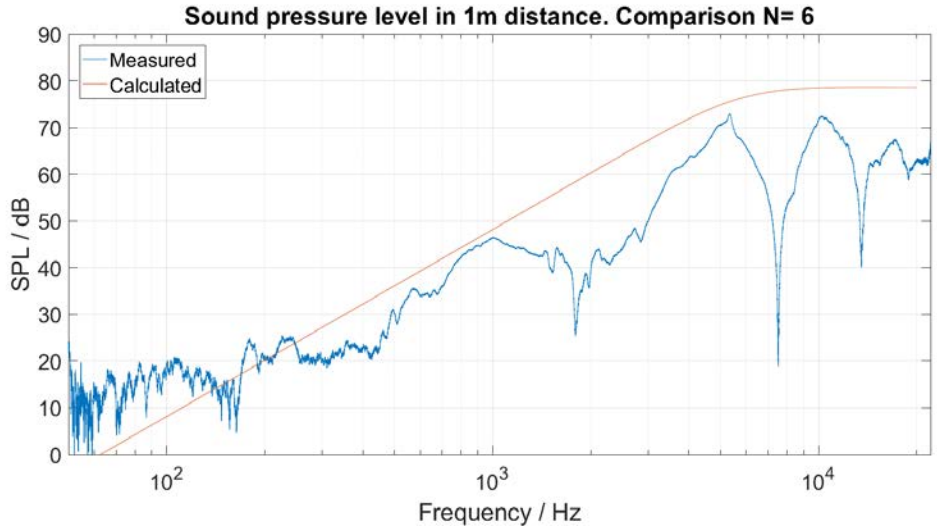

Figure 4.12: Measured frequency response of the 6-layered actuator. Measured with 2.0 kV bias voltage and 0.4 kV signal amplitude voltage.

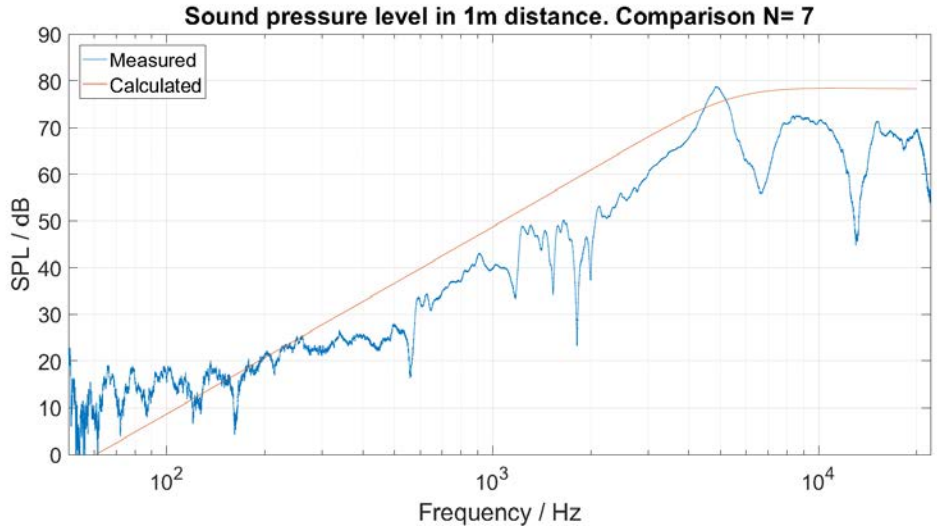

Figure 4.13: Measured frequency response of the 7-layered actuator. Measured with 2.0 kV bias voltage and 0.4 kV signal amplitude voltage.

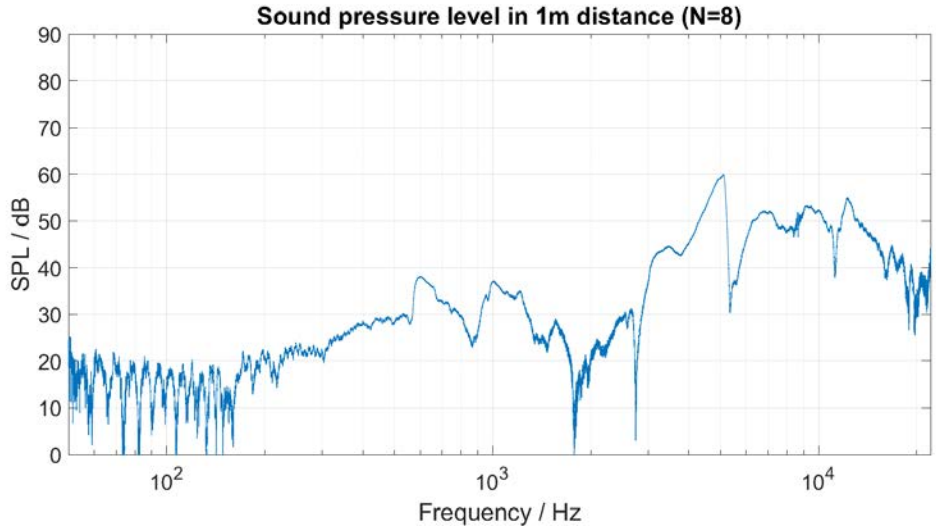

Figure 4.14: Measured frequency response of the 8-layered actuator. Measured with 2.0 kV bias voltage and 0.4 kV signal amplitude voltage. Sample is regarded as faulty.

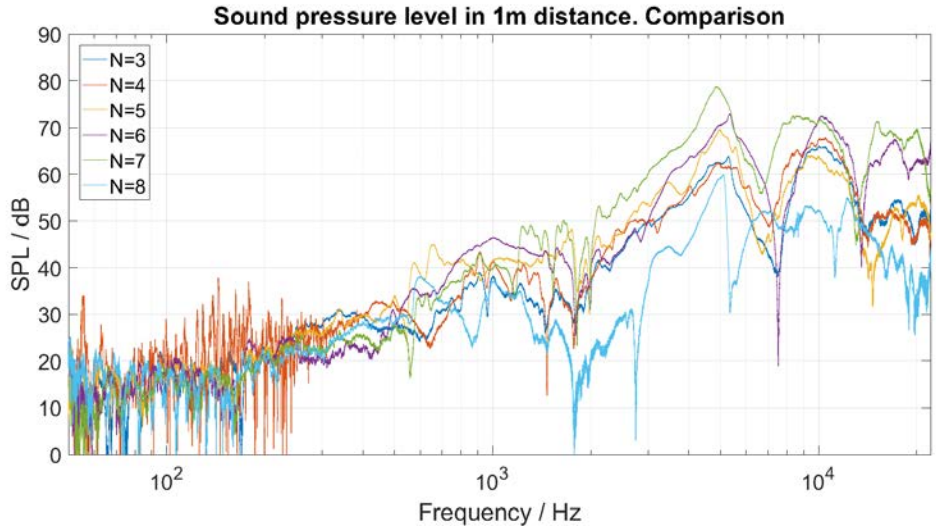

Figure 4.15: Comparison of frequency responses. Measured with 2.0 kV bias voltage and 0.4 kV signal amplitude voltage.

Calculations of the membrane transfer function Eq. 2.119 are based on a viscoelastic loss factor of 0.1 % which is only roughly estimated. Finding a value to fit the measured data does not serve the purpose of this work. Too many unknown variables contribute to the system, such as hysteresis and membrane inhomogeneities.

The abundance of modal frequencies from Eq.2.1 can hardly be associated to the various dips in the frequency responses. Also, the membrane can not be regarded as uniform, the frame exhibits irregularities and clamping the membrane into the frame results in compressive forces at the edges. Boundary conditions thus, are arbitrary and different for each sample and cannot be formulated satisfyingly in mathematical terms.

The measured curve of the 3-layered sample (Fig. 4.9) is about 12 dB below the model. The peak value at $f_0 \approx 5$ kHz is in accordance with the model. It can be assumed, that viscoelastic loss is indeed in the range of 0.1 %, as even small deviations would result in different peak frequencies.
The 4-layered actuator shows very similar behaviour and deviations to the calculated curve are almost identical to the 3-layered sample.
For each layer added to the actuators, the model seems to fit the measurements better. The 6- and 7-layered loudspeakers performed best, as the difference of calculated to measured frequency responses is less than 3 dB at the middle peak of 1 kHz and the peak at f_0. In between these frequencies however, the SPL is much lower than expected. Membrane movement is highly irregular as the very soft rubber-like material of the silicone allows a variety of partial oscillations.

The acoustic model can be regarded as confirmed by the measurements, though the abundance of naturals frequencies by Tab. 2.1 lead to deviations.

4.3 Total harmonic distortion (THD)

Figs. 4.16-4.18 show the results for the THD+N measurements. Each figure shows the THD+N for every sample at a given voltage amplitude. As the values do not seem to be dependent on the sample, the mean THD+N is also depicted. For better comparison the mean values are shown in Fig. 4.19.

The difference of THD+N for lower frequencies is mostly because of the noise at low frequencies. Higher levels of signal voltage generate higher pressure amplitudes, and thus THD+N decreases (see Eq.3.1, as the signal-to-noise-ratio (SNR) increases.
THD decreases with the same slope the frequency response increases with frequency (-6 dB/octave). THD for all samples and for all signal-to-bias ratios converges to -30 dB (3.2 %), which is reached at $\sim$3 kHz for all samples for all signal voltages. THD+N therefore also seems independent of

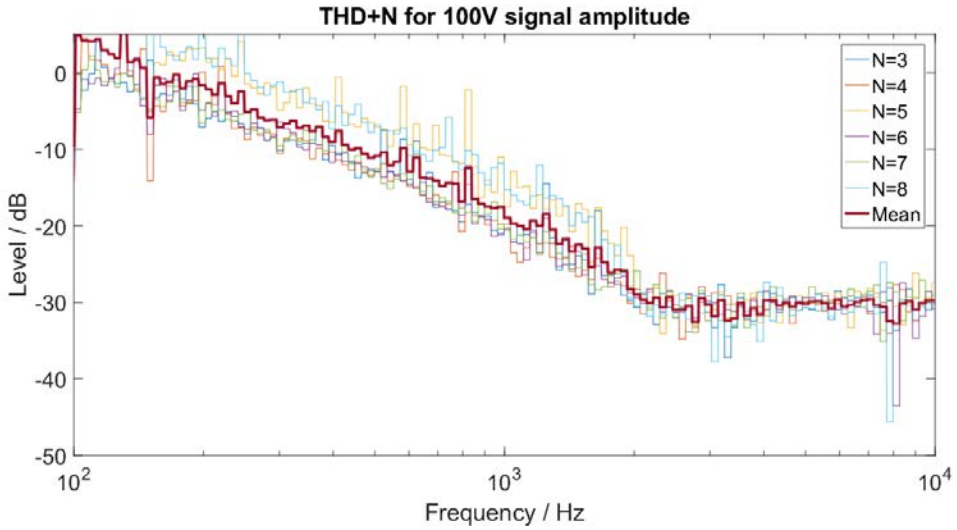

Figure 4.16: THD+N for every DUT at a signal voltage of 0.1 kV and a bias voltage of 2.0 kV.

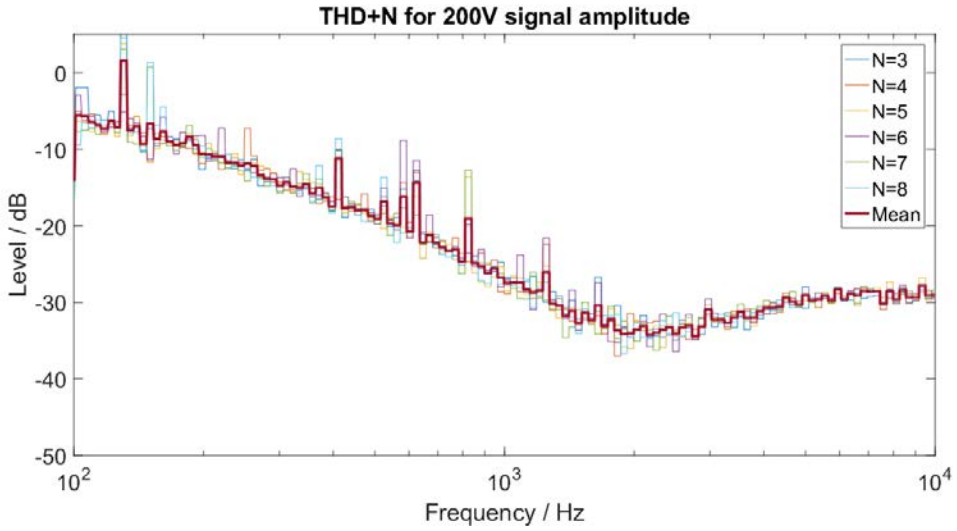

Figure 4.17: THD+N for every DUT at a signal voltage of 0.2 kV and a bias voltage of 2.0 kV.

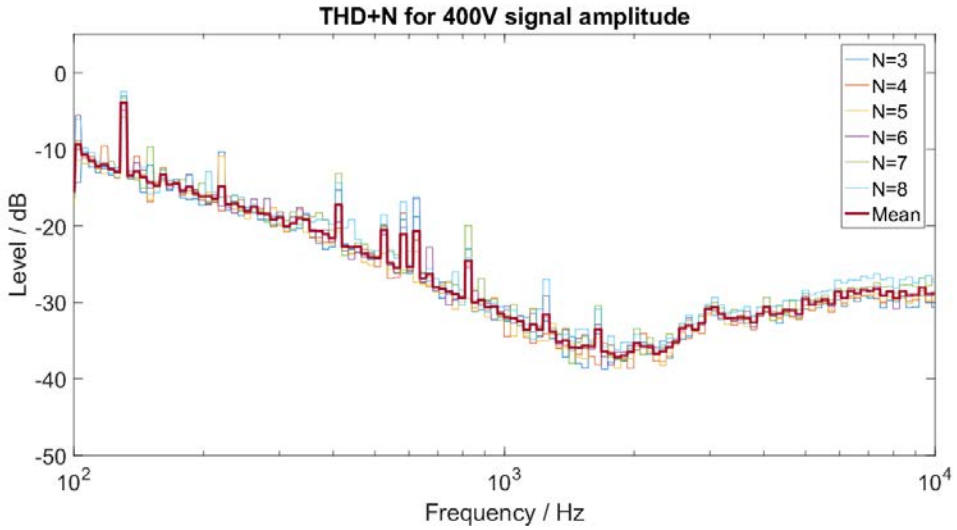

Figure 4.18: THD+N for every DUT at a signal voltage of 0.4 kV and a bias voltage of 2.0 kV.

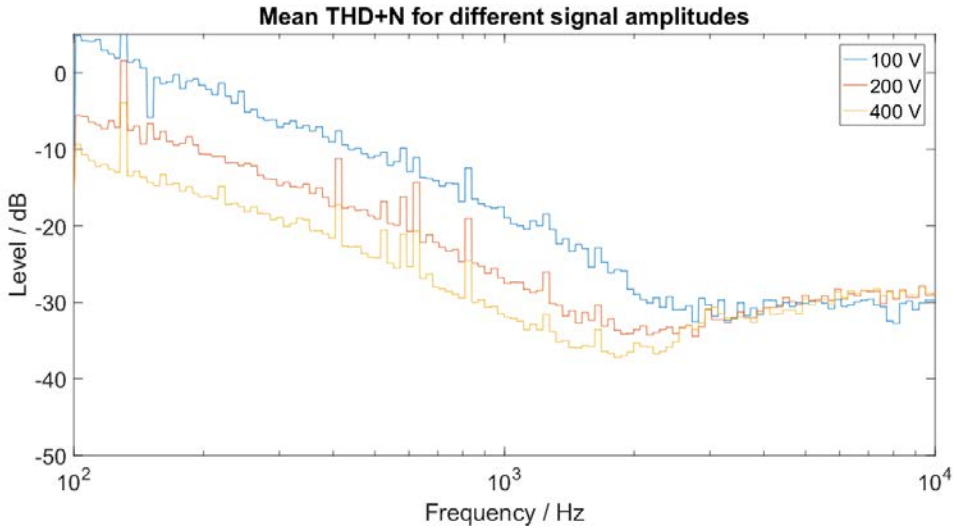

Figure 4.19: Comparison of the mean THD+N for different signal amplitudes.

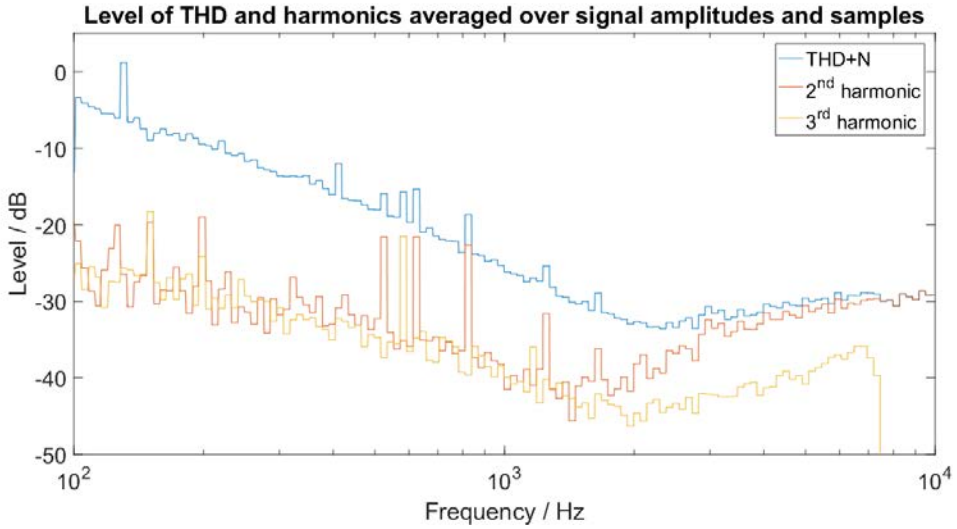

Figure 4.20: Level of THD+N, the 2nd and 3rd harmonics. Averaged over signal voltages and samples.

signal-to-bias ratio, contrary to observations in [15] but in accordance with measurements of [45]. Even better values of −38 dB are reached for frequencies in the range of 1.5 kHz to 2.5 kHz for 0.4 kV signal amplitude.

The level of the 2nd and 3rd harmonics are depicted in Fig. 4.20. The difference of the total THD+N at low frequencies to the level of the harmonics indicates, that prior assumption is correct: A large fraction of the THD here is the result of noise. Higher order harmonics usually have far lower levels than the 2nd and 3rd, so the total THD would only be about 6 dB above the level of the harmonics, if it wasn't due to noise.
The level of the harmonics is almost equal up to frequencies of 2 kHz, where the 2 curves begin to part.
Significance of Fig. 4.20 is only from that frequency upwards, as the THD+N varies for different amplitudes below that frequency (see Fig. 4.19).
As can be seen, the level of the 2nd harmonic increases and is the main contributor to THD+N.

For conventional loudspeaker THD+N is usually specified as $< 1\,\% = -40\,\mathrm{dB}$, which is about 10 dB better value than the presented prototypic DE loudspeaker. Main reason for the high THD+N is the quadratic behaviour of the strain-to-voltage relation [15].

The frequency response is calculated in terms cap height ($p \propto h^2$) as seen in Eq. 2.104. The

voltage-to-strain behaviour is given by

$$\frac{N}{N-1} E d_0^2 \cdot (\lambda^3 - \lambda^2) = \epsilon\epsilon_0 V^2 \tag{4.3}$$

with

$$\lambda = \frac{R_b^2 + h_0^2}{R_b^2 + h^2} \tag{4.4}$$

A sinusoidal stimulus $V = V_{\text{bias}} + \hat{V}\sin(\omega t)$ then results in

$$A\sin(\omega t) + B\sin(2\omega t) \propto \left(\frac{C}{p}\right)^3 - \left(\frac{C}{p}\right)^2 \tag{4.5}$$

(With A, B and C constants), which leads to

$$p \propto \frac{\sqrt[3]{c_1 \sin^2(\omega t) \cdot \sin^2(2\omega t) + \sqrt{c_2 \sin^4(\omega t)\sin^4(2\omega t) + c_3 \sin^3(\omega t)\sin^3(2\omega t)}}}{c_4 \sin(\omega t)\sin(2\omega t)} - \frac{c_5}{\sqrt[3]{c_1 \sin^2(\omega t) \cdot \sin^2(2\omega t) + \sqrt{c_2 \sin^4(\omega t)\sin^4(2\omega t) + c_3 \sin^3(\omega t)\sin^3(2\omega t)}}} \tag{4.6}$$

which highlights the complex harmonic structure of the system and explains the high THD+N. Harmonics of up to the 6^{th} order are expected.

The level peaks in Fig. 4.20 between 500 Hz to 800 Hz are significant, but in this range no corresponding feature can be found in the frequency response, which varies widely among different samples. The reason for these peaks remains unknown.

4.4 Conclusion

Static deflection tests turned out to fit well with the analytical model for samples with layers $N = 3$, 5 and 8, where elastic moduli similar to values found in literature are fitted. Small deviations are most probably due to electrode stiffness. A small contribution to the difference might be due the determination of the initial cap-height h_0.
Relative displacements of up to 60 % are achieved with the 3-layered actuator, where an elastic modulus of 1.18 MPa is found.

Contrary to expectations, samples with higher found elastic moduli do not perform worse in the acoustic measurements. Conversely, the 8-layered actuator, which shows very good accordance with the model (see Fig. 4.7) has to be regarded as faulty in the following acoustic measurements (see Fig. 4.14).
In the modelled curve of Sec. 4.2 the previously determined elastic moduli were used. The re-

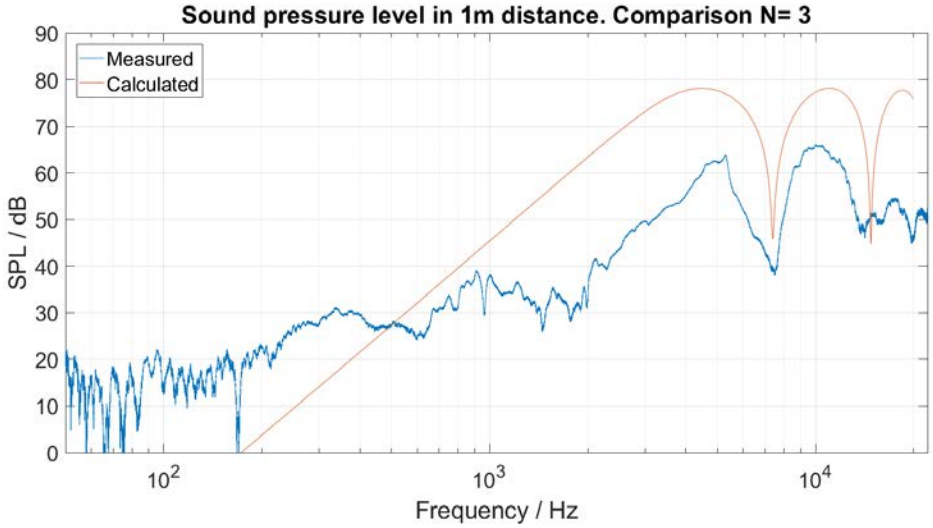

Figure 4.21: Comparison of calculated and measured frequency response of the 3-layered actuator. Effect of acoustic short-circuit considered

sulting shift of the natural frequency however, is not observed in the measurements. The peak level remained to be around 5 kHz and does not reflect the static measurements, despite the same samples are examined. This indicates, that some of the layers are not conductively connected to the power supply as stated. A maximum SPL of almost 80 dB at the natural frequency, radiated in the half space in 1 m distance is a good result for a loudspeaker of only 8 mm size. The level discrepancy of measured to modelled frequency responses is most probably due to the hysteresis, as depicted in Fig. 4.1 and due to the modal frequencies.
All together, the measurements are satisfactory, as the static as well as the acoustic model can be confirmed. Hardest to include in the calculations and hardest to comply with measurements are the modal frequencies, which causes the level deficits of measured to modelled frequency responses. Also natural frequencies, sub and super-harmonic resonances (see Eq. 2.120) are not visible in the curves, probably as they are concealed by the modal resonances.

The steep declines in SPL at ∼7.5 kHz and ∼15 kHz are a major performance deficit. An erroneous measurement setup is suspected. Sound radiated from the back of the transducer is measured with a delay of $\Delta T = \frac{\Delta x}{c}$. With the size of the actuator of 4 cm and a thickness of 0.6 cm, sound waves from the back and front annihilate at a frequency of $f = \frac{1}{\Delta T} = \frac{340\ \frac{\mathrm{m}}{\mathrm{s}}}{4.6\ \mathrm{cm}} \approx 7.4\,\mathrm{kHz}$.
Adjusted calculated curves are seen in Fig.4.21-4.25. As the calculated curves match with the suspected diagnosis, the loudspeaker, when its back is acoustically isolated, should indeed feature the calculated frequency responses. The steep dips are merely the unfortunate result of bad sealing between the transducer and the sound baffle during measurement. In an appropriate enclosure (e.g. loudspeaker box) the back of the transducer is acoustically isolated, and these

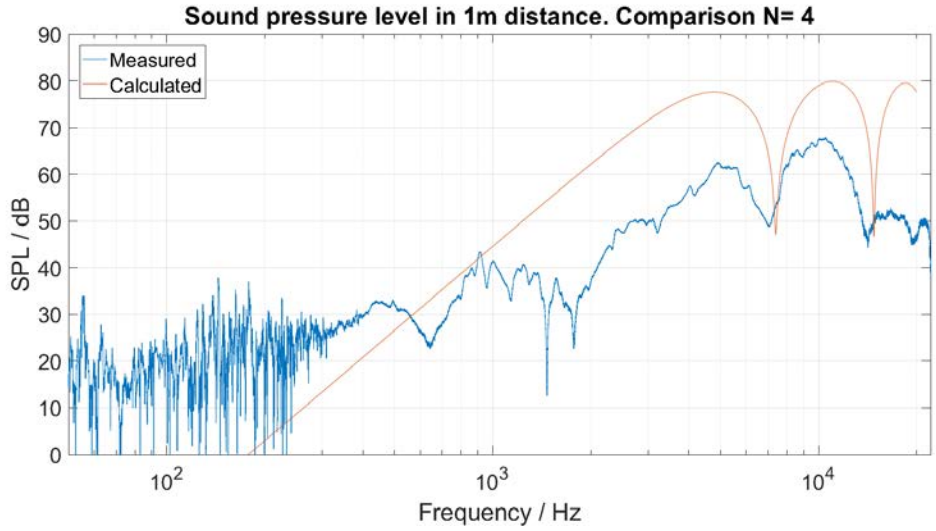

Figure 4.22: Comparison of calculated and measured frequency response of the 4-layered actuator. Effect of acoustic short-circuit considered

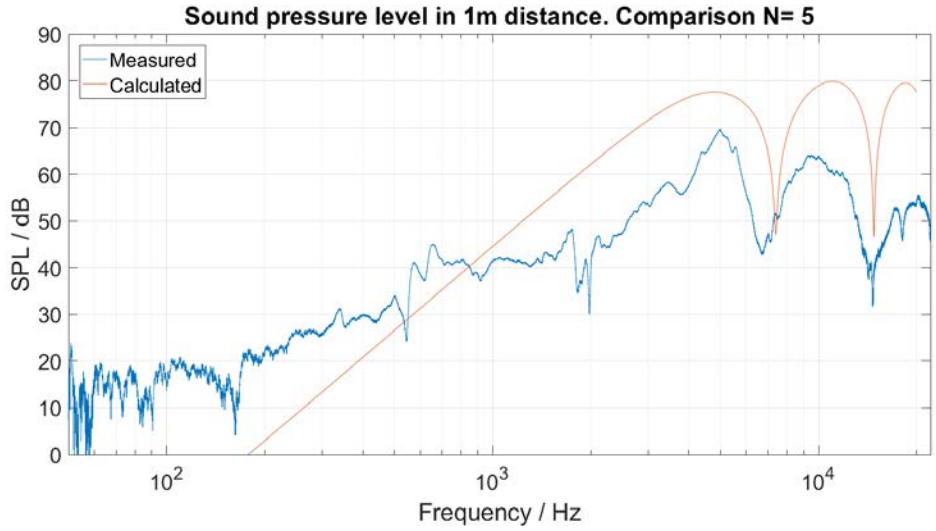

Figure 4.23: Comparison of calculated and measured frequency response of the 5-layered actuator. Effect of acoustic short-circuit considered

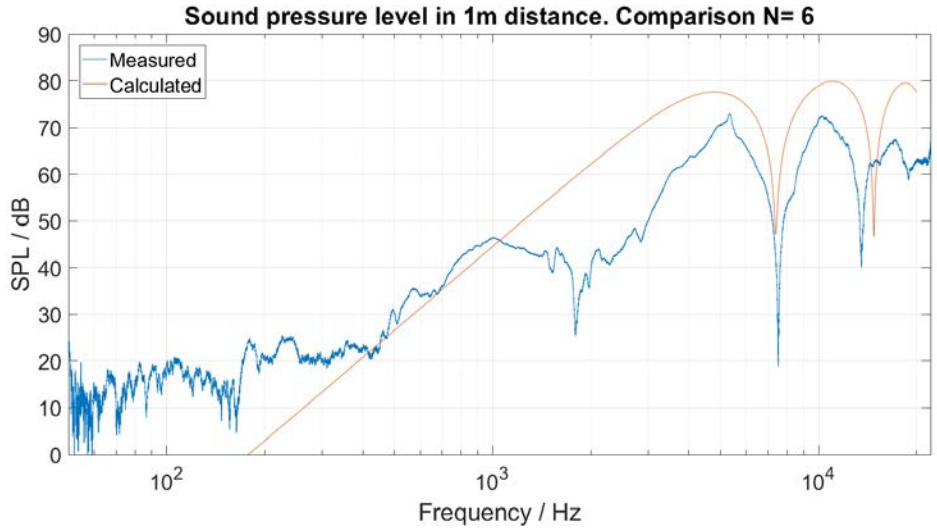

Figure 4.24: Comparison of calculated and measured frequency response of the 6-layered actuator. Effect of acoustic short-circuit considered

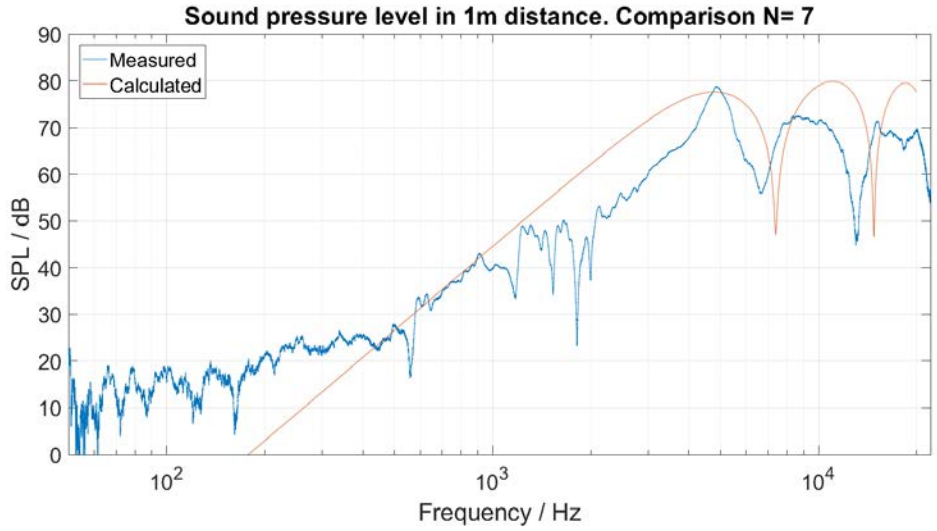

Figure 4.25: Comparison of calculated and measured frequency response of the 7-layered actuator. Effect of acoustic short-circuit considered

dips should not appear.

Chapter 5

Discussion

This last chapter critically reflects on the work. The prototypic loudspeaker is compared to other conceptual DE loudspeaker as well as to conventional drivers.
As the goal of the work is it to only develop but not to optimise an innovative loudspeaker, a short section on possibilities to do so is added.

5.1 Comparison to other Loudspeakers

The biggest problem of the presented speaker seems to be the high driving voltage and the large amount of modal frequencies, which lower the SPL significantly. The high voltages necessary to cause actuation is shared among other prototypic loudspeakers.
The first ever presented DE loudspeaker by Heydt et al [15], whose frequency response is depicted in Fig. 1.12 used a driving voltage of 0.6 kV with 1.5 kV bias voltage. His frequency response is significantly flatter and thus, seems to perform better. The active area however is much larger with 50 mm × 50 mm and 72 film elements are driven in parallel.
At such an area about 40 elements of the here presented speaker would fit, resulting in an SPL about 32 dB higher than the measured curves! This would allow the use of equalizers to lower some of the most prominent peaks. Using a softer material ($E = 0.1$ MPa and thicker membrane ($d_0 = 86\,\mu$m), the natural frequency of his design was at ca.1.4 kHz and thus, had a much wider operating range.
Non-linear distortion is similar for both concepts.
The more recent prototypes of Sugimoto et al [48] and Rustighi et al [45] also show frequency responses with better midrange capabilities than the BDEA of this thesis and similar values for THD were measured. Although again, the active area for both concepts is much larger.
Biggest advantage over other DE loudspeaker is its simplicity in production and operation. No underlying pressure chamber has to be used and no prestretch is necessary. Additionally, the polymer material and the plastic frames are inexpensive.

Conventional piezo and electrodynamic loudspeakers still outperform the presented prototype. The high voltages necessary to rive the speaker inhibits not only the risk of electric failures, but might also cause the system to generate much excess heat, as the electrode resistance is quite high. At low frequencies, its SPL is far from that of electrodynamic systems. At high frequencies, horn-loudspeakers outperform the presented prototype.
However, for applications, were small and lightweight tweeters are required, the presented prototype comes just right.

The frequency response does not seem to decline for high frequencies. Possible use of that is in the application as ultrasound loudspeakers.

The highly irregular frequency response and high THD impedes its use as high-fidelity loudspeaker unless major design optimizations are implemented.

5.2 Improvements

The high driving voltage is probably one of the main reasons, DE technology has not entered the commercial market on large scale, yet.
The decrease of driving voltage is solely a matter of the material and its thickness. As is highlighted in the equation for the generated stress by applied voltage Eq. 1.1, the parameters to be adressed by material scientists are the Young's modulus E and the dielectric constant ϵ. An increase of the factor ϵ/E decreases the necessary driving voltage [35]. Blending of dielectric fillers into the silicone is reported to increase the dielectric constant, and thus reduces the needed voltage. As [35] reported, copper elements in silicone lead to an increase in ϵ of almost 80 %.
Use of plasticisers also showed success on improving actuation. A decrease of Young's modulus from 1.6 MPa to 0.75 MPa was achieved by adding epoxidised soybean oil to the silicone, while dielectric constant lowered only by a small fraction. This led to an increase in actuation strain of 100 % [54]. The same authors also investigated the positive effect of titanium dioxide particles, which increased the dielectric constant.

Unfortunately, the use of filler elements as means of increasing ϵ seems to lower the dielectric breakdown strength of the material. Thus, the necessary voltage reduces but so does the maximum applicable voltage.
To compensate for that, Molberg et al [32] experimented with encapsulation of polyaniline in polydivinyl benzene. The encapsulated material was used as filler elements and led to 3-fold higher dielectric breakdown field.

Far easier than chemical manipulation of the material is to decrease film-thickness. Film thickness is quadratic to strain and linear to voltage in Eq.1.1. So, with same voltage and half-thickness of the film fourfold strain may be achieved. Or, for same strain only half the voltage is needed for halved film thickness. The maximum applicable voltage reduces by the same factor.

The presented loudspeakers are the result of a fast-prototyping process. Focus has never been on material quality, so different concepts could be tried in short time. The 3D-printed frame is of bad quality and has sharp edges along its inner cavity, where the membrane buckles up. Irregular behaviour and much deviation in performance among the samples are the result.
A standardized and reproducible fabrication process would allow to take on more actions on improving the quality, as the issues would become more clear and can be tackled.
Modal examination of the driven membrane would allow to gather more information necessary for tuning of the loudspeaker.

The frequency response is highly irregular with several dips and peaks for the full operating range. Higher damping factors of the material would broaden those peaks and potentially smooth the curve. Hysteresis however, might be negatively affected by such measures as well as response time.

More elements packed into an array would multiply the rather low SPL. A possible way to build a broadband speaker with an operating range from 300 Hz and above may be, to pack enough elements together, to lift up the SPL at 300 Hz to a desired level, i.e. 70 dB (corresponding to a level difference of 45 dB). About 200 elements are needed to achieve that. To compensate for the increasing frequency response of ca. 6 dB/octave, an analogous filter could be easily implemented.
Larger diameter of the elements would help to increase the level at low frequencies aswell. Fig. 5.1 applies the model to an actuator of 20 mm diameter and 10 layers. The predicted SPL is significantly higher for the full range. Material parameters of the *Silicone TC-5005, BJB Enterprises Inc., USA* are fitted. ($E = 60\,\mathrm{kPa}, \epsilon = 5.3, d_0 = 100\,\mu\mathrm{m}$).

As Heydt et al [15] demonstrated, square-root shaping of the signal lowers the THD to less than 1 %. As the initial aim was to develop a small loudspeaker for WFS, signal preprocessing is done anyway. An additional operation to lower the THD could be implemented easily.

This work proposes and proofs the concept of a lightweight and scalable tweeter loudspeaker and proposes the basis for possible future research. As the material and fabrication is potentially very low, cheap loudspeakers with reasonable performance might be produced automatically.

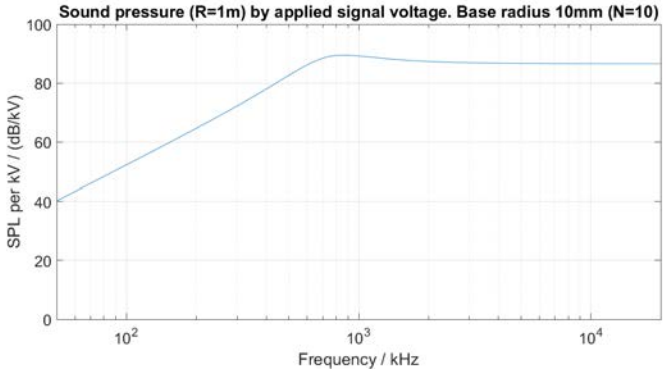

Figure 5.1: Predicted frequency response for an actuator of 10 layers with diameter 20 mm

Chapter 6

Appendix

6.1 Velocity of the membrane

Eq. 2.86 then reads as

$$\begin{aligned}
\mathbf{x}' &= (r+\hat{r}e^{i\omega t})\cdot\begin{pmatrix}\cos\left(\frac{\theta}{\theta_{max}}\theta'_{max}\right)\\ \sin\left(\frac{\theta}{\theta_{max}}\theta'_{max}\right)\end{pmatrix}+\begin{pmatrix}\sqrt{(r^2-R_B^2)}-\sqrt{r'^2-R_B^2}\\ 0\end{pmatrix}\\
&= (r+\hat{r}e^{i\omega t})\cdot\begin{pmatrix}\cos\left(\frac{\theta}{\theta_{max}}\theta'_{max}\right)\\ \sin\left(\frac{\theta}{\theta_{max}}\theta'_{max}\right)\end{pmatrix}+\begin{pmatrix}\sqrt{(r^2-R_B^2)}-\sqrt{(r+\hat{r}e^{i\omega t})^2-R_B^2}\\ 0\end{pmatrix} \qquad (6.1)\\
&= (r+\hat{r}e^{i\omega t})\cdot\begin{pmatrix}\cos\left(\frac{\theta}{\theta_{max}}\arcsin\left(\frac{R_b}{r'}\right)\right)\\ \sin\left(\frac{\theta}{\theta_{max}}\arcsin\left(\frac{R_b}{r'}\right)\right)\end{pmatrix}+\begin{pmatrix}\sqrt{(r^2-R_B^2)}-\sqrt{(r+\hat{r}e^{i\omega t})^2-R_B^2}\\ 0\end{pmatrix}
\end{aligned}$$

Differentiating by time provides the membrane velocity

$$\begin{aligned}
\mathbf{v} &= i\omega\hat{r}e^{i\omega t}\cdot\begin{pmatrix}\cos\left(\frac{\theta}{\theta_{max}}\arcsin\left(\frac{R_b}{r'}\right)\right)\\ \sin\left(\frac{\theta}{\theta_{max}}\arcsin\left(\frac{R_b}{r'}\right)\right)\end{pmatrix}\\
&- i\omega\hat{r}e^{i\omega t}\begin{pmatrix}-\sin\left(\frac{\theta}{\theta_{max}}\arcsin\left(\frac{R_b}{r'}\right)\right)\\ \cos\left(\frac{\theta}{\theta_{max}}\arcsin\left(\frac{R_b}{r'}\right)\right)\end{pmatrix}\cdot\frac{\theta}{\xi_{max}}\frac{R_B}{\sqrt{r'^2-R_b^2}} \qquad (6.2)\\
&- i\omega\hat{r}e^{i\omega t}\begin{pmatrix}\frac{r'}{\sqrt{r'^2-R_B^2}}\\ 0\end{pmatrix}
\end{aligned}$$

Which splits into a radial, a tangential and a axial term. The axial term is split into radial and tangential terms. With $\hat{r} \leqq r \to r' \approx r_0$ and $\theta_{max} \approx \theta'_{max}$

6.2 Acoustic potential

Considering the velocity is zero for all angles $\theta > \theta_{max}$, the integration area on the left hand side reduces.

$$
\begin{aligned}
& i\omega\hat{r}e^{i\omega t}\int_0^{\theta_{max}}\left(1-\cos(\theta)\frac{r}{\sqrt{r^2-R_B^2}}\right)P_m(\cos(\theta))\sin(\theta)\,\mathrm{d}\theta \\
& =\sum_{n=0}^{\infty}A_n\frac{\partial h_n^{(2)}(kR)}{\partial R}\int_0^{\pi}P_n(\cos(\theta))P_m(\cos(\theta))\sin(\theta)\,\mathrm{d}\theta\ \Big|_{R=r}
\end{aligned}
\tag{6.3}
$$

$$
\begin{aligned}
& \to i\omega\hat{r}e^{i\omega t}\left[\sin(\theta_{max})P_m^{-1}(\cos(\theta_{max}))-\frac{r}{\sqrt{r^2-R_B^2}}\int_0^{\theta_{max}}P_m(\cos(\theta))\cos(\theta)\sin(\theta)\,\mathrm{d}\theta\right] \\
& =\sum_{n=0}^{\infty}A_n\frac{\partial h_n^{(2)}(kR)}{\partial R}\cdot\frac{2\delta_{mn}}{2n+1}=A_m\frac{\partial h_m^{(2)}(kR)}{\partial R}\cdot\frac{2}{2m+1}\ \Big|_{R=r}
\end{aligned}
\tag{6.4}
$$

The remaining integral is [3]

$$
\begin{aligned}
& \int_0^{\theta_{max}}P_m(\cos(\theta))\cos(\theta)\sin(\theta)\,\mathrm{d}\theta= \\
& \qquad\begin{cases}
\frac{\sin^2(\theta_{max})}{2} & \text{for } m=0 \\
\frac{1-\cos^3(\theta_{max})}{3} & \text{for } m=1 \\
-\sin^2(\theta_{max})\frac{P_m(\cos(\theta_{max}))+\cot(\theta_{max})P_m^1(\cos(\theta_{max}))}{(m-1)(m+2)} & \text{for } m\geq 2
\end{cases}
\end{aligned}
\tag{6.5}
$$

With the radial derivative of the m$^{\text{th}}$ hankel function h_m

$$
\frac{\partial h_m^{(2)}(kR)}{\partial R}=\frac{k}{2m+1}\Big(mh_{m-1}^{(2)}(kR)-(m+1)h_{m+1}^{(2)}(kR)\Big) \tag{6.6}
$$

and substituting $R=r$, the A_n are

$$
\begin{aligned}
A_n= & \frac{(2n+1)^2}{2k\Big(nh_{n-1}^{(2)}(kr)-(n+1)h_{n+1}^{(2)}(kr)\Big)}\cdot i\omega\hat{r}e^{i\omega t} \\
& \cdot\Bigg[\sin(\theta_{max})P_n^{-1}(\cos(\theta_{max}))- \\
& \frac{r}{\sqrt{r^2-R_B^2}}\begin{cases}
\frac{\sin^2(\theta_{max})}{2} & \text{for } n=0 \\
\frac{1-\cos^3(\theta_{max})}{3} & \text{for } n=1 \\
-\sin^2(\theta_{max})\frac{P_n(\cos(\theta_{max}))+\cot(\theta_{max})P_n^1(\cos(\theta_{max}))}{(n-1)(n+2)} & \text{for } n\geq 2
\end{cases}\Bigg]
\end{aligned}
\tag{6.7}
$$

Bibliography

[1] N. A. Alfutov, editor. *Stability of elastic Structures*. Springer, 2000.

[2] W. Becker and D. Gross, editors. *Mechanik elastischer Körper und Strukturen*. Springer, 2002.

[3] Leo L. Beranek and Tim J. Mellow. *Acoustics: Sound Fields and Transducers*. Elsevier, 2012.

[4] Paul Brochu and Qibing Pei. Advances in dielectric elastomers for actuators and artificial muscles. *Macromolecular Rapid Communications*, 2010.

[5] Witold Brostow, editor. *Performance of Plastics*. Hanser, 2001.

[6] F. Carpi, G. Fantoni, P. Guerrini, and D. de Rossi. Buckling dielectric elastomer actuators and their use as motors for the eyeballs of an android face. *Smart Structures and Materials*, 2006.

[7] Federico Carpi, Stanisa Raspopovic, Gabriele Frediani, and Danilo De Rossi. Real-time control of dielectric elastomer actuators via bioelectric and biomechanical signals, 2009.

[8] Federico Carpi, Danilo De Rossi, Roy Kornbluh, Ronald Pelrine, and Peter Sommer-Larsen, editors. *Dielectric Elastomers as Electromechanical Transducers*. Elsevier, 2007.

[9] Klaus Ehrenfried. Lecture notes: Strömungsakustik 1. University Lecture, 2002.

[10] Paulo B. Goncalves, Renata M. Soares, and Djenane Pamplona. Nonlinear vibrations of a radially stretched circular hyperelastic membrane. *Journal of Sound and Vibration*, 2009.

[11] Nakhiah Goulbourne, Eric Mockensturm, and Mary Frecker. A nonlinear model for dielectric elastomer membranes. *Journal of Applied Mechanics*, 2005.

[12] C. Graf, D. Tepel, D. Cording, and J. Maas. Design, operation and evaluation of polymer loudspeakers. *Actuator Conference*, 2012.

[13] Vincenzo Guarino, Simona Zuppolini, Anna Borriello, and Luigi Ambrosio. Electro-active polymers (eaps): A promising route to design bio-organic/bioinspired platforms with on demand functionalities. *Multidisciplinary Digital Publishing Institute (MDPI)*, 2016.

[14] R. Heydt, R. Kornbluh, R. Pelrine, and V. Mason. Design and performance of an electrostrictive-polymer-film acoustic actuator. *Journal of Sound and Vibration*, 1998.

[15] Richard Heydt, Ron Pelrine, Jose Joseph, Joseph Eckerle, and Roy Kornbluh. Acoustical performance of an electristrictive polymer film loudspeaker. *Journal of the Acoustical Society of America*, 2000.

[16] Gerhard A. Holzapfel. *Nonlinear Solid Mechanics, a Continuum Approach for Engineering*. John Wiley & Sons, Ltd, 2001.

[17] Naoki Hosoya, Shun Baba, and Shingo Maeda. Hemispherical breathing mode speaker using a dielectric elastomer actuator. *The Journal of the Acoustical Society of America*, 2015.

[18] Hartmut Janoscha. *Unkonventionelle Aktoren*. Oldenbourg Verlag, 2 edition, 2013.

[19] C. Jean-Mistral, S. Basrour, J.J. Chaillour, and A. Bonvilain. A complete study of electroactive polymers for energy scavengeing: Modelling and experiments. *EDA Publishing/DTIP*, 2007.

[20] Kun Jia, Tongqing Lu, and T.J. Wang. Response time and dynamic range for a dielectric elastomer actuator. *Sensors and Actuators A: Physical*, 2016.

[21] Kwangmok Jung, Kwang J. Kim, and Hyouk Ryeol Choi. A self-sensing dielectric elastomer actuator. *Sensors and Actuators A*, 2007.

[22] Kwang J. Kim and Satoshi Tadokoro, editors. *Electroactive Polymers for Robotic Applications*. Springer, 2007.

[23] Guggi Kofod. The static actuation of dielectric elastomer actuators: How does pre-stretch improve actuation. *Journal of Physics D: Applied Physics*, 2008.

[24] Roy D. Kornbluh, Ron Pelrine, Qibing Pei, Richard Heydt, Scott Stanford, Seajin Oh, and Joseph Eckerle. Electroelastomers: Applications of dielectric elastomer transducers for actuation, generation and smart structures. *Smart Structures and Materials*, 2002.

[25] Luca Lampani. *Finite Element Modeling of Dielectric Elastomer Actuators for Space Applications*. PhD thesis, Università di Roma La Sapienza, 2010.

[26] Arthur W. Leissa, editor. *Vibration of Plates*. National Aeornautics and Space Administration (NASA), 1969.

[27] Tiefeng Li, Shaoxing Qu, and Wei Yang. Electromechanical and dynamic analyses of tunable dielectric elastomer resonator. *International Journal of Solids and Structures*, 2012.

[28] Liwu Liu, Yanju Liu, and Jinsong Leng. Theory progress and applications of dielectrc elastomers. *International Journal of Smart and Nano Materials*, 2013.

[29] Jürgen Maas, Dominik Tepel, and Thorben Hoffstadt. Actuator design and automated manufacturing process for deap-based multilayer stack-actuators. *Meccanica*, 2015.

[30] E. Magnucka-Blandzi, K. Wisniewska-Mleczko, M. J. Smyczynsi, and P. Kedzia. Buckling of a sandwich symmetrical circular plate with varying mechanical properties of the core. *Applied Mathematics and Mechanics*, 2018.

[31] Silvain Michel, Xuequn Q Zhang, Michael Wissler, Christian Löwe, and Gabor Kovacs. A comparison between silicone and acrylic elastomers as dielectric materials in electroactive polymer actuators. *Society of Chemical Industry*, 2009.

[32] Martin Molberg, Daniel Crespy, Patrick Rupper, Frank Nüesch, Jan-Anders E. Månson, Christion Löwe, and Dorina M. Opris. High breakdown field dielectric elastomer actuators using encapsulated polyaniline as high dielectric constant filler. *Advanced Functional Materials*, 2010.

[33] G. I. Montanari. Lettere inedite di Alessandro Volta. *Stamperia Nobili*, 1835.

[34] Michael Möser, editor. *Technische Akustik*. Springer, 2012.

[35] Ailish O'Halloran, Fergal O'Malley, and Peter McHugh. A review on dielectric elastomer actuators, technology, applications, and challenges. *Journal of Applied Physics*, 104, 2008.

[36] Tim A. Osswald and Georg Menges, editors. *Materials Science of Polymers for Engineers*. Hanser, 2 edition, 2003.

[37] Qibing Pei, Marcus Rosenthal, Ron Pelrine, Scott Stanford, and Roy Kornbluh. Multifunctional electroelastomer roll actuators and their application for biomimetic walking robots. *Smart Structures and Materials*, 2003.

[38] Ron Pelrine, Roy Kornbluh, Jose Joseph, Richard Heydt, Qibing Pei, and Seiki Chiba. High-field deformation of elastomeric dielectrics for actuators. *Materials Science and Engineering: C*, 1999.

[39] Ron Pelrine, Roy Kornbluh, Qibing Pei, Scott Stanford, Seajin Oh, Joe Eckerle, Robert Full, Marcus Rosenthal, and Kenneth Meijer. Dielectric elastomer artificial muscle actuators: Toward biomimetic motion. *Smart Structures and Materials 2002: Electroactive Polymer Actuators and Devices*, 2002.

[40] Ron Pelrine, Roy Kornbluh, Qibnig Pei, and Jose Joseph. High-speed electrically actuated elastomers with strain greater than 100%. *Science*, 287, 2000.

[41] Ronald E. Pelrine, Roy D. Kornbluh, and Jose P. Joseph. Electrostriction of polymer dielectrics with compliant electrodes as a means of actuation. *Sensors and Actuators A: Physical*, 1998.

[42] Wilhelm Conrad Röntgen. About the changes in shape and volume of dielectrics caused by electricity. *Annua Physics and Chemistry Series*, 11, 1880.

[43] L. J. Romasante, M. A. Lopez-Manchado, and R. Verdejo. Increasing the performance of dielectric elastomer actuators: A review from the materials perspective. *Progress in Poylmer Science*, 2015.

[44] Samuel Rosset, Muhamed Niklaus, Philippe Dubois, and Herbert R. Shea. Large-stroke dielectric elastomer actuators with ion-implanted electrodes. *Journal of Microelectromechanical Systems*, 2009.

[45] Emiliano Rustighi, William Kaal, Sven Herold, and Ahmed Kubbara. Experimental characterisation of a flat dielectric elastomer loudspeaker. *Actuators*, 2018.

[46] Rahimullah Sarban, Benny Lassen, and Morten Willatzen. Dynamic electromechanical modeling of dielectric elastomer actuators with metallic electrodes. *IEEE/ASME Transactions on Mechatronics*, 2012.

[47] J. H. Streng. Sound radiation from circular stretched membranes in free space. *Audio Engineering Society*, 1989.

[48] Takehiro Sugimoto, Akio Ando, Kazuho Ono, Yuichi Morita, Kosuke Hosoda, Daisaku Ishii, and Kentaro Nakamura. A lightweight push-pull acoustic transducer composed of a pair of dielectric elastomer films. *The Journal of the Acoustical Society of America*, 2013.

[49] Takehiro Sugimoto, Kazuho Ono, Akio Ando, Hiroyuki Okubo, and Kentaro Nakamura. Flexible acoustic transducer from dielectric-compound elastomer film. *Audio Engineering Society*, 2012.

[50] Xiaoming Tao, editor. *Smart fibres, fabrics and clothing*. Woodhead Publishing Limited and The Textile Institute, 2001.

[51] Rocco Vertechy, Antonio Frisoli, Massimo Bergamasco, Federico Carpi, Gabriele Frediani, and Danilo De Rossi. Modeling and experimental validation of buckling dielectric elastomer actuators. *Smart Materials and Structures*, 2012.

[52] Stefan Weinzierl, editor. *Handbuch der Audiotechnik*. Springer, 2008.

[53] Michael Wissler and Edoardo Mazza. Modeling of a pre-strained circular actuator made of dielectric elastomers. *Sensors and Actuators A: Physical*, 2004.

[54] Dan Yang, Liqun Zhang, Nanying Ning, Dongdong Li, Zhao Wang, Toshio Nishi, Kohzo Ito, and Ming Tian. Large increase in actuated strain of hnbr dielectric elastomer by controlling molecular interaction and dielectric filler network. *RSC Advances*, 2013.

[55] Xiang Yu, Zhenbo Lu, Li Cheng, and Fangsen Cui. Vibroacoustic modeling of an acoustic resonator tuned by dielectric elastomer membrane with voltage control. *Journl of Sound and Vibration*, 2017.

[56] Xuan Yuan. Application review of dielectric electroactive polymers (deaps) and piezoelectric materials for vibration energy harvesting. *Journal of Physics: Conference Series*, 2016.

[57] Xuequn Zhang, Christiane Löwe, Michael Wissler, Bernd Jähne, and Gabor Kovacs. Dielectric elastomers in actuator technology. *Advanced Engineering Materials*, 2005.

[58] Ma Zhenyi, Jerry I. Scheinbeim, Jar Wha Lee, and Brian A. Newman. High field electrostrictive response of polymers. *Journal of Polymer Science: Part B: Polymer Physics*, 1994.

[59] J. Zhu, C.Q. Ru, and A. Mioduchowski. High-order subharmonic parametric resonance of nonlinearly coupled micromechanical oscillators. *The European Physics Journal B*, 2007.

[60] Jian Zhu, Shenqiang Cai, and Zhigang Suo. Resonant behavior of a membrane of a dielectric elastomer. *International Journal of Solids and Structures*, 2012.